Alma Mater Studiorum - University of Bologna

DEI - DEPARTMENT OF ELECTRICAL, ELECTRONIC, AND INFORMATION ENGINEERING "GUGLIELMO MARCONI"

PhD Course in Electronics Engineering, Telecommunications and Information Technology

XXV CYCLE - COMPETION SECTOR: 09/F2- TELECOMMUNICATIONS
SCIENTIFIC-DISCIPLINARY SECTOR: ING-INF/03 - TELECOMMUNICATIONS

COOPERATIVE WIRELESS SYSTEMS

Candidate:
Ing.
Cristina La Palombara

Supervisor:
Chiar. mo Prof.
Oreste Andrisano

PhD Course Coordinator:
Prof.
Alessandro Vanelli Coralli

Advisors:
Prof.
Andrea Conti

Final Examination Year 2013

1. ***Relay-Assisted Communications***
2. ***Cooperative Diversity***
3. ***Power Allocation Techniques***
4. ***Distributed coding***
5. ***Ultra-wideband***

Abstract

This Ph.D. dissertation reports on the work performed at the Wireless Communication Laboratory - University of Bologna and National Research Council - as well as, for six months, at the Fraunhofer Institute for Integrated Circuit (IIS) in Nürnberg.

The work of this thesis is in the area of wireless communications, especially with regards to cooperative communications aspects in narrowband and ultra- wideband systems, cooperative links characterization, network geometry, power allocation techniques, and synchronization between nodes. The underpinning of this work is devoted to developing a general framework for design and analysis of wireless cooperative communication systems, which depends on propagation environment, transmission technique, diversity method, power allocation for various scenarios and relay positions. The optimal power allocation for minimizing the bit error probability at the destination is derived. In addition, a syncronization algorithm for master-slave communications is proposed with the aim of jointly compensate the clock drift and offset of wireless nodes composing the network.

Contents

Abbreviations

Wi-MAX	Worldwide Interoperability for Microwave Access
Wi-Fi	Wireless Fidelity
LTE	Long Term Evolution
MANET	Mobile ad-hoc network
WMN	Wireless mesh network
WSN	Wireless sensor network
V2V	Vehicle-to-vehicle
GPS	Global Positioning System
UWB	Ultra-wide bandwidth
MIMO	Multiple-input multiple-output
WLAN	Wireless local area network
QoS	Quality of service
TDMA	Time division multiple access
FDMA	Frequency division multiple access
MAC	Multiple access channel
AF	Amplify and forward

LF	Linear-process and forward
nLF	Non-linear-process and forward
DemAF	Demodulation and forward
DF	Decode and forward
CF	Compress and forward
ARP	Adaptive relay protocol
RC	Repetition coding
UC	Unconstrained coding
CSI	Channel state information
CDMA	Code division multiple access
STC	Space-time code
P-STC	Pragmatic space-time code
BFC	Block fading channel
IID	Independent, identically distributed
PEP	Pairwise error probability
INID	Independent, non-identically distributed
AWGN	Additive white Gaussian noise
SV	Saleh-Valenzuela
SNR	Signal-to-noise ratio
BEP	Bit error probability
IPC	Ideal power control

BPSK	Binary phase shift keying
ROI	Region of interest
CM	Channel model
NLOS	Non-line-of-sight
LDPC	Low-density parity check
FEP	Frame error probability
QAM	Quadrature amplitude modulation
RFID	Radio frequency identification
NLOS	Non-line-of-sight
UHF	Ultra-high frequency
ppm	Parts per million
PI	Proportional-integrator
IR-UWB	Impulse-radio ultrawide bandwidth
ToA	Time-of-arrival
LOS	Line-of-sight
NCO	Numerically controlled oscillator

Introduction

THE interest for relay-assisted communications has increased to efficiently extend area coverage or improve the performance in wireless channels, by exploiting cooperative diversity. In fact relay-assisted transmissions and diversity methods improve wireless communications via nodes cooperation, multiple channels reception, and distributed processing. Analysis and design of relay-assisted diversity communications require to account for system setting, propagation environment, and resource allocation methods. Specifically, the contribution of this work has been to create a mathematical framework to analyze the performance at the destination depending on distributed coding, nodes spatial distribution, and power allocation among source and relay nodes. After a preliminary investigation of the impact of cooperative link characterization on the overall relay assisted communication, the work has been focused on the comparison of different power allocation techniques to identify the most cost effective based on the scenario and the relay position. The framework is built on a simple model for assessing the performance as a function of radio links characteristic, and enables a clear understanding of how aforementioned aspects affect the performance. The activity was conducted for both narrow-band and ultra-wideband systems and the transmission channels is correspondingly shaped to that choice [1–3]. In addition, the effect of timing synchronization errors among wireless nodes is investigated. The development and characterization of an algorithm for timing synchronization have been

proposed, focusing on a master-slave synchronization [4].

The remainder of the thesis is organized as follows. In Chapter 1 an overview of cooperative wireless communications is reported, highlighting the benefits of using them. Several relaying protocols and resource allocation strategies are recalled and some possible application scenarios are described.

In Chapter 2 the analytical framework for narrow-band systems is proposed and the impact of links characterization on the overall performance is evaluated. Results are given for two case studies in which P-STC[1] and LDPC[2] code are employed as distributed coding techniques. Analytical results are confirmed by simulations that are given to serve as benchmark for the considered cases.

In Chapter 3 a novel FEP[3]-optimal power allocation has been developed and compared with other allocation techniques such as uniform, destination-balanced, and relay-balanced. The framework enables the system designer to allocate power and individuate the best relay position to minimize the FEP. Results show the effectiveness of the novel power allocation technique for various distributed coding and provide insight into the operation of relay-assisted diversity systems.

In Chapter 4 an analytical framework for the performance evaluation of relay-assisted UWB communications are proposed. This accounts for new single link characterization in IEEE 802.15.4a channels, network topology, and various power allocation techniques. Starting from a new class of tight bounds characterizing the performance in each link, the framework enables to quantify the benefits of relaying for ideal power control, uniform power distribution and optimal power allocation minimizing the bit error probability (BEP).

In Chapter 5 the problem of synchronization between nodes is analyzed, in terms of master-slave synchronization. The work has been fo-

[1]Pragmatic space-time code
[2]Low-density parity check
[3]Frame error probability

cused on the estimation and compensation of the clock drift and clock offset of the slave nodes with respect to the reference clock. The overall performance has been evaluated as a function of the system configuration.

Chapter 1

Overview of Cooperative Wireless Systems

In the last few years the fast growth of wireless communications is unprecedented. The extraordinary progress has led to a wide diffusion of technologies in all human activities. Recently, wireless communication systems have experienced a huge increase in time sensitive traffic due to the significant growth in the number of users and development of new applications that require high transmission rates [5–7]. These aspects involve not only the mobile phone market using LTE[1], but also other wireless technologies, such as Wi-MAX[2] for metropolitan area networks, Wi-Fi[3] for local area networks, UWB[4] communications, wireless ad-hoc networks (i.e., MANETs[5], WMNs[6], WSNs[7]), and V2V[8] communications [8–11]. The environment complexity requires devices able to share a limited amount of resources in order to ensure reliable high-speed com-

[1]Long Term Evolution
[2]Worldwide Interoperability for Microwave Access
[3]Wireless Fidelity
[4]Ultra-wide bandwidth
[5]Mobile ad-hoc networks
[6]Wireless mesh networks
[7]Wireless sensor networks
[8]Vehicle-to-vehicle

munications with appropriate power allocation and interference mitigation techniques.

In this context, an important solution is provided by MIMO[9] systems, which use multiple antennas elements for transmission and reception of signals with the purpose of creating multiple independent channel for sending multiple data streams [12, 13]. MIMO technology converts the multipath propagation into a benefits through the use of the spacial dimension, that adds diversity in the system. In addition, MIMO can exploit random fading and multipath delay spread typical of wireless channel [14–17]. As results, the quality of the wireless communications is improved and the capacity of the link is increasing. Even though recent technological developments allow the implementation of multiple antennas maintaining an acceptable cost, the size of mobile devices limits the number of antennas that can be deployed.

To overcome the above limitations of MIMO systems, a new spatial diversity technique based on cooperative communications is considered, namely cooperative diversity [18–20]. Due to the broadcast nature of wireless channel, the information transmitted from a source node to a destination node can be overheard by neighboring nodes which cooperate together for distributed transmission and processing information. Using this point of view, cooperative communications, also called virtual MIMO, generate independent paths between the source and the destination by using an auxiliary relay channel in addition to the direct channel. Cooperative communications exploit some of the benefits of MIMO systems and provide fading robustness, performance improvement, coverage extension, and power saving [21].

This chapter provides an overview of cooperative wireless systems, in order to detail all the main aspects of relay-assisted communications. The reminder is organized as follows. Section 1.1 introduces the concept of cooperative communications and possible transmission protocols. Sec-

[9]Multiple-input multiple-output

tion 1.2 describes some practical application scenarios and Section 1.3 underlines the advantages and disadvantages of cooperative wireless communications. Section 1.4 details relaying protocols.

1.1 Fundamentals of Cooperative Wireless Communications

COOPERATIVE communications are based on the collaboration among several nodes, which create a virtual array through sharing their antennas. This type of communication differs from point-to-point communication in the use of a new element, called relay. The basic scheme of relay-assisted communication involves three nodes, as depicted in Fig. 1.1. The source node S wants to transmit information to the destination node D and the relay node R assists the communication.

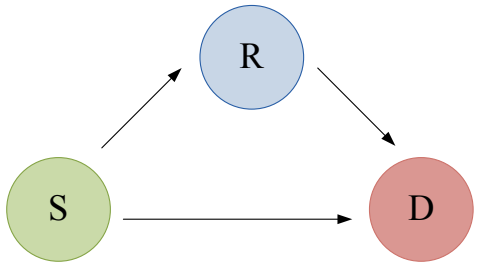

Figure 1.1: Relay-assisted communication scheme.

In general, the communication between devices can be full-duplex or half-duplex. In full-duplex communication a node can receive and transmit data at the same time or in the same band; in half-duplex communication a node cannot send and receive at the same time or in the same band. Unlike MIMO systems, additional channel resources are necessary in relay-assisted communications due to the radio technology limitations. Consequently, the relay is forced to work in half-duplex mode and the communication is divided in two orthogonal duplexing phases, namely relay-receive phase and relay-transmit phase. The phase separation can be done by TDMA[10] or FDMA[11]. In TDMA the received and the transmit information at the relay are divided into different time slots and share the

[10]Time division multiple access
[11]Frequency division multiple access

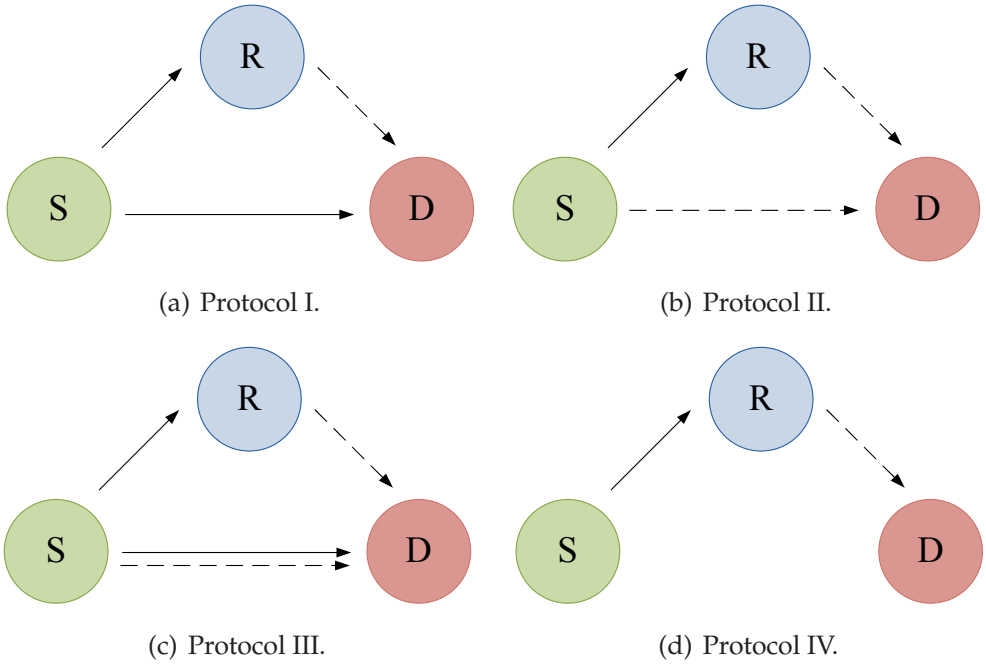

(a) Protocol I. (b) Protocol II.

(c) Protocol III. (d) Protocol IV.

Figure 1.2: Half-duplex relay protocols in a scenario with three nodes. Solid lines and dashed lines correspond to relay-receive and relay-transmit phase, respectively.

same frequency channel; this separation is used by regenerative relaying protocols. In FDMA the received and the transmit information at the relay are separated into different frequency band and share the same time slots; this division is utilized by regenerative and non-regenerative relaying protocols.

The possible transmission combinations lead to four half-duplex relay protocols among three nodes, as depicted in Fig. 1.2 where solid lines refer to relay-receive phase and dashed lines correspond to relay-transmit phase. These four protocols can be classified as follows:

- Protocol I. In the relay-receive phase the source broadcasts the information to the destination and the relay; in the relay-transmit phase the relay communicates with the destination, as shown in Fig. 1.2(a).
- Protocol II. In the relay-receive phase the source only transmits its

message to the relay and the destination is unable to receive the information; in the relay-transmit phase the source and the relay communicates simultaneously with the destination, as presented in Fig. 1.2(b). This protocol corresponds to a MAC[12] solution.

- Protocol III. In the relay-receive phase the source broadcasts the information to the destination and the relay; in the relay-transmit phase the source and the relay communicates simultaneously with the destination. This protocol combines protocol I and protocol II, as visualized in Fig. 1.2(c).

- Protocol IV, also known as forwarding protocol. In the relay-receive phase the source only transmits its message to the relay; in the relay-transmit phase the relay only communicates with the destination, as showm in Fig. 1.2(d).

In contrast to the traditional forwarding protocols, the first three protocols use also the source-destination link. However, if the source-destination link quality drops below a certain threshold, performances obtained from the first three protocols converge to those of the forwarding protocols.

Depending on the type of considered relay-assisted system and CSI[13] at the source, the duration of the relay-receive and relay-transmit phase can be previously assigned or not [22]. Static resource allocation relaying is assumed when the transmission is done into two time slots with fixed duration. Possible examples of application are a centralized cellular scenario based on TDMA or a system where the channel model is characterized by statistical information. On the contrary, dynamic resource allocation relaying requires that the source knows the all links qualities. Under that knowledge, the adaptive resource allocation on each phase maximizes the spectral efficiency of a relay-assisted communication.

[12]Multiple access channel
[13]Channel state information

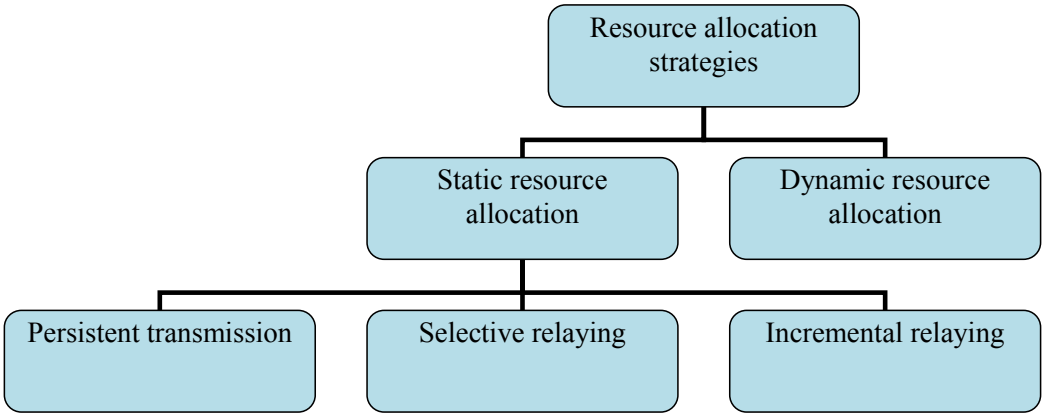

Figure 1.3: Resource allocation strategies in a relay-assisted communications.

Static resource allocation relaying may evaluate knowledge about the success of the transmission at the destination or at the relay and involves several retransmission schemes at the relay to increase spectral efficiency. The different types of static resource allocation strategies, shown in Fig. 1.3, can be summarized as follows:

- Persistent transmission. In this retransmission scheme the relay terminal may always transmit.

- Selective relaying. This retransmission scheme is enforced to the DF[14] strategy, because it considers the success or failure of the source-relay link. If the relay does not receive the signal properly or if the channel state of the source-relay link is below a threshold, the source retransmits the message while the relay remains silent. Otherwise if the relay receives correctly the signal coming from the source, the relay retransmits the message to the destination.

- Incremental relaying. This retransmission scheme considers the success or failure of the source-destination link during the relay-receive

[14]Decode and forward

phase. The relay transmits the information when the message at the destination is received in error.

The different retransmitting schemes at the relay for the available half-duplex protocols are presented in Table 1.1. All types of retransmitting schemes are possible for protocol I and protocol III. Incremental relaying scheme is not implementable for protocol II, where the source and the relay communicate simultaneously with the destination in the relay-transmit phase. Persistent transmission is the only implementable scheme for protocol IV, where is necessary that the relay always transmits.

Static resource allocation relaying	Half-duplex relay protocols			
	Protocol I	Protocol II	Protocol III	Protocol IV
Persistent transmission	√	√	√	√
Selective relaying	√	√	√	×
Incremental relaying	√	×	√	×

Table 1.1: Retransmitting schemes at the relay for different half-duplex relay protocols.

1.2 Application Scenarios

COOPERATIVE communications play an essential role in many application scenarios and permit to overcome issues related to the direct link communication [23]. The cooperation between nodes is beneficial in several practical applications, ranging from cellular networks to wireless sensor networks, as shown in Figs. 1.4- 1.9. In fact, the use of relays can provide a solution for problems of a network which are caused by a limited use of resources in terms of bandwidth and transmitted power.

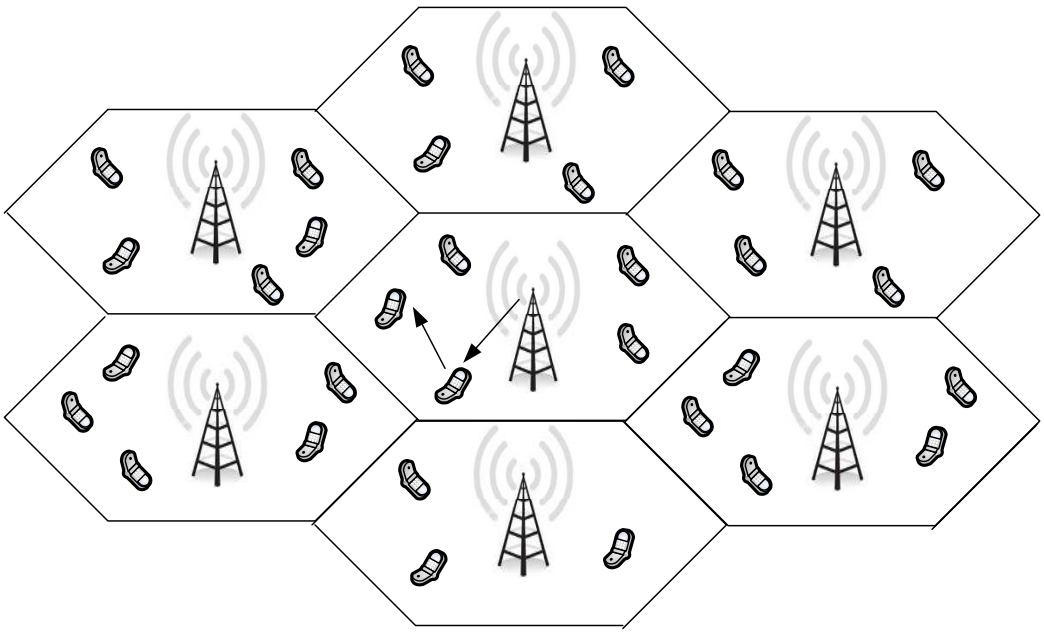

Figure 1.4: Cellular scenario: relaying improve performance of users in terms of capacity, coverage or interference.

1.2.1 Cellular Networks

Cellular networks are a typical scenario, which are limited in the resources per cell. By increasing the number of users per cell, resources are not able to satisfy the demand of users; consequently the offered cell

capacity becomes insufficient and the limit in transmitted power is reflected on the coverage. In addition, the inter-cell and intra-cell interference are detrimental performance factors. Capacity, coverage, and interference problems can be reduced using relay-assisted communications, where the cooperative transmission helps the direct link in order to guarantee better performance.

Figure 1.4 shows an example of cooperative cellular networks, where the network coverage is improved especially at the cell edge. In fact in this part of the cell, the signal received from the base station is characterized by a low SNR[15]. By using the relay-assisted communication, the total coverage area of the cell increase thanks to the the strong signal that the mobile station receives from the relay station. In addition, the improvement of the signal quality for user located in the cell edge lead to a decrease of required resources from the base station.

1.2.2 Wireless Local Area Networks

WLAN[16] supports network communication over short distances in a urban scenario, where the interference can significantly affect performance. The low cost and high bandwidth of these networks have allowed an increase of their use. The continuous data rate requirements for real time and non-real time web-based applications require new strategies to improve the performance of WLAN technologies. One method to improve network capacity is based on the use of intermediate relay nodes to boost the power of wireless signal. As for the cellular networks, cooperative communication is able to alleviate also problems in terms of coverage and interference in WLAN.

Figure 1.5 shows a WLAN example with home WLAN access points and users located in the street and in the house. In particular, the home access point can communicate with a user in the street using another user

[15]Signal-to-noise ratio
[16]Wireless local area network

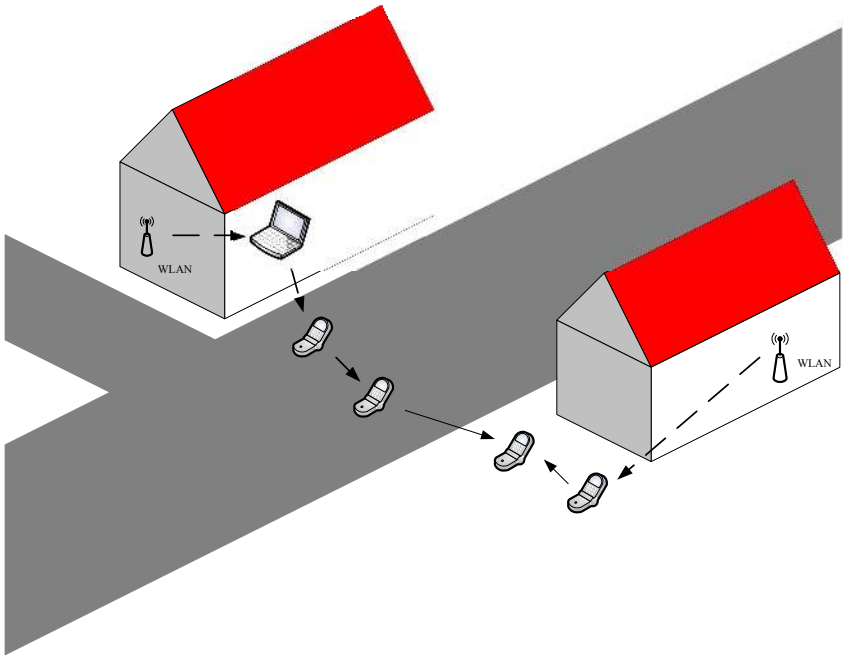

Figure 1.5: A WLAN station installed inside a house provides access to users in the street via relays.

that provides a relay-assisted communication.

1.2.3 Vehicle-to-Vehicle Communications

However, V2V communication systems are a type of networks where vehicles communicate with each others for exchange information, as shown in Fig. 1.6. In a urban and suburban scenario, this type of cooperative communication can deliver very significant benefit for traffic reduction, safety, parking problems. Data arising from vehicles, infrastructure and their interactions improve the mobility management and influence both the economic and social development of the country. This cooperative approach offers high link stability and can be more effective in avoiding accidents and traffic congestions.

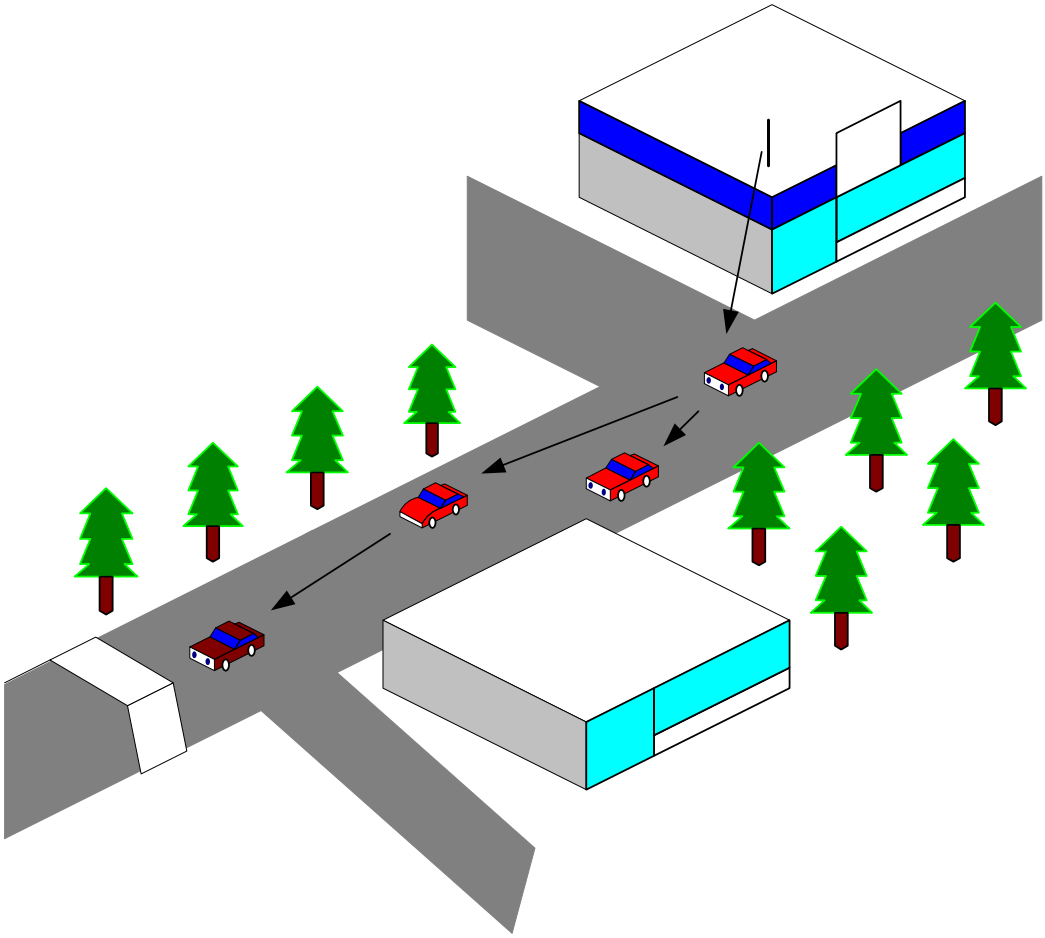

Figure 1.6: Distributed V2V communication scenario, where vehicles cooperate to reduce communication delays.

1.2.4 Wireless Sensor Networks

WSN must be properly designed to maximize the lifetime of the network, ensuring efficient communications between sensor nodes. In fact, the main problem of these networks is the limited battery power of sensor nodes. Also in this scenario, relay-assisted communications are beneficial to maintain network integrity avoiding the performance degradation. Figure 1.7 shows an example of cooperative WSN, where the sensor nodes are limited in coverage.

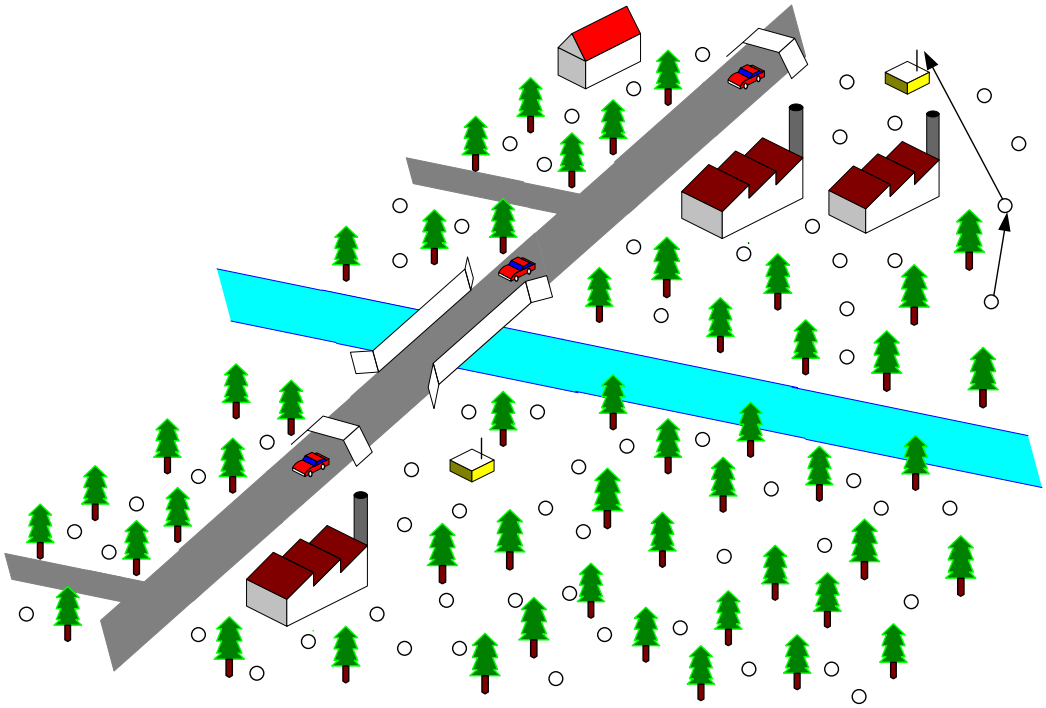

Figure 1.7: WSN scenario, where sensors cooperate to obtain a better coverage.

1.2.5 Networks Localization

Many applications require knowledge of the nodes position in order to know where the data are collected for perform data analyses or for determine what actions should be taken. Traditional methods of nodes localization include the attaching of a GPS[17] receiver in each node or the manual configuration of each nodes position. By increasing the scale of the networks, these methods become unfeasible for their high cost and inconvenience. The localization algorithms use some special nodes, called anchor nodes, which know their positions for facilitate the determination of the positions of the other nodes (called common nodes). An emerging paradigm is cooperative localization, in which nodes help each other to determine their locations. Cooperative localization has received exten-

[17]Global Positioning System

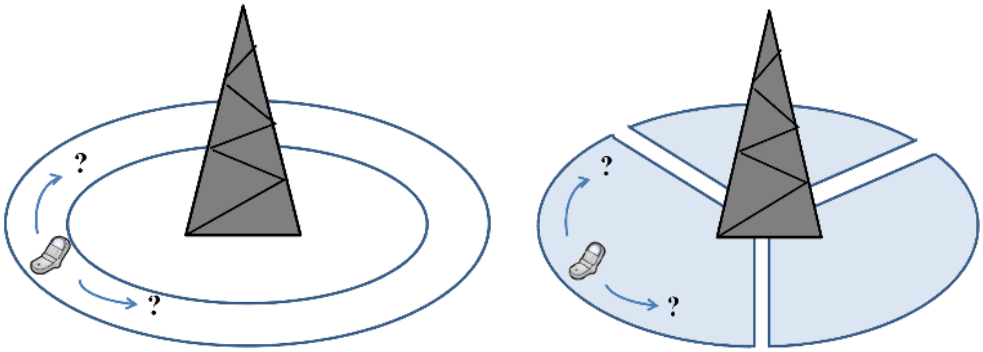

Figure 1.8: Area where it is more likely to find a mobile device if cooperation is not used.

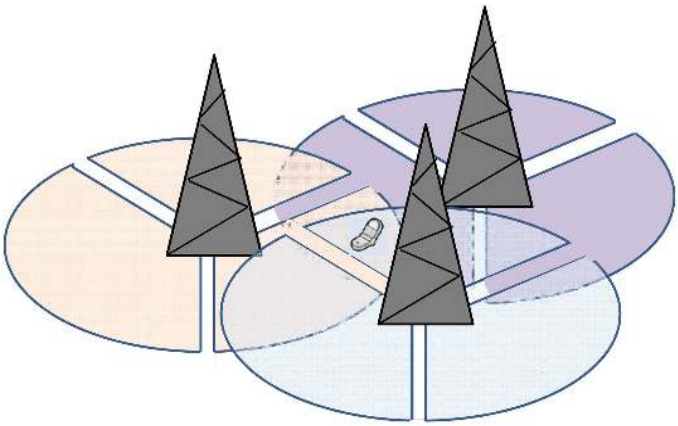

Figure 1.9: Area where it is more likely to find the mobile device if cooperation is used.

sive interest from the robotics, optimization, and wireless communications communities [24–27].

Figures. 1.8 and 1.9 show a simple example for comparing conventional and cooperative localization. A non-cooperative device can retrieve information from one base station only. These information could be used to determine a zone where the mobile may be located. This means that, given a received signal strength, it is assumed that the mobile is in a cer-

tain area defined by a certain tier, as shown in Fig. 1.8. In cellular networks a typical structure environment is the trisector, also known as clover, that is composed of three sectors, each of which is served by one separate antenna. Every sector has a separate direction of tracking of 120°with respect to the adjacent ones. Therefore it is possible to define a more precise zone of localization. In a cooperative scenario, two mobile phones can send their information using a short range communication technology. By exploiting the information received, the area of localization is now given by the intersection of the zones individuated by each information exchanged by cooperating, as shown in Fig. 1.9. In general, cooperative localization can dramatically increase localization performance in terms of accuracy and coverage.

1.3 Advantages and Disadvantages of Cooperation

THE cooperative communications allow several advantages in terms of link reliability, power consumption, coverage and capacity in wireless systems, resulting in wide interests in both academia and industry [28]. In order to realize practical systems, the choice of system design parameters must take into account the most important advantages and disadvantages of cooperative systems.

In the wide range of scenarios, the most favorable aspects of cooperation are:

- Reduced signal attenuation. The wireless channel is affected by pathloss, shadowing and fading effects. This implies an exponential decay of the signal strength with distance between source and destination. The increase of the distance leads to a greater attenuation of the signal, resulting in lack of communication between source and destination. On the contrary, in a relay-assisted communications the distance between source and relay and the distance between relay and destination are shortened. Accordingly the signal strength improves and the source can use higher modulation symbol alphabets to transmit more data in each channel. This circumstance increases the data rate transmitted to the user, resulting in increased system performance.

- Reduced shadowing effects. Big cities are characterized by many obstacles such as hills or large buildings, that obscure the main path between source and destination and affect the signal propagation. The relay-assisted communication creates an alternative route to avoid obstacles.

- Reduced fading effects. By exploiting the independently orthogonal

phases, cooperative diversity communications combat also the signal fluctuations caused by fading effects.

- QoS[18]. Relay-assisted communications balance capacity and coverage problems and provide an equal QoS for all users.

- Low cost. Cooperative communication is a cheaper solution compared to the cellular scenario, where the cost for building base stations is very high.

- Infrastructure-less deployment. The use of relay provides the lack of infrastructure. In disaster-struck areas, cooperation can be used to communicate in a simple way.

Despite all these advantages, there are also some disadvantages in relay-assisted communications, as summarized below:

- Increased overhead. Each link introduces overheads, such as synchronization and channel estimation. In some scenarios, CSI is required at each node resulting in a significant consumption of resources.

- Resource consumption. The relay-assisted communications establish extra links between nodes, which consume extra resources, such as battery, frequency or time.

- Increased interference and traffic. The transmitted data from each node can cause interference and can increase traffic for the overall system.

- Spectral efficiency loss. The relay assisted-communication is based on an half-duplex protocol, that leads to spectral efficiency loss compared to the direct transmission.

[18]Quality of service

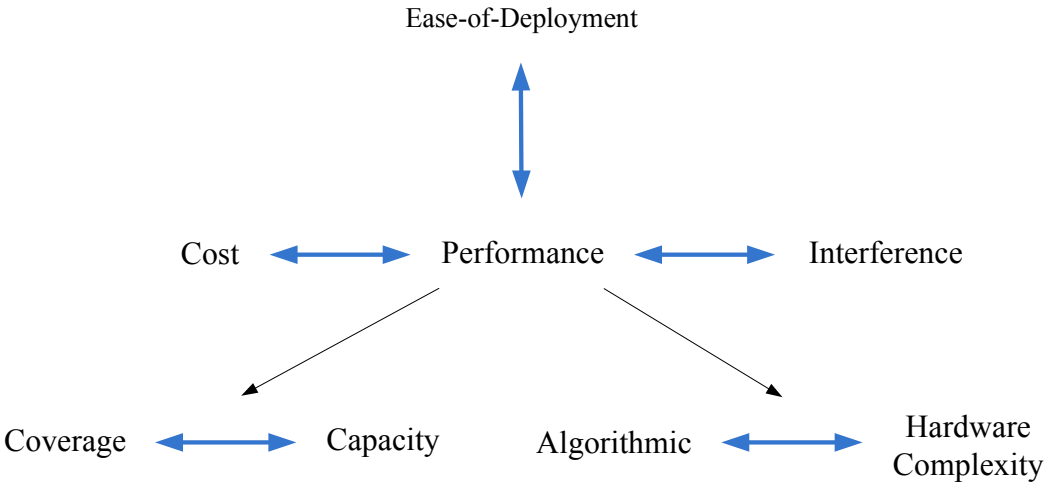

Figure 1.10: System trade-offs in cooperative networks.

The advantages and disadvantages of cooperative networks lead to a suitable choice of system design parameters, because the increase of a parameter implies a decrease of another parameter. Hence, a good decision can be obtained with a compromise solution, that finds the right trade-offs between the different involved aspects. Figure 1.10 shows these trade-offs and provides at a glance the system design parameters to be optimized. In particular, a good choice considers the following aspects:

- Coverage versus capacity. The designer must choose if increase the cell radius to provide greater coverage or increase the capacity of the system.
- Algorithmic versus Hardware Complexity. The relay has a relatively low hardware complexity compared to base stations. The low hardware complexity implies an increase in algorithmic complexity because of scheduling, synchronization, and handover.
- Interference versus performance. Relay-assisted communications ensure the transmission power reduction and performance improving in terms of coverage and capacity. On the other hand, relay causes extra traffic, which produces additional interference.

- Ease-of-deployment versus performance. The network designers can deploy relays in a planned and unplanned manner. In the former case, the placement and parametrization of the static relay node are optimized providing a complex task with superior performance. In the latter case, costs are significantly simplified but performance are worse.
- Cost versus Performance. The cost deeply impacts the performance of cooperative communications.

1.4 Relaying Protocols

In relay-assisted communications the relay assumes an essential role to achieve the desired performance. The relaying protocols [29] can be classified in two categories, namely non-regenerative and regenerative relaying protocols. The classification depends on the operations performed by the relay, which can modify or not the information. The performance of some of these protocols are examined for more realistic assumptions in [30]. Figure 1.11 shows the main protocols and provides at a glance the classification described in the following sections.

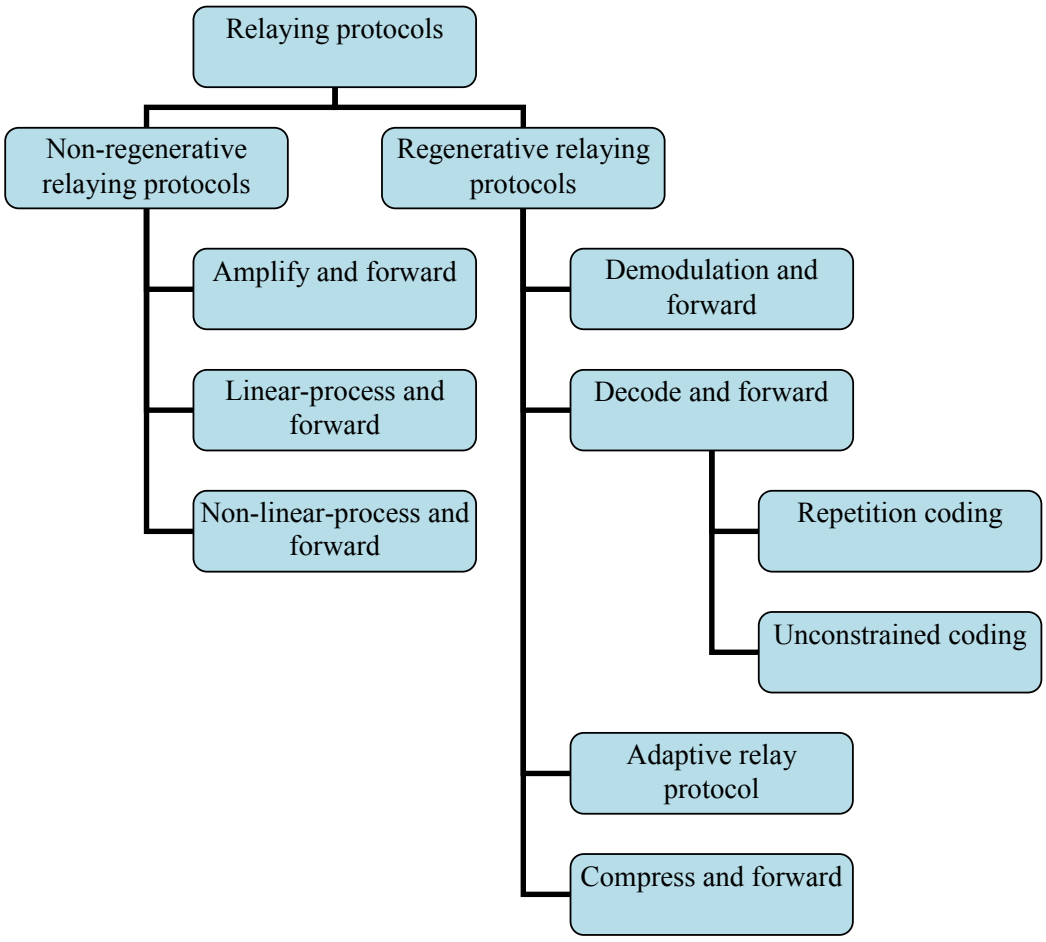

Figure 1.11: Classification of the main relaying protocols.

1.4.1 Non-Regenerative Relaying Protocols

In non-regenerative relaying protocols the relay performs simple operations, as amplify or phase rotation, without modify the signal coming from the source. Examples of non-regenerative relaying protocols are:

- AF[19] protocol [31, 32] is the simplest and most popular relay communication protocol, in which the relay amplifies the received signal coming from the source before retransmitting it to the destination. In other words, the relay transmits a scaled version of the signal received from the source, where the scale factor is the amplification gain. The final decision is carried out by the destination where the two copies of the received signal are combined properly. Obviously the drawback of this simple protocol is the noise amplification at the relay. In AF, the quality of channel estimates influences the overall performance of relay-assisted communications and might become a performance limiting factor [33, 34]. The performance of AF protocol degrades with the increase of the network size. For this reason it is important to find the trade-off between network size, rate, and diversity [35]. AF may minimize the outage probability using intelligent scheduling based on optimal selection and transmission of a single relay among a set of multiple AF [36].

- LF[20] protocol performs some simple linear operations in the analog domain after amplification. An example is provided by phase shifting. Note that the choice of the linear processing at the relay influences the performance of the overall system.

- nLF[21] protocol provides some non-linear operations in the analog domain before retransmitting. An example is provided by nonlinear amplification of the received signal [37].

[19] Amplify and forward
[20] Linear-process and forward
[21] Non-linear-process and forward

In non-regenerative relaying protocol the choice of the amplification factor is a very important design issue at the relay. Different solutions can be realized, namely

- Constant output power. The relay transmits with a constant output power that is set during node manufacturing or prior configuration. This is the simplest way to realize a non-regenerative protocol.

- Fixed gain amplification. In a given time window, the amplification factor assumes a constant value depending on long-term channel statistics. The amplification factor is usually inversely proportional to the average channel gain between source and relay. When channel conditions are very bad, the average channel gain between source and relay is low and consequently the amplification factor is high; in this situation, the maximum transmission power delimitates retransmitting signal leading to clipping effects.

- Variable gain amplification. In a given time window, the amplification factor is not constant and assumes a value that depending on instantaneous channel changes. Also in this case, the amplification factor is usually inversely proportional to the instantaneous channel gain between source and relay. When channel conditions are not good, the amplification factor is high for compensate the low value of the average channel gain between source and relay; in this situation, the maximum transmission power delimitates retransmitting signal introducing clipping effects.

1.4.2 Regenerative Relaying Protocols

In regenerative relaying protocol the relay modifies the information coming from the source, employing a more complex hardware and obtaining better performance. Examples of regenerative relaying protocols are:

- DemAF[22] protocol [38] overcomes the disadvantage of AF eliminating the effect of noise amplifications. The relay demodulates the signal received from the source, forms the estimation of the transmitted signals, and retransmits this estimation [39].

- DF protocol [32,40] considers a relay that decodes the signal received from the source and re-encodes the information before retransmitting it to the destination. The relay may use two different types of encoding: RC[23] or UC[24] [41]. In RC the relay retransmits symbols, using the same codeword as the source; in UC the relay employs a different codebook from the source. DF is more complex than AF and DemAF protocols, but it outperforms the performance compared to AF and DemAF. When the source-relay link suffers from deep fading, the relay may re-encode incorrect bits resulting in error propagation. This implies a severe performance degradation. On the contrary, when the quality of the source-relay channel is better than that of the source destination channel, DF achieves capacity.

- ARP[25] [42] exploits the advantages of AF and DF minimizing their disadvantages in terms of noise amplification and error propagation. The relay adaptively chooses which protocol is the best option to use in certain situation, based on the correct decoding. In other words if the relay successfully decodes the signal received from the source, DF protocol is used; if the relay fails to decode, AF protocol is employed.

- CF[26] protocol considers a relay that compresses the received signal from the source, using Wyner-Ziv coding for optimal compression. After the compression the relay forwards the signal to the destina-

[22]Demodulation and forward
[23]Repetition coding
[24]Unconstrained coding
[25]Adaptive relay protocol
[26]Compress and forward

tion. By considering the same situations, CF outperforms DF protocol [43].

Chapter 2

Link Characterization for Relay-Assisted Communications

COOPERATIVE diversity provides significative performance improvements in wireless networks. By exploiting virtual transmit diversity, cooperation allows single antenna devices to benefit of some of the advantages of MIMO systems, extending the coverage and improving the performance at the destination. In addition, the full spatial diversity achieved by cooperation [44, 45] together with power control techniques [46] allows drastic power savings for a target level of outage probability and a given communication rate. Hence, the paradigm of cooperative diversity has recently attracted considerable attention both in cellular systems and in decentralized ad-hoc networks as the way to efficiently share resources through distributed transmission and processing.

To increase network capacity and reliability, and to optimally allocate the transmitted power, various cooperation techniques can be considered: cooperation strategies based on CDMA[1] signals are proposed in [47] and [48]. Opportunistic relaying schemes are presented in [49] and [50], where also an evaluation of the outage probability under source power constraint

[1]Code division multiple access

in Rayleigh fading channels is proposed. An alternative approach for improving bandwidth efficiency, was proposed in [51] and [41], where cooperative diversity algorithms based on STCs[2] are adopted to offer full spatial diversity without feedback. In [52] P-STCs, consisting of standard convolutional encoders and Viterbi decoders over multiple transmitting and receiving antennas, have been proposed to simplify the encoder and decoder structures and to allow a feasible method to search for good codes in BFCs[3]. In [53] a design methodology for P-STCs in relay networks was proposed, and the derivation of the pairwise error probability, the asymptotic error probability bounds, and the design criteria to optimize diversity and coding gain were discussed. By exploiting P-STCs, in [54], the impact of the relay position on the performance at the destination was investigated by simulation and some insights on power consumption as a function of geometrical relaying conditions were generated.

Differently from these contributions, and with reference to a three nodes cooperation scheme, the key contributions of this chapter are [1,2]:

- development of a framework that jointly considers i) network geometry, ii) links characterization, iii) diversity methods, iv) distributed coding and constellation signaling, and v) power allocation.
- characterization of cooperative links by means of simple models, which depend on propagation environment, transmission technique, and diversity method.
- investigation of the impact of the link FEP characterization on the overall relay-assisted communication and comparison between analytical results and simulations, in the case studies of distributed P-STCs and LDPC codes.

The reminder of the chapter is organized as follows. Section 2.1 details the system model and the assumptions related to the used configuration.

[2]Space-time codes
[3]Block fading channels

Section 2.2 characterizes a simple model to approximate the FEP for each link of cooperative system. Section 2.3 provides numerical results for two case studies of distributed coding: P-STCs [55] and LDPC codes [56].

2.1 Relay-Assisted Communication Model

In this section the system and channel models for design and analysis of relay-assisted diversity communications are presented and the received signals on each antenna is defined. In addition, assumptions related to the relay-assisted system are proposed.

2.1.1 System Model

The communication scheme consists of a general three-node relay-assisted system, where the communication from source S to destination D is assisted by relay R. Figure 2.1 shows the considered scenario. Decode and forward, where the relay decodes the received signals and re-encodes them before forwarding to the destination, is considered. When the channel quality in the link between the source and relay is sufficient, the process of decoding and re-encoding provides more powerful error correcting capabilities than amplify and forward and demodulation and forward [47, 51]. The communication is based on two orthogonal phases: in the first phase the source broadcasts its message, which is forwarded in the second phase by the relay (if capable to decode it). The destination jointly decodes the signals received in the two phases.[4] The source and the relay employ n_{S} and n_{R} transmitting antennas, respectively, and that m_{R} and m_{D} are the number of receiving antennas at the relay and at the destination, respectively.

Each transmission from the source employs energy E_{S}, while that from the relay employs energy E_{R}, with corresponding energy per coded symbols $E_{\mathrm{S}}/n_{\mathrm{S}}$ and $E_{\mathrm{R}}/n_{\mathrm{R}}$.[5] To account for various power allocations, the assumptions $E_{\mathrm{S}} = x_{\mathrm{S}}E$ and $E_{\mathrm{R}} = x_{\mathrm{R}}E$ are considered, where E is the energy

[4] The destination decodes only the signal received in the first phase when the relay is not able to forward the message.

[5] In each transmission, n_{S} and n_{R} coded symbols are sent in parallel over transmitting antennas from the source and the relay, respectively.

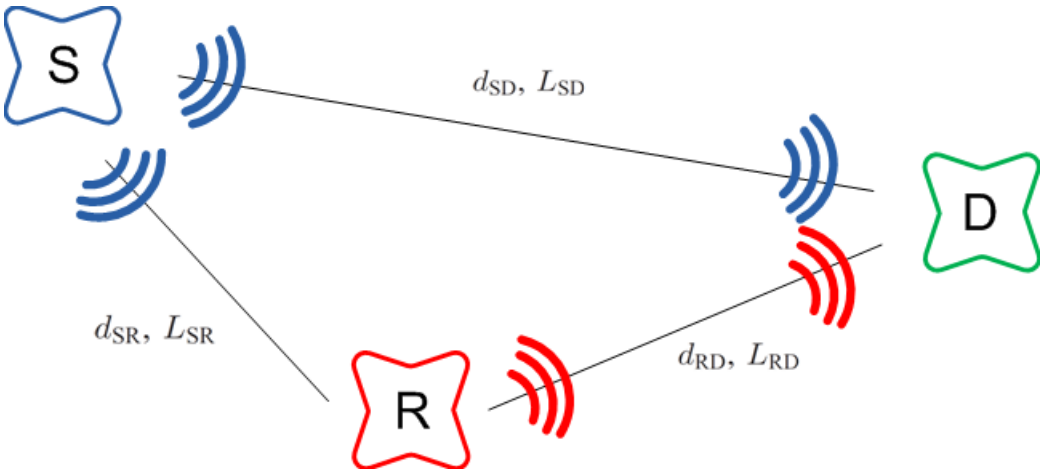

Figure 2.1: Relay-assisted communication system with a source S, a relay R, and a destination D.

averaged over the two phases given by

$$E = \frac{N_S E_S + N_R E_R}{N_S + N_R} \tag{2.1}$$

with N_S and N_R being the number of transmissions in the first and the second phase, respectively. It follows that the constraint on the total energy over the two phases requires

$$a_S x_S + a_R x_R = 1 \tag{2.2}$$

with $a_S = N_S/(N_S+N_R)$, $a_R = 1-a_S = N_R/(N_S+N_R)$, $x_S \in [0, 1/a_S]$, and $x_R \in [0, 1/a_R]$. The same amount of information bits is transmitted in the two phases, which gives $\rho \triangleq a_S/a_R = N_S/N_R = R_{CR} n_R/(R_{CS} n_S)$, where R_{CS} and R_{CR} are the code-rates at the source and at the relay, respectively. Thus, the mean energy transmitted per information bit is $E_b = E/(a_S R_{CS} n_S)$.

2.1.2 Channel Model

For a compact notation $\mathbb{L} \in \{SD, SR, RD\}$ indicates the link source-destination (SD), source-relay (SR), and relay-destination (RD), respectively. The cooperative system follows a BFC model in each link with fading level

constant over a block of B consecutive transmitted symbols and independent from block to block (i.e., if the codeword length is N, the fading levels per codeword are $M = N/B$). Perfect CSI is available at the receivers, whereas the transmitters only know the mean channel gains, averaged over fading, which will be exploited for power allocation. The channel is spatially uncorrelated with INID[6] complex Gaussian gains having mean zero (i.e., Rayleigh fading) and variance

$$\Delta_{\mathbb{L}} = \left(\frac{d_{\mathbb{L}}}{d_0}\right)^{-\beta} \tag{2.3}$$

where d_0 is a reference distance (i.e., the channel gain of each link is normalized to have unitary path loss at distance d_0), $d_{\mathbb{L}}$ is the distance between the transmitter and the receiver for the link $\mathbb{L}$, and β is the path loss exponent. The channel model includes AWGN[7], assumed IID[8] at the relay and at the destination, with mean zero and variance $N_0/2$ per dimension.

The channel gain of the link $\mathbb{L}$ between transmitting antenna i ($i \in \{1, 2, ..., n_{\mathrm{S}}\}$ at the source and $i \in \{1, 2, ..., n_{\mathrm{R}}\}$ at the relay), and receiving antenna j ($j \in \{1, 2, ..., m_{\mathrm{R}}\}$ at the relay and $j \in \{1, ..., m_{\mathrm{D}}\}$ at the destination) is denoted with $h^{\mathbb{L}}_{i,j}$.

2.1.3 Received Signals

The coded symbols, transmitted from the antenna i with unitary energy constellation signaling, are $c_{\mathrm{S},i}$ when the source transmits and $c_{\mathrm{R},i}$ when the relay transmits. The received signal on the antenna j is $r^{\mathbb{L}}_j$, which can be written for the links $\mathbb{L}$ = SD and $\mathbb{L}$ = SR as

$$r^{\mathbb{L}}_j = \sqrt{\frac{E_{\mathrm{S}}}{n_{\mathrm{S}}}} \sum_{i=1}^{n_{\mathrm{S}}} h^{\mathbb{L}}_{i,j} c_{\mathrm{S},i} + \eta^{\mathbb{L}}_j \tag{2.4}$$

[6]Independent, non-identically distributed
[7]Additive white Gaussian noise
[8]Independent, identically distributed

and for the link $\mathbb{L}$ = RD as

$$r_j^{\mathrm{RD}} = \sqrt{\frac{E_{\mathrm{R}}}{n_{\mathrm{R}}}} \sum_{i=1}^{n_{\mathrm{R}}} h_{i,j}^{\mathrm{RD}} c_{\mathrm{R},i} + \eta_j^{\mathrm{RD}} . \tag{2.5}$$

In particular, following the time-division scheme considered, (2.4) and (2.5) refer to the first and the second phase, respectively.

2.2 Links and Performance Characterization

THE framework is built on the analysis of the FEP at the destination for cooperating links and distributed coding, where the FEP represents the probability that a frame (a codeword) is not correctly decoded. When the decoding on the link SR is correct (hence, relay R forwards the information to destination D) the destination performs joint decoding of the signals received from S and R. When the decoding on the link SR is incorrect (the relay R does not forward the information to destination D), the destination decodes only the signal received from S. Therefore, the FEP at the destination depends on the quality of links SD, SR, and RD. Specifically, by denoting the FEP as $P_{\mathrm{e}}^{(\mathrm{SD})}$ and $P_{\mathrm{e}}^{(\mathrm{SR})}$ for links SD and SR, respectively, the overall FEP at the destination is given by [54]

$$P_{\mathrm{e}} = P_{\mathrm{e}}^{(\mathrm{SD})} P_{\mathrm{e}}^{(\mathrm{SR})} + P_{\mathrm{e}}^{(\mathrm{SRD})} \left[1 - P_{\mathrm{e}}^{(\mathrm{SR})}\right] \tag{2.6}$$

where $P_{\mathrm{e}}^{(\mathrm{SRD})}$ is the FEP at the destination when signals received from S and R are jointly decoded (the probability that relay forward the message is $1 - P_{\mathrm{e}}^{(\mathrm{SR})}$). The FEP components are function of the received SNRs over the involved links, in particular

$$P_{\mathrm{e}}^{(\mathbb{L})} = g_{\mathbb{L}}(\overline{\gamma}_{\mathbb{L}}) \tag{2.7}$$

where $\bar{\gamma}_{\mathbb{L}}$ is the mean SNR at the receiver of link $\mathbb{L}$, which depends on $\bar{\gamma} \triangleq E/N_0$ through

$$\bar{\gamma}_{\mathrm{SD}} = x_{\mathrm{S}} \Delta_{\mathrm{SD}} \bar{\gamma} \tag{2.8a}$$

$$\bar{\gamma}_{\mathrm{SR}} = x_{\mathrm{S}} \Delta_{\mathrm{SR}} \bar{\gamma} \tag{2.8b}$$

$$\bar{\gamma}_{\mathrm{RD}} = x_{\mathrm{R}} \Delta_{\mathrm{RD}} \bar{\gamma} \tag{2.8c}$$

and

$$P_{\mathrm{e}}^{(\mathrm{SRD})} = g_{\mathrm{SRD}} \left(\bar{\gamma}_{\mathrm{SD}}, \bar{\gamma}_{\mathrm{RD}}\right) . \tag{2.9}$$

The function $g_{\mathbb{L}}\left(\bar{\gamma}_{\mathbb{L}}\right)$ in (2.7) is the generic error probability function for the link $\mathbb{L}$, which depends on the modulation and used coding scheme,

whereas $g_{\text{SRD}}\left(\bar{\gamma}_{\text{SD}}, \bar{\gamma}_{\text{RD}}\right)$ is the error probability after joint decoding of the composite link SRD.

To characterize the composite link SRD, it is important underline that $g_{\text{SRD}}\left(\bar{\gamma}_{\text{SD}}, 0\right) = g_{\text{SD}}\left(\bar{\gamma}_{\text{SD}}\right)$ and $g_{\text{SRD}}\left(0, \bar{\gamma}_{\text{RD}}\right) = g_{\text{RD}}\left(\bar{\gamma}_{\text{RD}}\right)$. This behavior can be explained as follows: a receiver with perfect CSI would not base its decision on the contributions received via the unreliable link. Moreover, the PEP[9] of distributed codes for the composite link SRD, at large SNRs, is given by the product of the PEPs referred to links SD and RD.[10] These observations motivate the approximation of the error probability over the composite link SRD as

$$g_{\text{SRD}}\left(\bar{\gamma}_{\text{SD}}, \bar{\gamma}_{\text{RD}}\right) \simeq k_{\text{SRD}}\, g_{\text{SD}}\left(\bar{\gamma}_{\text{SD}}\right) g_{\text{RD}}\left(\bar{\gamma}_{\text{RD}}\right) \tag{2.10}$$

where k_{SRD} is a constant tailored to tight the approximation.

The analysis of the FEP at destination through (2.6) requires the characterization of (2.7) and (2.10) via suitable models for the error probabilities $g_{\mathbb{L}}\left(\bar{\gamma}_{\mathbb{L}}\right)$ for each link. Each $g_{\mathbb{L}}\left(\bar{\gamma}_{\mathbb{L}}\right)$ can be approximated with one-slope or two-slope functions by means of the local bounds [57] or through the asymptotic behavior.

2.2.1 One-Slope Approximation

The error probability of each link in Rayleigh fading channel with diversity L is upper bounded by $k_{\mathbb{L}}/\bar{\gamma}_{\mathbb{L}}^{L}$, where $k_{\mathbb{L}}$ is a constant determined from the asymptotic behavior [58]. This motivates the following one-slope FEP approximation

$$g_{\mathbb{L}}(\bar{\gamma}_{\mathbb{L}}) \simeq \min\left\{a_{\mathbb{L}}, \frac{k_{\mathbb{L}}}{\bar{\gamma}_{\mathbb{L}}^{L_{\mathbb{L}}}}\right\} \tag{2.11}$$

[9] Pairwise error probability

[10] For instance, focusing on distributed STCs (see [54]), the eigenvalues set of the pairwise codeword matrix, which is block diagonal, is the union of the two sets of eigenvalues referred to the component matrices of each single link. Since, for large SNR, the PEP is a function of the product of the eigenvalues, it also becomes the product of the PEPs referred to single links. Similar considerations arise for other distributed coding schemes.

where $L_{\mathbb{L}}$ is the diversity degree of link $\mathbb{L}$ and $a_{\mathbb{L}} \in [0,1]$ is a constant that depends on modulation and coding scheme [57].[11] This solution is very tight for both large and small values of $\bar{\gamma}_{\mathbb{L}}$, whereas it can be not accurate for moderate values of $\bar{\gamma}_{\mathbb{L}}$ around $k_{\mathbb{L}}/a_{\mathbb{L}}$.

2.2.2 Two-Slope Approximation

The two-slope error probability on each single link $\mathbb{L}$ is given by

$$g^{(\mathbb{L})} \simeq \begin{cases} a_{\mathbb{L}} & \text{if } \bar{\gamma}_{\mathbb{L}} < \bar{\gamma}_1 \\ \frac{\breve{k}_{\mathbb{L}}}{\bar{\gamma}_{\mathbb{L}}^{\breve{L}_{\mathbb{L}}}} & \text{if } \bar{\gamma}_1 < \bar{\gamma}_{\mathbb{L}} < \bar{\gamma}_2 \\ \frac{k_{\mathbb{L}}}{\bar{\gamma}_{\mathbb{L}}^{L_{\mathbb{L}}}} & \text{otherwise} \end{cases} \tag{2.12}$$

where

$$\bar{\gamma}_1 = \breve{k}_{\mathbb{L}}^{\frac{1}{L_{\mathbb{L}}}} \tag{2.13}$$

$$\bar{\gamma}_2 = \left(\frac{k_{\mathbb{L}}}{\breve{k}_{\mathbb{L}}}\right)^{\frac{1}{L_{\mathbb{L}}}} \tag{2.14}$$

with same parameters as for the one-slope case with $\breve{L}_{\mathbb{L}} = L_{\mathbb{L}}/2$. This solution is very tight for both large and small values of $\bar{\gamma}_{\mathbb{L}}$ and provides a good approximation also for moderate values of $\bar{\gamma}_{\mathbb{L}}$ around $k_{\mathbb{L}}/a_{\mathbb{L}}$.

Equations (2.11) and (2.12) have the advantage of easily capturing the performance behavior on each link as a function of system configuration and propagation environment. By considering the same modulation format on each link, $a_{\mathbb{L}} = \alpha \ \forall \ \mathbb{L}$. Moreover, for the composite link SRD, $k_{\text{SRD}} = 1/\alpha$ gives $g_{\text{SRD}}(0, \bar{\gamma}_{\text{RD}}) = g_{\text{RD}}(\bar{\gamma}_{\text{RD}})$ and $g_{\text{SRD}}(\bar{\gamma}_{\text{SD}}, 0) = g_{\text{SD}}(\bar{\gamma}_{\text{SD}})$.

[11] Note, for instance, that for the error probability of a binary uncoded link, it results $a_{\mathbb{L}} = 0.5$. However, for coded systems with a large number of symbols per codeword, $a_{\mathbb{L}}$ is close to 1.

2.3 Numerical Results

To show the range of validity of the analysis, two case studies for distributed coding with different numbers of transmitting and receiving antennas in each single link are considered. In particular, the first case study refers to a 8-state rate $1/4$ ($R_{\mathrm{CS}} = R_{\mathrm{CR}} = 1/2$) distributed P-STC [53,54] with generators $(13, 15)_8$ at the source and $(11, 17)_8$ at the relay, BPSK[12] modulation, $n_{\mathrm{S}} = n_{\mathrm{R}} = 2$ transmitting antennas, $m_{\mathrm{R}} = 2$ receiving antennas at the relay, and $m_{\mathrm{D}} = 1$ receiving antenna at the destination. The second case study refers to a binary rate $1/4$ LDPC distributed code with a four levels QAM[13], and $n_{\mathrm{S}} = n_{\mathrm{R}} = m_{\mathrm{D}} = m_{\mathrm{R}} = 2$. The LDPC code is constructed according to [59] and using a repetition code in the second phase ($R_{\mathrm{CS}} = R_{\mathrm{CR}} = 1$).

The values of $k_{\mathbb{L}}$ and $\breve{k}_{\mathbb{L}}$, obtained from the asymptotic behavior of the simulated FEP $g_{\mathbb{L}}(\cdot)$ of link $\mathbb{L}$ are presented in Table 4.1 for both case studies. Different combinations of spatial diversity degrees for the three links are considered: $L_{\mathrm{SR}} = n_{\mathrm{S}} m_{\mathrm{R}}$, $L_{\mathrm{SD}} = n_{\mathrm{S}} m_{\mathrm{D}}$, and $L_{\mathrm{RD}} = n_{\mathrm{R}} m_{\mathrm{D}}$ in quasi-static channel for the considered full diversity distributed codes.

Distributed P-STCs	k_{SD}	k_{SR}	k_{RD}	$\breve{k}_{\mathrm{SD}}$	$\breve{k}_{\mathrm{SR}}$	$\breve{k}_{\mathrm{RD}}$
$L_{\mathrm{SD}} = L_{\mathrm{RD}} = 2, L_{\mathrm{SR}} = 4$	10.14	8.62	10.08	1.25	0.54	1.26
Distributed LDPC codes	k_{SD}	k_{SR}	k_{RD}	$\breve{k}_{\mathrm{SD}}$	$\breve{k}_{\mathrm{SR}}$	$\breve{k}_{\mathrm{RD}}$
$L_{\mathrm{SD}} = L_{\mathrm{SR}} = L_{\mathrm{RD}} = 4$	16.12	16.12	16.12	1.9	1.9	1.9

Table 2.1: Values of $k_{\mathbb{L}}$ and $\breve{k}_{\mathbb{L}}$ for distributed P-STCs and LDPC codes.

2.3.1 Evaluation of Single Link Approximation

Figures 2.2- 2.7 show the behavior of the one-slope analytical approximations on each link given by (2.11), the behavior of the two-slope analyt-

[12]Binary phase shift keying
[13]Quadrature amplitude modulation

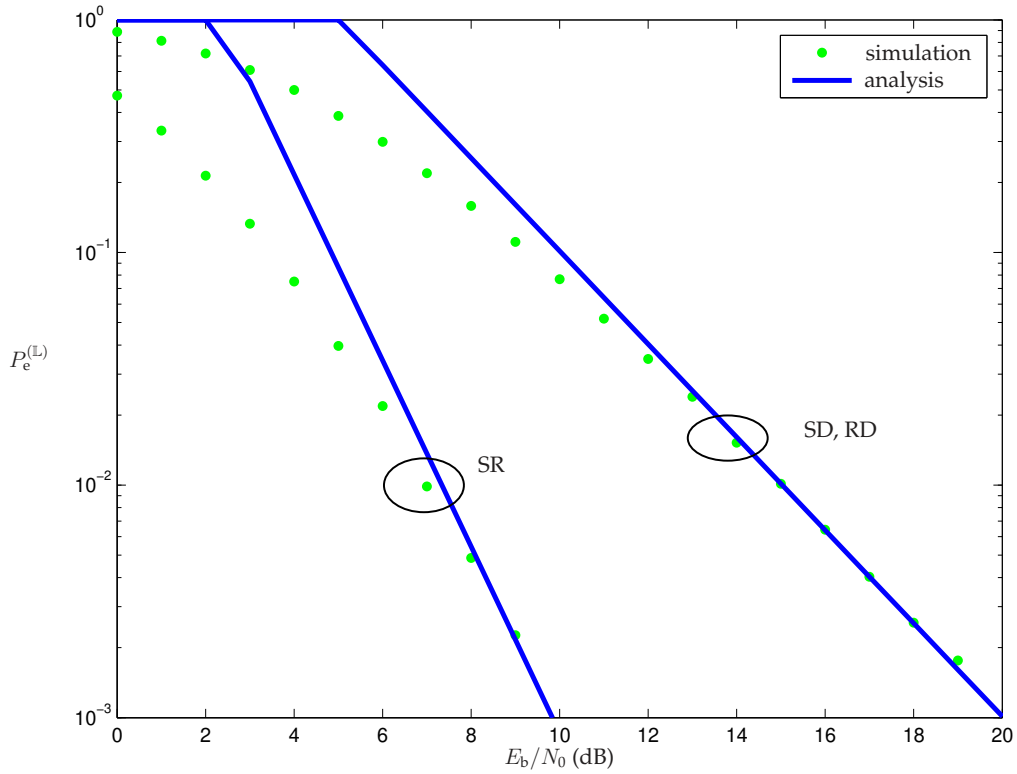

Figure 2.2: P-STCs case study. $P_e^{(\mathbb{L})}$ vs. E_b/N_0 (dB): comparison between one-slope analytical approximation (2.11) and simulation.

ical approximations on each link given by (2.12), and the approximation on $P_e^{(\mathrm{SRD})}$ given by (2.10), all compared with simulation.

In particular, Fig. 2.2 shows the behavior of the one-slope analytical approximations on each link $\mathbb{L}$ given by (2.11) as a function of E_b/N_0 (dB) for P-STC case study. Links working with the same diversity conditions (SD and RD) practically have the same performance behavior, even if they are using codes with different generators. This is the reason why the curves of $P_e^{(\mathrm{SD})}$ and $P_e^{(\mathrm{RD})}$ are coincident whereas $P_e^{(\mathrm{SR})}$ has a different behavior due to the diversity degree. As can be observed, the approximation is very good for high SNRs (i.e., $P_e^{(\mathbb{L})} < 10^{-2}$), but the distance with the simulated curve is not negligible when the SNR decreases.

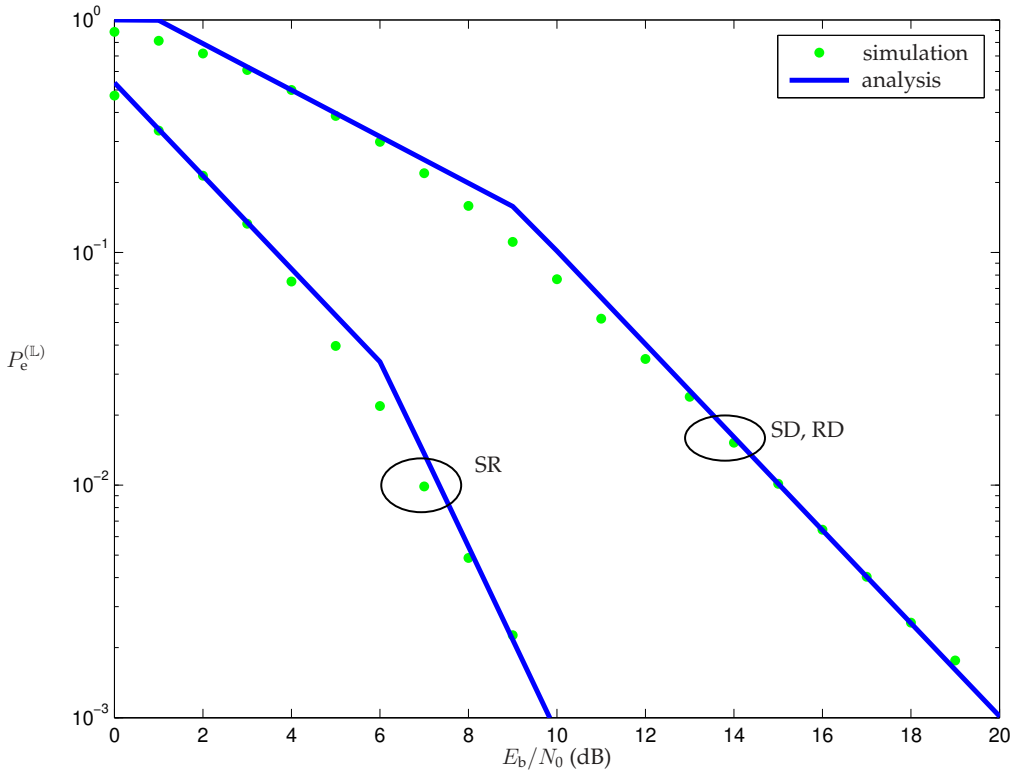

Figure 2.3: P-STCs case study. $P_e^{(\mathbb{L})}$ vs. E_b/N_0 (dB): comparison between two-slope analytical approximation (2.12) and simulation.

Figure 2.3 shows the two-slope analytical approximation on each link $\mathbb{L}$ given by (2.12) as a function of E_b/N_0 (dB) for P-STC case study. By comparing Figs. 2.2 and 2.3, the remarkable improvement given by the two-slope approximation with respect to one-slope can be observed on each link $\mathbb{L}$, especially for low SNRs, typically representing the limit of the asymptotic approximation.

Figure 2.4 shows the FEP on the composite link SRD given by (2.10) as a function of $\bar{\gamma}_{SD}$ and $\bar{\gamma}_{RD}$ for P-STC case study, and a good agreement with simulation, thus validating also the approximation on the cooperative link error probability.

Similar considerations arise from Figs. 2.5, 2.6, and 2.7 referred to the

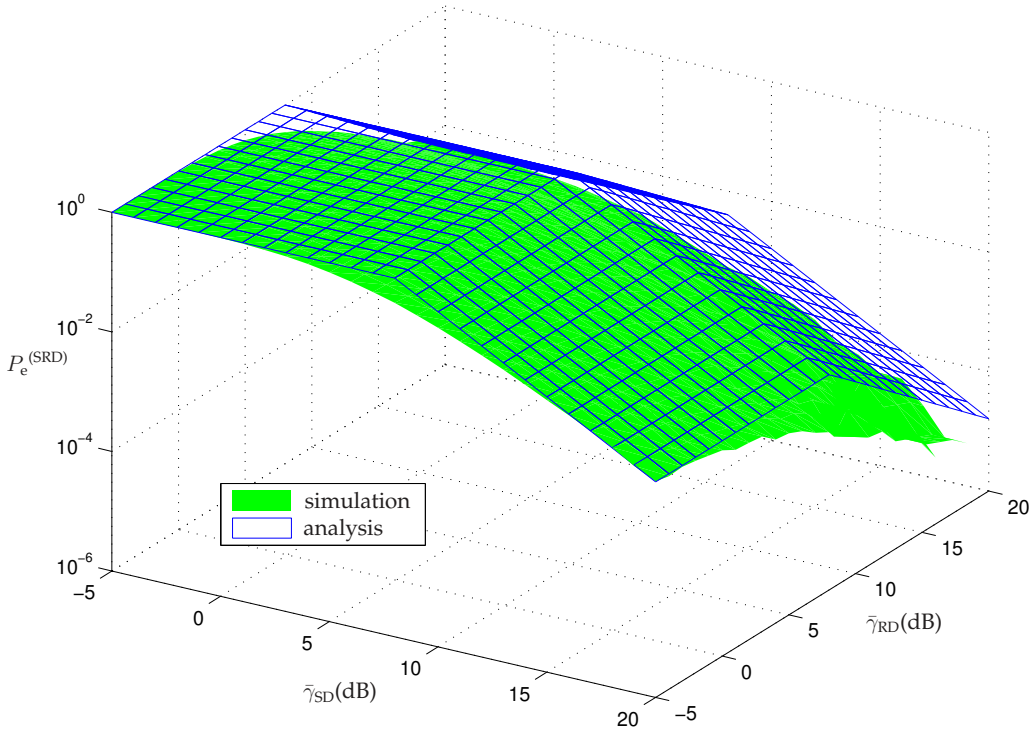

Figure 2.4: P-STCs case study. $P_e^{(SRD)}$ vs. SNR (dB) on the links SD and RD: comparison between analytical approximation (2.9) and simulation.

case study with LDPC distributed codes. As can be observed comparisons with simulation show a good agreement with the analysis also for the case study of LDPC codes. In particular, Figs. 2.5 and 2.6 highlights the validity of the asymptotical approximation given by (2.11) and (2.12), respectively, as a function of E_b/N_0 (dB) for each single link $\mathbb{L}$. In the case of distributed LDPC codes, the same diversity conditions are considered over the three links SD, SR, RD. For this reason, performance over the three links are coincident.

Figure 2.5 shows the approximation on $P_e^{(SRD)}$ given by (2.10) as a function of $\bar{\gamma}_{SD}$ and $\bar{\gamma}_{RD}$, compared with simulation.

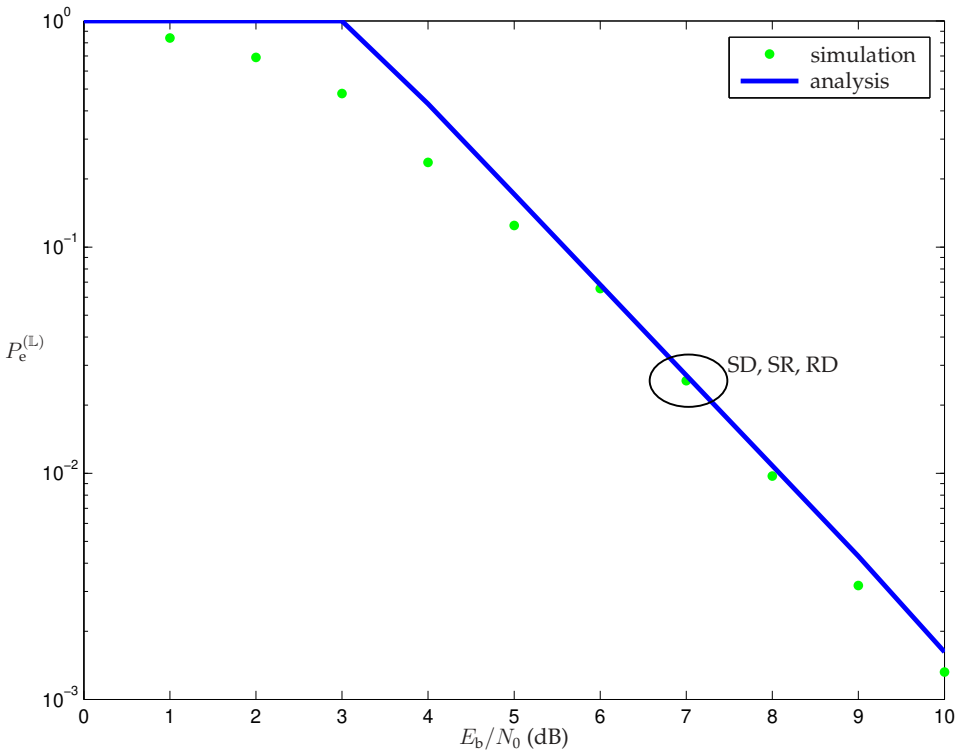

Figure 2.5: LDPC codes case study. $P_e^{(\mathbb{L})}$ vs. E_b/N_0 (dB): comparison between one-slope analytical approximation (2.11) and simulation.

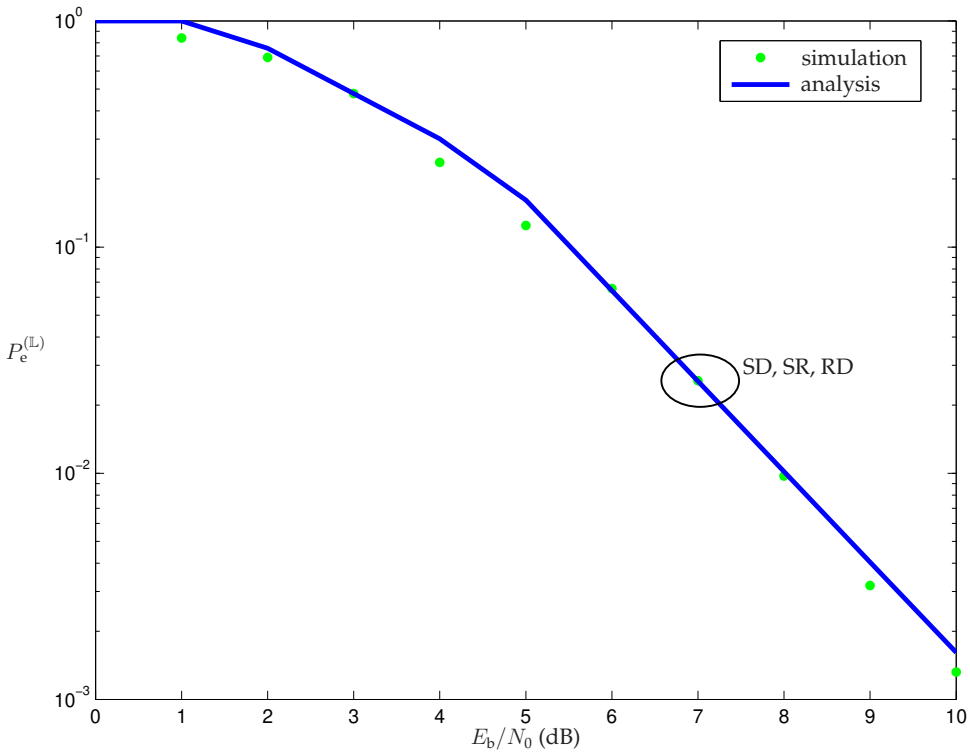

Figure 2.6: LDPC codes case study. $P_{\mathrm{e}}^{(\mathbb{L})}$ vs. E_{b}/N_0 (dB): comparison between two-slope analytical approximation (2.12) and simulation.

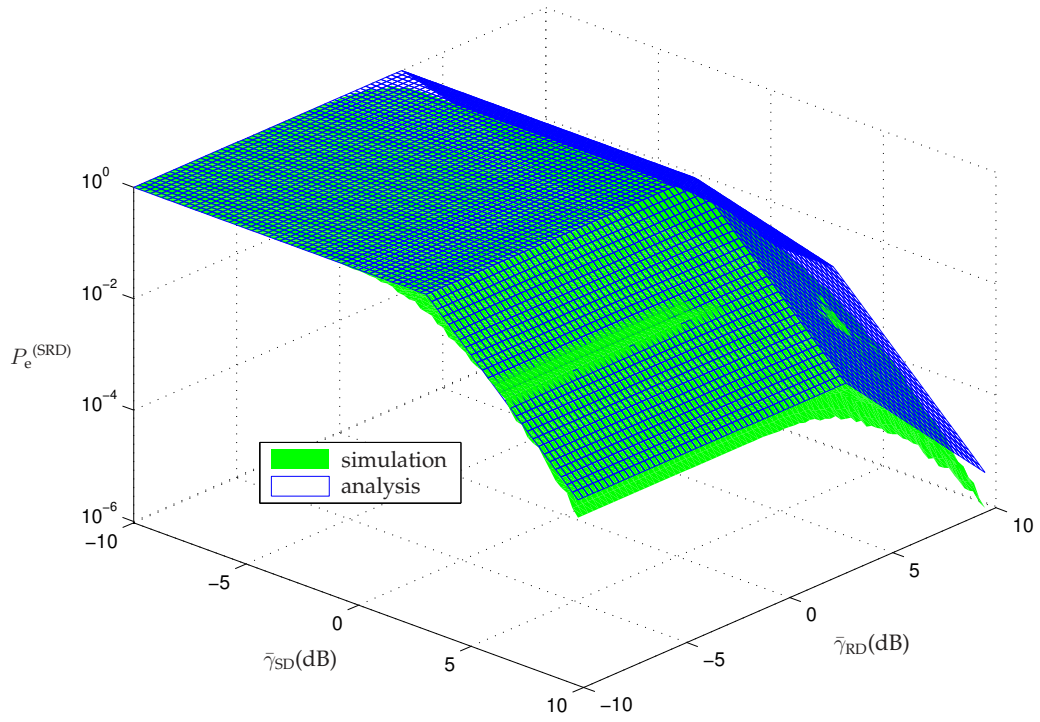

Figure 2.7: LDPC codes case study. $P_e^{(SRD)}$ vs. SNR (dB) on the links SD and RD: comparison between analytical approximation (2.9) and simulation.

2.3.2 Performance Evaluation

The FEP at the destination is evaluated through (2.6) by exploiting the approximations (2.10) and (2.11). Specifically, the parameter $k_{\mathbb{L}}$ in (2.11) is extracted from the asymptotic behavior of $g_{\mathbb{L}}(\bar{\gamma}_{\mathbb{L}})$ which is evaluated through off-line simulations of communications over link $\mathbb{L}$. This approach is validated here by comparison with simulative results for the case studies of P-STC and LDPC distributed codes.

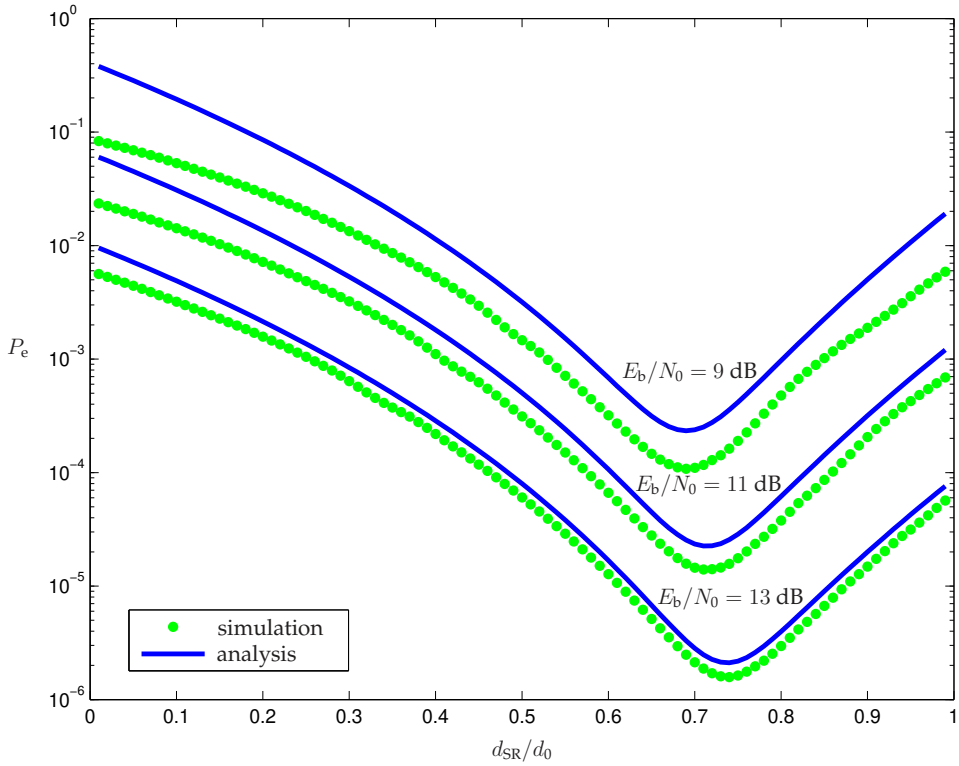

Figure 2.8: P-STCs case study: P_{e} as a function of d_{SR}/d_0 for different values of E_{b}/N_0 (dB); comparison between (2.6) and simulations.

In particular, Figs. 2.8 and 2.9 show the overall FEP as a function of normalized SR distance d_{SR}/d_0 at different values of E_{b}/N_0 (dB) when P-STC and LDPC distributed codes are employed, respectively. Simulated FEP is compared with the FEP evaluated through (2.6) by using the one-

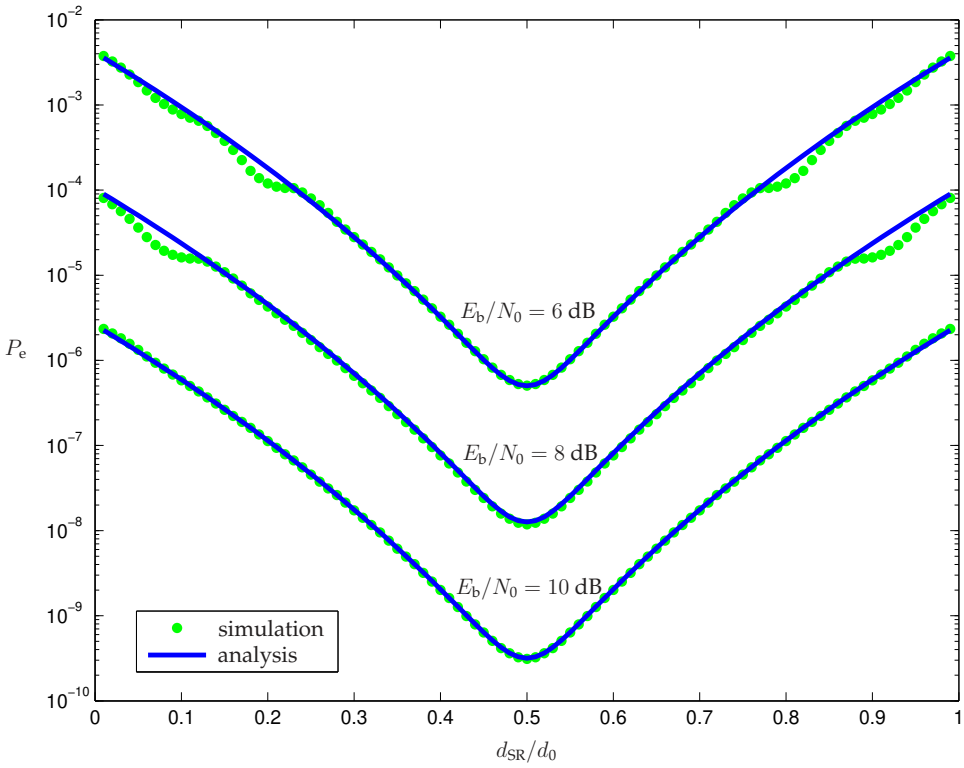

Figure 2.9: LDPC codes case study: P_e as a function of d_{SR}/d_0 for different values of E_b/N_0; comparison between (2.6) and simulations.

slope approximation (2.11) for each single link $\mathbb{L}$ and the approximation (2.10) for the composite link SRD. These figures highlight the validity of the proposed approximations at different SNRs and relay's positions, specially in providing indications of the relay's position minimizing the overall P_e.

The small gap between analysis and simulation in Fig. 2.8 is because of the one-slope approximation of the FEP on each link $\mathbb{L}$. This approximation has the advantage of allowing to simply capture the slope of the performance as a function of system parameters and propagation environment; it represents a tight approximation for values of SNRs such that $P_e^{(\mathbb{L})}$ lower than 10^{-2}.

Chapter 3

A General Model for the Evaluation of Optimal Power Allocation

COOPERATION among nodes provides a form of diversity that can be exploited to improve the performance of wireless systems [44, 51, 60]. In addition to cooperative diversity, power allocation can allow a significative energy saving for a target level of outage probability and communication rate [46, 61, 62]. This results into an increasing of research and standardization activities on relay-assisted wireless communications [63, 64].

Design and analysis of relay-assisted diversity communication systems require a clear understanding of how system configuration, propagation environment, modulation and coding scheme, power allocation, and diversity method affect the system performance. The literature on relay-assisted communications mainly covers these aspects separately. For instance, relaying techniques and communication protocols are proposed in [45, 47, 49, 65, 66]; adaptive modulation schemes are assessed in [67–69]; distributed coding methods are evaluated in [44, 51, 53, 60, 70–72]; and diversity methods are devised in [41, 50, 73, 74]. In addition, distributed

power allocation techniques between the source and the relays are analyzed in [54,75–77].

This chapter provides a simple and general framework for design and analysis of relay-assisted diversity communications with various system configuration [1]. Specifically, the key contributions of the chapter can be summarized as follows:

- proposal of new FEP-optimal power allocation technique and comparison with destination-balanced, relay-balanced, and uniform power allocation techniques under a common setting.
- evaluation of the performance for several power allocation techniques, thus identifying the most convenient on the basis of the scenario and the relay position.

As case studies the proposed methodology is applied to evaluate the performance of relay-assisted diversity communication systems employing two kinds of distributed coding: P-STCs [55] and LDPC codes [56]. Results provide the essence of how to exploit all forms of diversity based on nodes positions, links characteristics, and power allocation.

This chapter exploits models and assumptions related to the relay system, the cooperative channels, and the received signals described in Section 2.1. Furthermore, all the following considerations are developing starting from the analysis introduced in Section 2.2. The reminder of the chapter is organized as follows. Section 3.1 introduces different power allocation techniques. Section 3.2 analyzes the new FEP-optimal power allocation technique and Section 3.3 provides results for two case studies.

3.1 Power Allocation Techniques

POWER allocation is extremely important in relay-assisted communications. Several power allocation techniques for relay-assisted networks are present in the literature (see, e.g., [54, 61]). A new power allocation technique, namely FEP-optimal power allocation, is proposed and its performance is compared with that of other power allocation techniques, such as destination-balanced (D-balanced), relay-balanced (R-balanced), and uniform power allocation.

The techniques used as benchmarks are summarized below.

3.1.1 Uniform Power Allocation

The power allocation to the source and the relay is adjusted so that the two nodes transmit with the same energy per symbol. Hence, independently of the relay position, the portion x_{S} of transmitted energy per symbol at the source is equal to the portion x_{R} of transmitted energy per symbol at the relay. In other words, the power allocation is given by

$$x_{\mathrm{S}} = x_{\mathrm{R}} = 1\,. \tag{3.1}$$

3.1.2 Destination-Balanced Power Allocation

The power is allocated to the source and the relay so that the average received power at the destination from source and relay is the same, that is $\bar{\gamma}_{\mathrm{SD}} = \bar{\gamma}_{\mathrm{RD}}$. Hence, the portion x_{S} of transmitted energy per symbol at the source depends on the relay position as

$$x_{\mathrm{S}} = \frac{\Delta_{\mathrm{RD}}}{a_{\mathrm{R}}\Delta_{\mathrm{SD}} + a_{\mathrm{S}}\Delta_{\mathrm{RD}}}\,. \tag{3.2}$$

At the relay, from (2.2) and (3.2), x_{R} becomes

$$x_{\mathrm{R}} = \frac{\Delta_{\mathrm{SD}}}{a_{\mathrm{R}}\Delta_{\mathrm{SD}} + a_{\mathrm{S}}\Delta_{\mathrm{RD}}}\,. \tag{3.3}$$

3.1.3 Relay-Balanced Power Allocation

The power is allocated to the source and the relay so that the average received power at the relay and at the destination is the same, that is $\bar{\gamma}_{\mathrm{SR}} = \bar{\gamma}_{\mathrm{RD}}$. Hence, the portion x_{S} of transmitted energy per symbol at the source depends on the relay position as

$$x_{\mathrm{S}} = \frac{\Delta_{\mathrm{RD}}}{a_{\mathrm{R}}\Delta_{\mathrm{SR}} + a_{\mathrm{S}}\Delta_{\mathrm{RD}}}\,. \tag{3.4}$$

At the relay, from (2.2) and (3.4), x_{R} becomes

$$x_{\mathrm{R}} = \frac{\Delta_{\mathrm{SR}}}{a_{\mathrm{R}}\Delta_{\mathrm{SR}} + a_{\mathrm{S}}\Delta_{\mathrm{RD}}}\,. \tag{3.5}$$

3.1.4 FEP-Optimal Power Allocation

The new FEP-optimal power allocation is determined by evaluating the values of x_{S} and x_{R} that minimize the FEP at the destination in (2.6) as a function of the relay position and system configuration. Specifically, it can be determined by

$$(x_{\mathrm{S}}^{\star}, x_{\mathrm{R}}^{\star}) = \underset{(x_{\mathrm{S}},x_{\mathrm{R}})\in\mathcal{X}}{\arg\min}\, P_{\mathrm{e}}(x_{\mathrm{S}}, x_{\mathrm{R}}, \bar{\gamma}) \tag{3.6}$$

where $\mathcal{X} = \{x_1, x_2 \text{ s.t. } a_{\mathrm{S}}x_1 + a_{\mathrm{R}}x_2 = 1 \text{ and } x_1, x_2 \geq 0\}$ and $P_{\mathrm{e}} = P_{\mathrm{e}}(x_{\mathrm{S}}, x_{\mathrm{R}}, \bar{\gamma})$ is the expression obtained from (2.6), (2.7), (4.6), and (2.9). In the Section 3.2 some closed form approximated solutions of (3.6) are proposed. These solutions are based on the analytical model for the FEP at the destination derived in Section 2.2, which includes the dependence on the allocated power, system setting, and propagation conditions.

3.2 FEP-Optimal Power Allocation

In this Section, the values of $x_{\mathrm{S}}^{\star}$ and $x_{\mathrm{R}}^{\star}$ minimizing the FEP at the destination solving (3.6) are derived. From (2.6), (2.7), (4.6), and (2.9), it is possible write the FEP as

$$\begin{aligned} P_{\mathrm{e}}(x_{\mathrm{S}}, x_{\mathrm{R}}, \bar{\gamma}) &= g_{\mathrm{SD}}\left(\bar{\gamma}_{\mathrm{SD}}\right) g_{\mathrm{SR}}\left(\bar{\gamma}_{\mathrm{SR}}\right) + g_{\mathrm{SRD}}\left(\bar{\gamma}_{\mathrm{SD}}, \bar{\gamma}_{\mathrm{RD}}\right)\left[1 - g_{\mathrm{SR}}\left(\bar{\gamma}_{\mathrm{SR}}\right)\right] \\ &= g_{\mathrm{SD}}(x_{\mathrm{S}}\Delta_{\mathrm{SD}}\bar{\gamma}) g_{\mathrm{SR}}(x_{\mathrm{S}}\Delta_{\mathrm{SR}}\bar{\gamma}) \\ &\quad + g_{\mathrm{SRD}}(x_{\mathrm{S}}\Delta_{\mathrm{SD}}\bar{\gamma}, x_{\mathrm{R}}\Delta_{\mathrm{RD}}\bar{\gamma})\left[1 - g_{\mathrm{SR}}(x_{\mathrm{S}}\Delta_{\mathrm{SR}}\bar{\gamma})\right] . \end{aligned} \tag{3.7}$$

Even if the FEP can be analytically evaluated using approximations in (2.10) and (2.11), it is still difficult to find closed-form solution for problem (3.6). For this reason, two simple closed-form approximations of (3.6), denoted as $\tilde{x}_{\mathrm{S}}$ and $\tilde{x}_{\mathrm{R}}$, are proposed. These solutions are based on the analytical model for the FEP at the destination derived in Section 2.2, which includes the dependence on the allocated power, system setting, and propagation conditions. They hold for sufficiently large values of $\bar{\gamma}$ and are applicable, without significant errors, in a large range of operating conditions. Specifically, in (3.7) the following expression for $g_{\mathbb{L}}(\cdot)$ is used

$$g_{\mathbb{L}}(\bar{\gamma}_{\mathbb{L}}) \simeq \frac{k_{\mathbb{L}}}{\bar{\gamma}_{\mathbb{L}}^{L_{\mathbb{L}}}} \tag{3.8}$$

that holds when $k_{\mathbb{L}}/\bar{\gamma}_{\mathbb{L}}^{L_{\mathbb{L}}} \leq a_{\mathbb{L}}$ and $a_{\mathbb{L}} = 1$. Thus

$$\begin{cases} x_{\mathrm{S}}\Delta_{\mathrm{SD}}\bar{\gamma} \geq {k_{\mathrm{SD}}}^{1/L_{\mathrm{SD}}} \\ x_{\mathrm{S}}\Delta_{\mathrm{SR}}\bar{\gamma} \geq {k_{\mathrm{SR}}}^{1/L_{\mathrm{SR}}} \\ x_{\mathrm{R}}\Delta_{\mathrm{RD}}\bar{\gamma} \geq {k_{\mathrm{RD}}}^{1/L_{\mathrm{RD}}} . \end{cases} \tag{3.9}$$

Consequently, $\tilde{x}_{\mathrm{S}} \in [x_{\mathrm{L}}, x_{\mathrm{H}}]$ and $\tilde{x}_{\mathrm{R}} \in [(1 - a_{\mathrm{S}}x_{\mathrm{H}})/a_{\mathrm{R}}, (1 - a_{\mathrm{S}}x_{\mathrm{L}})/a_{\mathrm{R}}]$, where

$$x_{\mathrm{L}} = \max\left\{ \frac{{k_{\mathrm{SR}}}^{\frac{1}{L_{\mathrm{SR}}}}}{\Delta_{\mathrm{SR}}\bar{\gamma}}, \frac{{k_{\mathrm{SD}}}^{\frac{1}{L_{\mathrm{SD}}}}}{\Delta_{\mathrm{SD}}\bar{\gamma}} \right\} \tag{3.10}$$

$$x_{\mathrm{H}} = \frac{1}{a_{\mathrm{S}}}\left(1 - \frac{a_{\mathrm{R}}{k_{\mathrm{RD}}}^{\frac{1}{L_{\mathrm{RD}}}}}{\Delta_{\mathrm{RD}}\bar{\gamma}}\right) . \tag{3.11}$$

Note that, for high $\bar{\gamma}$, x_{L} approaches 0 and x_{H} approaches $1/a_{\mathrm{S}}$. Therefore, from (2.10) and (2.11) the FEP in (3.7) becomes

$$P_{\mathrm{e}} \simeq g_{\mathrm{SD}}(y_{\mathrm{S}}\Delta_{\mathrm{SD}})g_{\mathrm{SR}}(y_{\mathrm{S}}\Delta_{\mathrm{SR}}) + g_{\mathrm{SD}}(y_{\mathrm{S}}\Delta_{\mathrm{SD}})g_{\mathrm{RD}}\left(\frac{\bar{\gamma}-a_{\mathrm{S}}y_{\mathrm{S}}}{a_{\mathrm{R}}}\Delta_{\mathrm{RD}}\right) \times [1-g_{\mathrm{SR}}(y_{\mathrm{S}}\Delta_{\mathrm{SR}})] \tag{3.12}$$

where $y_{\mathrm{S}} \triangleq x_{\mathrm{S}}\bar{\gamma}$.

Since P_{e} is a continuous function of x_{S}, the optimal value of x_{S} can be determined from the derivative of P_{e} in (3.12) with respect to y_{S}, which is given by

$$\begin{aligned} P_{\mathrm{e}}{}' = \frac{dP_{\mathrm{e}}}{dy_{\mathrm{S}}} &= g'_{\mathrm{SD}}(y_{\mathrm{S}}\Delta_{\mathrm{SD}})\Delta_{\mathrm{SD}}g_{\mathrm{SR}}(y_{\mathrm{S}}\Delta_{\mathrm{SR}}) + g_{\mathrm{SD}}(y_{\mathrm{S}}\Delta_{\mathrm{SD}})g'_{\mathrm{SR}}(y_{\mathrm{S}}\Delta_{\mathrm{SR}})\Delta_{\mathrm{SR}} \\ &\quad + g'_{\mathrm{SD}}(y_{\mathrm{S}}\Delta_{\mathrm{SD}})\Delta_{\mathrm{SD}}g_{\mathrm{RD}}\left(\frac{\bar{\gamma}-a_{\mathrm{S}}y_{\mathrm{S}}}{a_{\mathrm{R}}}\Delta_{\mathrm{RD}}\right)[1-g_{\mathrm{SR}}(y_{\mathrm{S}}\Delta_{\mathrm{SR}})] \\ &\quad - g'_{\mathrm{SR}}(y_{\mathrm{S}}\Delta_{\mathrm{SR}})\Delta_{\mathrm{SR}}g_{\mathrm{SD}}(y_{\mathrm{S}}\Delta_{\mathrm{SD}})g_{\mathrm{RD}}\left(\frac{\bar{\gamma}-a_{\mathrm{S}}y_{\mathrm{S}}}{a_{\mathrm{R}}}\Delta_{\mathrm{RD}}\right) \\ &\quad - g'_{\mathrm{RD}}\left(\frac{\bar{\gamma}-a_{\mathrm{S}}y_{\mathrm{S}}}{a_{\mathrm{R}}}\Delta_{\mathrm{RD}}\right)\frac{a_{\mathrm{S}}}{a_{\mathrm{R}}}\Delta_{\mathrm{RD}}g_{\mathrm{SD}}(y_{\mathrm{S}}\Delta_{\mathrm{SD}})\,[1-g_{\mathrm{SR}}(y_{\mathrm{S}}\Delta_{\mathrm{SR}})] \end{aligned} \tag{3.13}$$

where $g'_{\mathbb{L}}(\bar{\gamma}_{\mathbb{L}}) = -k_{\mathbb{L}}L_{\mathbb{L}}/\bar{\gamma}_{\mathbb{L}}^{L_{\mathbb{L}}+1}$.

The value of $\tilde{x}_{\mathrm{S}}$ is then found among the roots of (3.13); after simple mathematical manipulation it is possible write

$$\begin{aligned} &- {y_{\mathrm{S}}}^{-1}L_{\mathrm{SD}}\left\{\frac{k_{\mathrm{SR}}}{(y_{\mathrm{S}}\Delta_{\mathrm{SR}})^{L_{\mathrm{SR}}}} + \frac{k_{\mathrm{RD}}}{\left[\left(\frac{\bar{\gamma}-a_{\mathrm{S}}y_{\mathrm{S}}}{a_{\mathrm{R}}}\right)\Delta_{\mathrm{RD}}\right]^{L_{\mathrm{RD}}}}\left[1-\frac{k_{\mathrm{SR}}}{(y_{\mathrm{S}}\Delta_{\mathrm{SR}})^{L_{\mathrm{SR}}}}\right]\right\} \\ &- \frac{k_{\mathrm{SR}}}{(y_{\mathrm{S}}\Delta_{\mathrm{SR}})^{L_{\mathrm{SR}}}}L_{\mathrm{SR}}{y_{\mathrm{S}}}^{-1}\left\{1-\frac{k_{\mathrm{RD}}}{\left[\left(\frac{\bar{\gamma}-a_{\mathrm{S}}y_{\mathrm{S}}}{a_{\mathrm{R}}}\right)\Delta_{\mathrm{RD}}\right]^{L_{\mathrm{RD}}}}\right\} + \frac{k_{\mathrm{RD}}}{\left[\left(\frac{\bar{\gamma}-a_{\mathrm{S}}y_{\mathrm{S}}}{a_{\mathrm{R}}}\right)\Delta_{\mathrm{RD}}\right]^{L_{\mathrm{RD}}}} \\ &\times \left[1-\frac{k_{\mathrm{SR}}}{(y_{\mathrm{S}}\Delta_{\mathrm{SR}})^{L_{\mathrm{SR}}}}\right]L_{\mathrm{RD}}\left(\frac{\bar{\gamma}-a_{\mathrm{S}}y_{\mathrm{S}}}{a_{\mathrm{R}}}\right)^{-1}\rho = 0\,. \end{aligned} \tag{3.14}$$

By defining $\xi_{\mathrm{SR}} \triangleq k_{\mathrm{SR}}/(y_{\mathrm{S}}\Delta_{\mathrm{SR}})^{L_{\mathrm{SR}}}$, (3.14) becomes

$$\frac{k_{\mathrm{SR}}}{k_{\mathrm{RD}}}\left(L_{\mathrm{SD}}+L_{\mathrm{SR}}\right)\frac{\Delta_{\mathrm{RD}}^{L_{\mathrm{RD}}}}{\Delta_{\mathrm{SR}}^{L_{\mathrm{SR}}}} = \frac{{y_{\mathrm{S}}}^{L_{\mathrm{SR}}}}{\left(\frac{\bar{\gamma}-a_{\mathrm{S}}y_{\mathrm{S}}}{a_{\mathrm{R}}}\right)^{L_{\mathrm{RD}}}} \times\left[\frac{L_{\mathrm{RD}}y_{\mathrm{S}}(1-\xi_{\mathrm{SR}})\rho}{\frac{\bar{\gamma}-a_{\mathrm{S}}y_{\mathrm{S}}}{a_{\mathrm{R}}}}-L_{\mathrm{SD}}(1-\xi_{\mathrm{SR}})+L_{\mathrm{SR}}\xi_{\mathrm{SR}}\right]. \tag{3.15}$$

From the definition of y_{S} and from (2.2), equation (3.15) results in

$$\frac{k_{\mathrm{SR}}}{k_{\mathrm{RD}}}\frac{L_{\mathrm{SD}}+L_{\mathrm{SR}}}{L_{\mathrm{RD}}}\frac{1}{1-\xi_{\mathrm{SR}}}\frac{\Delta_{\mathrm{RD}}^{L_{\mathrm{RD}}}}{\Delta_{\mathrm{SR}}^{L_{\mathrm{SR}}}} = \bar{\gamma}^{(L_{\mathrm{SR}}-L_{\mathrm{RD}})}\frac{{x_{\mathrm{S}}}^{L_{\mathrm{SR}}}}{{x_{\mathrm{R}}}^{L_{\mathrm{RD}}}} \times\left(\rho\frac{x_{\mathrm{S}}}{x_{\mathrm{R}}}-\frac{L_{\mathrm{SD}}}{L_{\mathrm{RD}}}+\frac{L_{\mathrm{SR}}}{L_{\mathrm{RD}}}\frac{\xi_{\mathrm{SR}}}{1-\xi_{\mathrm{SR}}}\right). \tag{3.16}$$

Note that $\xi_{\mathrm{SR}} \ll 1$ for high values of $\bar{\gamma}$, from which it is possible determine an approximated solution of (3.16) as given by

$$\frac{k_{\mathrm{SR}}}{k_{\mathrm{RD}}}\frac{L_{\mathrm{SD}}+L_{\mathrm{SR}}}{L_{\mathrm{RD}}}\frac{\Delta_{\mathrm{RD}}^{L_{\mathrm{RD}}}}{\Delta_{\mathrm{SR}}^{L_{\mathrm{SR}}}} = \bar{\gamma}^{(L_{\mathrm{SR}}-L_{\mathrm{RD}})}\frac{{x_{\mathrm{S}}}^{L_{\mathrm{SR}}}}{{x_{\mathrm{R}}}^{L_{\mathrm{RD}}}}\left(\rho\frac{x_{\mathrm{S}}}{x_{\mathrm{R}}}-\frac{L_{\mathrm{SD}}}{L_{\mathrm{RD}}}\right). \tag{3.17}$$

For single antenna links ($L_{\mathrm{SD}} = L_{\mathrm{SR}} = L_{\mathrm{RD}} = 1$) with quasi-static fading channel, (3.17) reduces to

$$2\frac{k_{\mathrm{SR}}}{k_{\mathrm{RD}}}\frac{\Delta_{\mathrm{RD}}}{\Delta_{\mathrm{SR}}} = \frac{x_{\mathrm{S}}}{x_{\mathrm{R}}}\left(\rho\frac{x_{\mathrm{S}}}{x_{\mathrm{R}}}-1\right) \tag{3.18}$$

and its solution results in closed form as

$$\frac{\tilde{x}_{\mathrm{S}}}{\tilde{x}_{\mathrm{R}}} = \frac{1}{2\rho}\left(1+\sqrt{1+8\rho\frac{k_{\mathrm{SR}}}{k_{\mathrm{RD}}}\frac{\Delta_{\mathrm{RD}}}{\Delta_{\mathrm{SR}}}}\right). \tag{3.19}$$

To solve (3.17) for the generic diversity case, the parameter $z \geq 0$ is defined as

$$z \triangleq \frac{k_{\mathrm{SR}}}{k_{\mathrm{RD}}}\frac{L_{\mathrm{SD}}+L_{\mathrm{SR}}}{L_{\mathrm{RD}}}\frac{\Delta_{\mathrm{RD}}^{L_{\mathrm{RD}}}}{\Delta_{\mathrm{SR}}^{L_{\mathrm{SR}}}}\frac{1}{\rho}\bar{\gamma}^{(L_{\mathrm{RD}}-L_{\mathrm{SR}})} \tag{3.20}$$

and rewritten (3.17) as

$$z = \frac{{x_{\mathrm{S}}}^{L_{\mathrm{SR}}}}{{x_{\mathrm{R}}}^{L_{\mathrm{RD}}}}\left(\frac{x_{\mathrm{S}}}{x_{\mathrm{R}}}-\frac{L_{\mathrm{SD}}}{L_{\mathrm{RD}}}\frac{1}{\rho}\right) \tag{3.21}$$

which can be easily solved numerically.

3.2.1 Asymptotic Approximation

To find simple closed-form solutions for $\tilde{x}_{\mathrm{S}}$ and $\tilde{x}_{\mathrm{R}}$, it is important to focus on asymptotic behavior of (3.21) for large and small values of z. In particular, when $z \to \infty$, (thus x_{S} approaching $1/a_{\mathrm{S}}$ and x_{R} approaching 0), (3.21) becomes

$$z \simeq \frac{{a_{\mathrm{S}}}^{-L_{\mathrm{SR}}-1}}{{x_{\mathrm{R}}}^{L_{\mathrm{RD}}+1}} \tag{3.22}$$

and consequently

$$\tilde{x}_{\mathrm{S}} \simeq \frac{1}{a_{\mathrm{S}}}\left[1 - a_{\mathrm{R}}\left(\frac{{a_{\mathrm{S}}}^{-L_{\mathrm{SR}}-1}}{z}\right)^{\frac{1}{L_{\mathrm{RD}}+1}}\right], \tag{3.23}$$

$$\tilde{x}_{\mathrm{R}} \simeq \left(\frac{{a_{\mathrm{S}}}^{-L_{\mathrm{SR}}-1}}{z}\right)^{\frac{1}{L_{\mathrm{RD}}+1}}. \tag{3.24}$$

This approximation looses validity for $z \to 0$ for which the solution of (3.21) would give

$$\tilde{x}_{\mathrm{S}} \simeq \frac{1}{a_{\mathrm{S}}}\frac{L_{\mathrm{SD}}}{L_{\mathrm{SD}} + L_{\mathrm{RD}}} \tag{3.25}$$

$$\tilde{x}_{\mathrm{R}} \simeq \frac{1}{a_{\mathrm{R}}}\frac{L_{\mathrm{RD}}}{L_{\mathrm{SD}} + L_{\mathrm{RD}}}. \tag{3.26}$$

Thus, modified allocations are proposed as

$$\tilde{x}_{\mathrm{S}} \simeq {x_{\mathrm{S}}}^{(\mathrm{as})} = \frac{1}{a_{\mathrm{S}}}\left[1 - a_{\mathrm{R}}\left(\frac{{a_{\mathrm{S}}}^{-L_{\mathrm{SR}}-1}}{z+\Lambda}\right)^{\frac{1}{L_{\mathrm{RD}}+1}}\right] \tag{3.27}$$

and

$$\tilde{x}_{\mathrm{R}} \simeq {x_{\mathrm{R}}}^{(\mathrm{as})} = \frac{1 - a_{\mathrm{S}}{x_{\mathrm{S}}}^{(\mathrm{as})}}{a_{\mathrm{R}}} \tag{3.28}$$

where Λ is a suitable constant to better approximate $\tilde{x}_{\mathrm{S}}$ behavior also for $z \to 0$. Note that for $z \to \infty$, (3.27) has the same behavior of $\tilde{x}_{\mathrm{S}}$ in (3.23), whereas when $z \to 0$ it gives a constant value that depends on Λ. The value of Λ is determined so that $\tilde{x}_{\mathrm{S}}$ approaches $(L_{\mathrm{SD}}/a_{\mathrm{S}})/(L_{\mathrm{SD}} + L_{\mathrm{RD}})$ for $z \to 0$, resulting in

$$\Lambda = {a_{\mathrm{R}}}^{L_{\mathrm{RD}}+1}{a_{\mathrm{S}}}^{-L_{\mathrm{SR}}-1}\left(1 + \frac{L_{\mathrm{SD}}}{L_{\mathrm{RD}}}\right)^{L_{\mathrm{RD}}+1}.$$

This approximated solution looses accuracy for intermediate values of z. Then, in the following section a local solution is proposed, which is valid in the range where (3.27) deviates.

3.2.2 Local Approximation

This section proposes a local approximation for the solution of (3.21) that holds for intermediate values of z, more precisely for x_{R} around $\eta = L_{\mathrm{RD}}/[2a_{\mathrm{R}}(L_{\mathrm{RD}} + L_{\mathrm{SD}})]$. When $x_{\mathrm{R}} = \eta$, $x_{\mathrm{S}} = (1 - a_{\mathrm{R}}\eta)/a_{\mathrm{S}}$ is obtained from (2.2), and $x_{\mathrm{S}}/x_{\mathrm{R}} = (2L_{\mathrm{SD}} + L_{\mathrm{RD}})/\rho L_{\mathrm{RD}}$. The corresponding value of z is given from (3.21) as

$$z = \frac{(1 - a_{\mathrm{R}}\eta)^{L_{\mathrm{SR}}}}{{a_{\mathrm{S}}}^{L_{\mathrm{SR}}}\eta^{L_{\mathrm{RD}}}} \frac{L_{\mathrm{SD}} + L_{\mathrm{RD}}}{\rho L_{\mathrm{RD}}} \,. \tag{3.29}$$

The local approximation is obtained by taking the natural logarithm of (3.21) and then by replacing the right-hand side with its first order approximation around the point $x_{\mathrm{S}} \simeq (1 - a_{\mathrm{R}}\eta)/a_{\mathrm{S}}$ and $x_{\mathrm{R}} \simeq \eta$. The natural logarithm of (3.21) is

$$\ln z = L_{\mathrm{SR}} \ln x_{\mathrm{S}} - L_{\mathrm{RD}} \ln x_{\mathrm{R}} + \ln\left(x_{\mathrm{S}} - \frac{L_{\mathrm{SD}}}{\rho L_{\mathrm{RD}}} x_{\mathrm{R}}\right) - \ln x_{\mathrm{R}} \,. \tag{3.30}$$

The first order approximation of $\ln x$ around a point x_0 is $\ln x_0 - 1 + x/x_0$. Therefore, after simple mathematical manipulations the first order approximation of (3.30) can be written as

$$\begin{aligned} \ln z \simeq\ & L_{\mathrm{RD}} - L_{\mathrm{SR}} + \frac{L_{\mathrm{SR}}}{1 - a_{\mathrm{R}}\eta} - \ln(2a_{\mathrm{S}}) + L_{\mathrm{SR}} \ln\left(\frac{1 - a_{\mathrm{R}}\eta}{a_{\mathrm{S}}}\right) + 2 \\ & -(L_{\mathrm{RD}} + 1)\ln(\eta) - x_{\mathrm{R}}\left(\frac{2}{\eta} + \frac{L_{\mathrm{RD}}}{\eta} + \frac{a_{\mathrm{R}} L_{\mathrm{SR}}}{1 - a_{\mathrm{R}}\eta}\right) \end{aligned} \tag{3.31}$$

from which

$$\begin{aligned} \tilde{x}_{\mathrm{S}} \simeq x_{\mathrm{S}}^{(\mathrm{loc})} = \frac{1}{a_{\mathrm{S}}} & + \frac{\ln z - L_{\mathrm{RD}} + L_{\mathrm{SR}} - 2 + \ln(2a_{\mathrm{S}}) - \frac{L_{\mathrm{SR}}}{1 - a_{\mathrm{R}}\eta}}{\rho\left(\frac{2}{\eta} + \frac{L_{\mathrm{RD}}}{\eta} + \frac{a_{\mathrm{R}} L_{\mathrm{SR}}}{1 - a_{\mathrm{R}}\eta}\right)} \\ & - \frac{L_{\mathrm{SR}} \ln\left(\frac{1 - a_{\mathrm{R}}\eta}{a_{\mathrm{S}}}\right) - (L_{\mathrm{RD}} + 1)\ln(\eta)}{\rho\left(\frac{2}{\eta} + \frac{L_{\mathrm{RD}}}{\eta} + \frac{a_{\mathrm{R}} L_{\mathrm{SR}}}{1 - a_{\mathrm{R}}\eta}\right)} \,. \end{aligned} \tag{3.32}$$

3.3 Numerical Results

In this section results related to power allocation and FEP in various system configurations are provided. Specially, the three-node relay-assisted system, described in Chapter 2, is considered with distances normalized to $d_0 = d_{\mathrm{SD}}$, path loss exponent $\beta = 3.5$, and two transmission phases of equal duration ($N_{\mathrm{S}} = N_{\mathrm{R}}$) with $a_{\mathrm{S}} = a_{\mathrm{R}} = 1/2$.
The two case studies described in Section 2.3 are considered, employing distributed P-STCs [53] and distributed LDPC codes [59]. The results are provided for two scenarios:

- one-dimensional scenario with the relay placed in a segment between S and D;
- bi-dimensional scenario with the relay moving on a plane, with S at (0,0) and D at (d_0,0) coordinates.

3.3.1 One-Dimensional Scenario

Figures 3.1 and 3.2 show the portion x_{S} of power allocated as a function of the normalized distance d_{SR}/d_0 for P-STC at $E_{\mathrm{b}}/N_0 = 13$ dB and LDPC codes at $E_{\mathrm{b}}/N_0 = 6$ dB, respectively, with different power allocation techniques.[1] From these figures, it can be observed how the power is allocated between the source and the relay. In the case of uniform allocation, the source and relay transmit with the same power and x_{S} is constant and equal to 1 independently on the distance. For all the other power allocation techniques, x_{S} increases when the relay moves from the source to the destination, as expected. In particular, in case of D-balanced power allocation, x_{S} assumes the higher values; in fact, the power allocated to the source has to be high enough to guarantee $\bar{\gamma}_{\mathrm{SD}} = \bar{\gamma}_{\mathrm{RD}}$. Opposite is the behavior of R-balanced, where x_{S} has to be allocated so that $\bar{\gamma}_{\mathrm{SR}} = \bar{\gamma}_{\mathrm{RD}}$:

[1] These two values of SNR provide similar performance for the two distributed coding techniques.

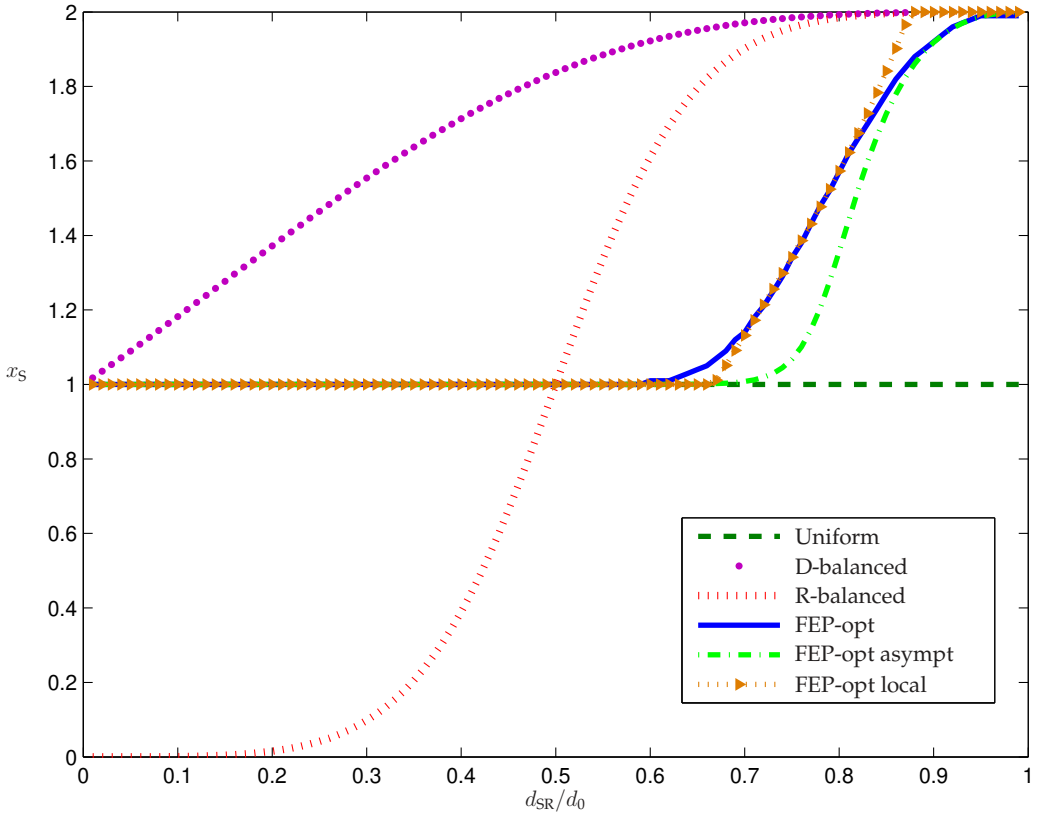

Figure 3.1: P-STCs case study: portion x_S of power allocated to the source as a function of d_{SR}/d_0 at $E_b/N_0 = 13$ dB. Comparison among different power allocation techniques.

in this case $x_S \simeq 0$ when the relay is near to the source and $x_S = x_R = 1$ when the relay is exactly at half way between the source and the destination. In the considered case, FEP-optimal behaves as uniform power allocation when the relay is near to the source because $g_{SRD}\left(\bar{\gamma}_{SD}, \bar{\gamma}_{RD}\right) \simeq k_{SRD}\, g_{SD}\left(\bar{\gamma}_{SD}\right) g_{RD}\left(\bar{\gamma}_{RD}\right)$ and same diversity on the SD and RD links. When the relay moves toward the destination, x_S increases as per the FEP minimization as given by new (3.7). Note that, power allocation significantly impacts the FEP. Focusing on FEP-optimal power allocation, one can compare the numerical solution of (3.6) with the asymptotical approximation (3.27) and the local approximation (3.32). It can be observed that the

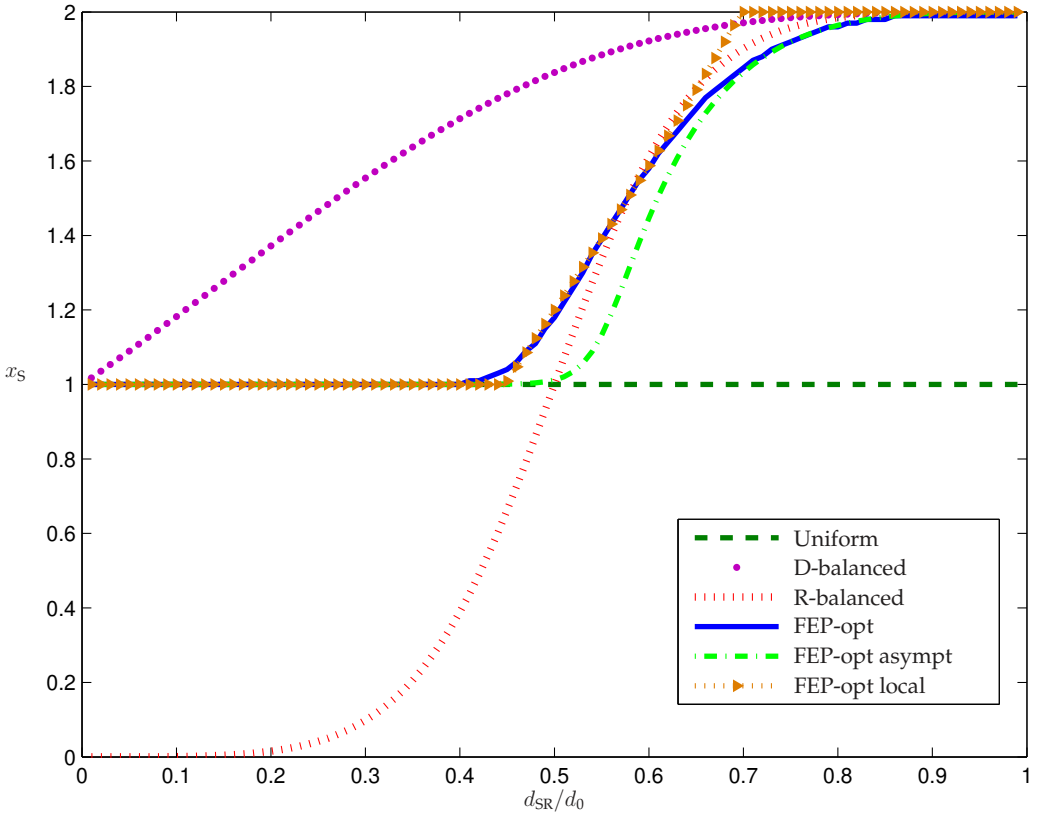

Figure 3.2: LDPC codes case study: portion x_S of power allocated to the source as a function of d_{SR}/d_0 at $E_b/N_0 = 6$ dB. Comparison among different power allocation techniques.

asymptotical approximation (3.27) provides a good approximation when the relay approaches the source or the destination, whereas for some intermediate relay positions (i.e., d_{SR}/d_0 in the range [0.65, 0.85] for P-STCs in Fig. 3.1 and d_{SR}/d_0 in the range [0.4, 0.65] for LDPC codes in Fig. 3.2), the local approximation (3.32) is more tight to (3.6). Note that, power allocation significantly impacts the FEP.

These considerations on power allocations, in fact, translate on the behaviors of the curves presented in Figs. 3.3 and 3.4, where the overall FEP is plotted as a function of d_{SR}/d_0 with different power allocation techniques for P-STCs at $E_b/N_0 = 13$ dB and LDPC codes at $E_b/N_0 = 6$ dB, re-

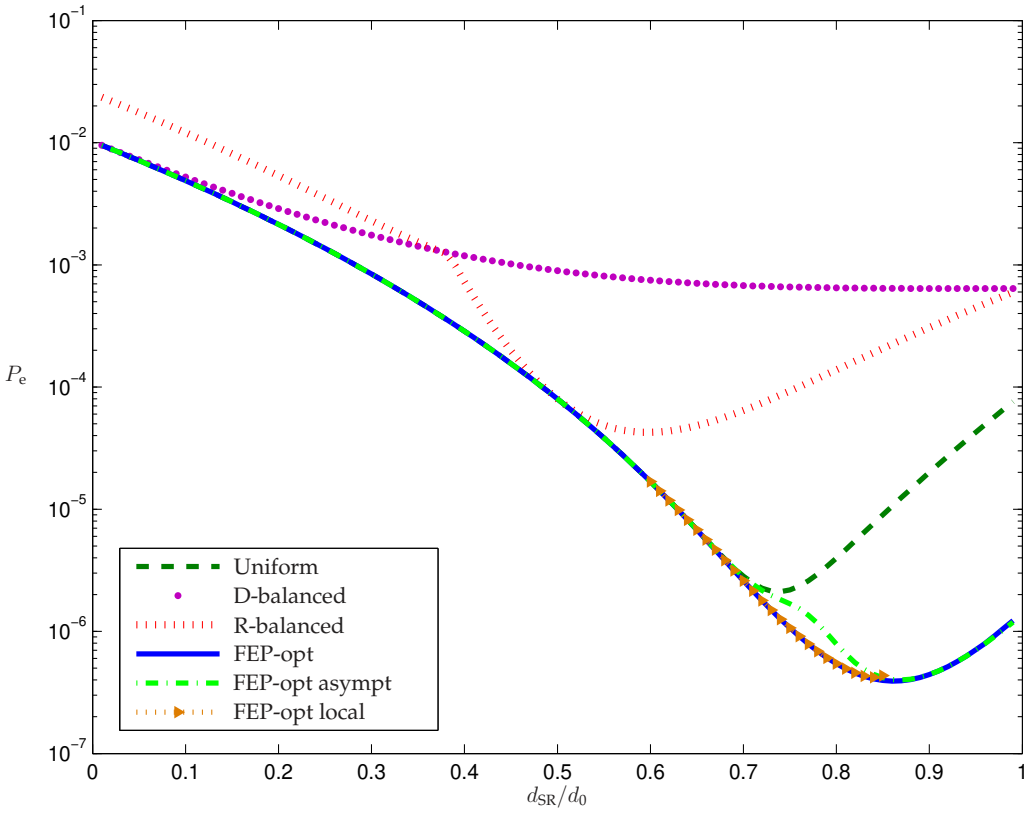

Figure 3.3: P-STCs case study: P_e as a function of d_{SR}/d_0 at $E_b/N_0 = 13$ dB. Comparison among different power allocation techniques.

spectively. In fact, FEP-optimal has the same behavior of uniform power allocation when the relay is near to the source and always outperforms the other power allocation techniques as expected. D-balanced gives the worst performance and R-balanced power allocation performs differently than uniform power allocation. Figure 3.4 referred to LDPC codes case study, where uniform power allocation is closed to FEP-optimal for the relay near to the source ($d_{SR}/d_0 < 0.48$) and FEP-optimal always outperforms R-balanced exception made for $d_{SR}/d_0 \in [0.55, 0.65]$ where they coincide. It is also possible to observe that (3.27) represents a very good approximation of the numerical solution, with exception for the range [0.7, 0.85] for P-STCs in Fig. 3.3 and [0.45, 0.65] for LDPC codes in Fig. 3.4. In these

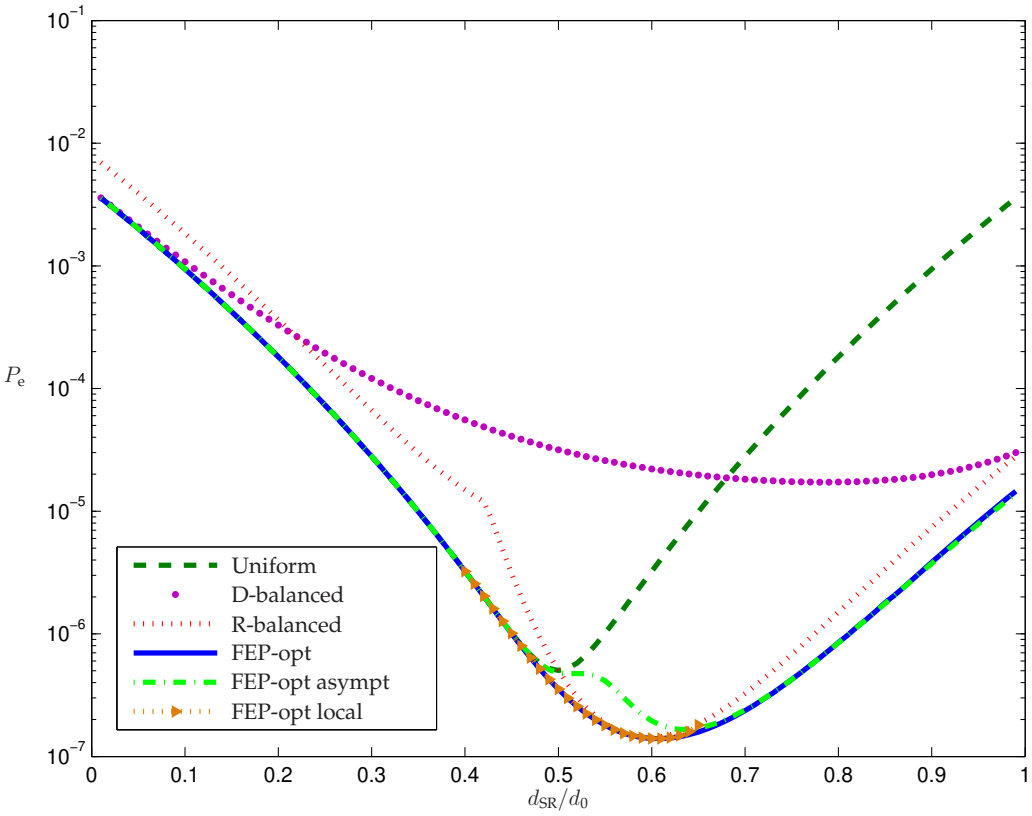

Figure 3.4: LDPC codes case study: P_e as a function of d_{SR}/d_0 at $E_b/N_0 = 6$ dB. Comparison among different power allocation techniques.

ranges, (3.32) may be adopted. The comparison with uniform, D-balanced, and R-balanced techniques quantifies the benefit of FEP-optimal power allocation with respect to the others, for both distributed coding techniques. In addition, it can be observed that FEP-optimal power allocation provides a larger range of possible relay positions for a given target FEP compared to other power allocations.

3.3.2 Bi-Dimensional Scenario

Figures 3.5 and 3.6 show the FEP contours at 10^{-5} in a bi-dimensional scenario, with source S and destination D located at the coordinates $(0, 0)$ and $(d_0, 0)$, respectively, and the relay moving on the entire plane. Re-

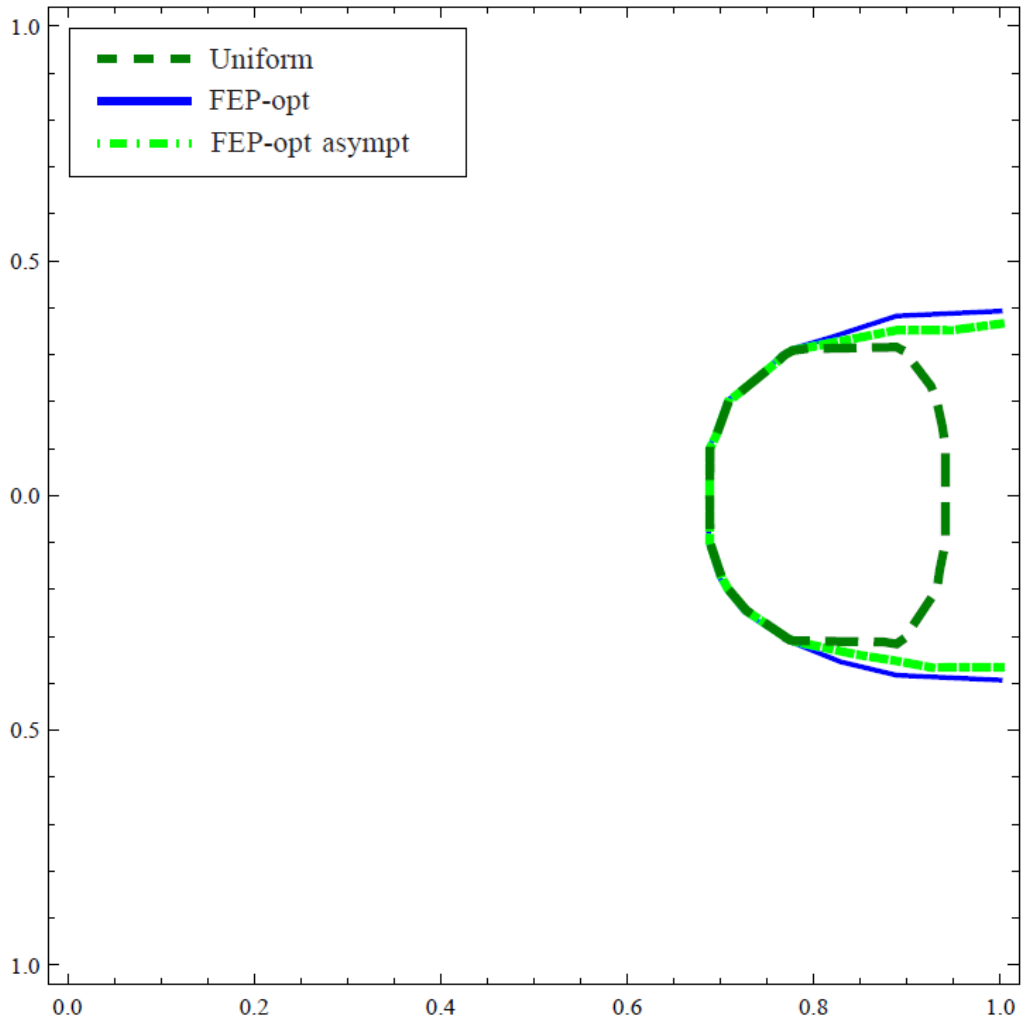

Figure 3.5: P-STCs case study: FEP contours at 10^{-5} as function of relay position at $E_b/N_0 = 13$ dB in a bi-dimensional scenario. Comparison among different power allocation techniques.

sults are presented for uniform,D-balanced, R-balanced, and FEP-optimal power allocation techniques, when the two case studies of P-STCs and LDPC codes are considered. Specially, the region of relay positions providing the required FEP can be observed for all power allocations (those not shown do not fulfill the target FEP). It highlights at a glance which is the most suitable region for the relay position by varying the power al-

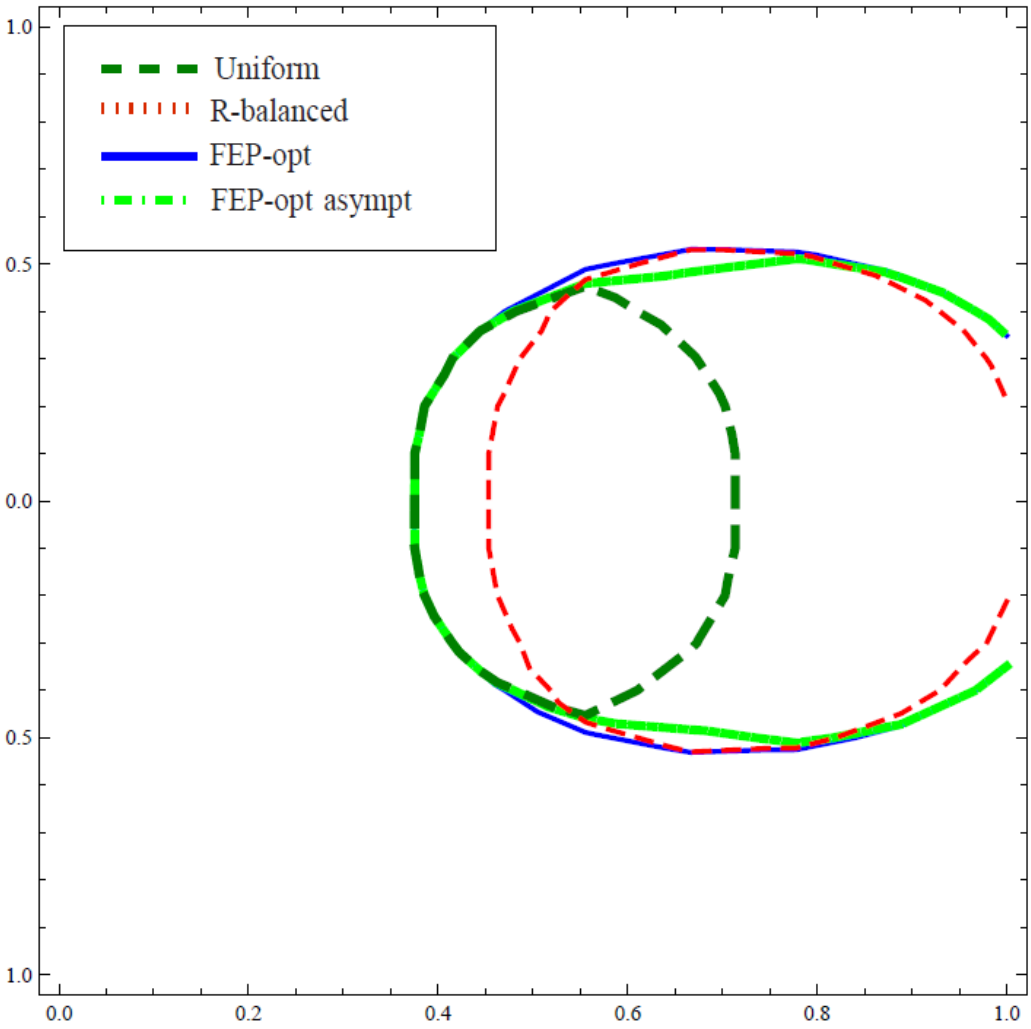

Figure 3.6: LDPC codes case study: FEP contours at 10^{-5} as function of relay position at $E_b/N_0 = 6$ dB in a bi-dimensional scenario.Comparison among different power allocation techniques

location techniques. It can be observed that for all the considered power allocation techniques, the minimum FEP can be obtained when the relay is located in a region between the source and the destination, also confirming that when extending the dimension of the scenario, the behavior is similar to the one dimensional case. It can be noticed that the FEP-optimal power allocation provides a larger region for the relay position providing

the target FEP. Figures 3.5 and 3.6 also remark the very good approximation provided by the asymptotical approximation in (3.27) for all regions of interest and that the optimal relay position as a function of the various power allocation techniques is always between the source and the destination.

Chapter 4

Cooperation in Ultra-Wide Bandwidth Communications

UWB technology is considered for short range high data rate communications with extremely low power spectral density [78,79]. In addition, the UWB signal characteristics enable high accuracy localization [80–82]. This is reflected in the standard IEEE 802.15.4a, which is the first for wireless personal area networks with both communication and high accuracy localization capabilities [83]. The limitations on the UWB emission mask, imposed by regulation bodies worldwide in the last decade, call for techniques to enlarge the coverage still maintaining a target performance. In particular, an important solution is given by relay-assisted UWB communications.

Cooperation via relay represents a new communication paradigm that involves both transmission and distributed processing to increase the capacity and diversity gain in wireless networks [41,47–49,84]. The performance achievable in UWB communications assisted by relays with decode-and-forward protocol has been recently investigated. An analysis through characteristic functions and numerical evaluations has been proposed in [85] by modeling the links according to IEEE 802.15.4a standards, while in [86] UWB MIMO systems with power allocation have been investigated,

where each link is modeled with tapped-delay-lines, Nakagami-m fading, and exponential power delay profile.

The performance at the destination, in terms of BEP[1], depends on network topology, propagation conditions, and power allocation between source and relay. The design of an UWB relay-assisted communication system requires a joint analysis of all these aspects. Therefore, a mathematical framework based on a careful characterization of the performance in each single link (source-destination, source-relay, and relay-destination) is proposed. Instead of time-consuming bit-level simulations, a class of tight bounds for the BEP in a ROI[2] is suggested. This enables the evaluation of the BEP at the destination for various power allocation techniques and relay positions.

The key contributions of the chapter are [3]:

- a performance assessment of relay-assisted UWB communications;
- a new class of tight bounds for UWB single link performance characterization in IEEE 802.15.4a channels;
- the proposal of a new BEP-optimal power allocation technique and its comparison with others techniques, such as uniform power allocation and IPC[3];
- a mathematical framework for the performance evaluation at the destination which jointly considers single link characteristics, power allocation techniques, and network topology.

The remainder of the chapter is organized as follows. Section 4.1 introduces the system model. Section 4.2 describes the single link characterization and the relay-assisted performance. Section 4.3 discusses several power allocation techniques. Section 4.4 combines the different aspects and provides numerical results.

[1]Bit error probability
[2]Region of interest
[3]Ideal power control

4.1 System Model

THE considered relay-assisted communication scheme is illustrated in Fig. 4.1, where the source S transmits to the destination D and a relay R decodes the message from the source and forwards it to the destination to provide cooperation diversity. The communication is characterized by two phases: the transmitting node is the source in the first phase and the relay in the second phase. The three involved links are considered statistically independent. The channels between nodes S, R, and D follow the modified SV[4] model as per the UWB channel model provided by the IEEE 802.15.4a standard [87]. According to this model the channel impulse-response can be represented as $\sqrt{Kd^{-\beta}}h'(t)$ where $h'(t)$ is the model for short-term multipath fading, d is the distance and K is a frequency-dependent constant.

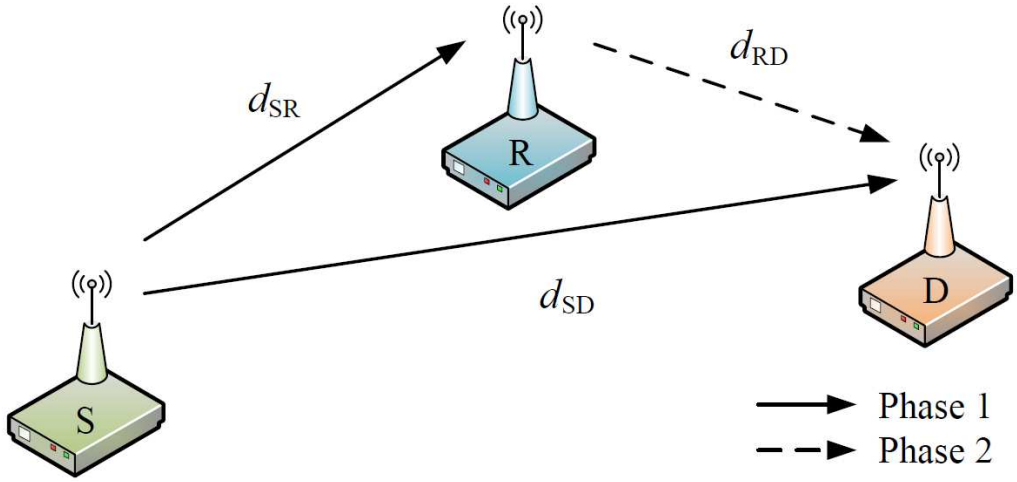

Figure 4.1: Cooperative communication system, with a source S, a relay R and a destination D.

Remark: when using the channel model, each channel realization has to be suitably normalized such that the short-term averaged power gain of

[4]Saleh-Valenzuela

the channel in the signal bandwidth is $Kd^{-\beta}$, that is the inverse of distance-dependent path-loss of the channel.

The average energy per symbol used in each phase of relay-assisted communication is E_{S}. This means that a total energy $2E_{\mathrm{S}}$ is spent to transfer a symbol from the source to destination. The portion of the total energy per symbol transmitted by the source and the relay are indicated with x_{S} and x_{R}, respectively. Thus, the total energy constraint[5] over the two phases results in

$$x_{\mathrm{S}} + x_{\mathrm{R}} = x_{\mathrm{T}} = 2 \tag{4.1}$$

with $x_{\mathrm{S}}, x_{\mathrm{R}} \in [0, x_{\mathrm{T}}]$.

The reference SNR is E_{S}/N_0, N_0 being the one-sided power spectral density of the thermal noise. This SNR is evaluated as short-term averaged at the destination D by assuming that the path-loss on link SD is normalized to 1 to enable network scaling. Consequently, the constant K for each link $\mathbb{L}$ ($\mathbb{L}$ is SD, SR, and RD for the source-destination, source-relay, and relay-destination link, respectively) is replaced with the deterministic component $\Delta_{\mathbb{L}}$ that identifies the inverse path-loss normalized to that in the link SD. This results in

$$\begin{cases} \Delta_{\mathrm{SD}} = 1 \\ \Delta_{\mathrm{RD}} = \left(\frac{d_{\mathrm{RD}}}{d_{\mathrm{SD}}}\right)^{-\beta} \\ \Delta_{\mathrm{SR}} = \left(\frac{d_{\mathrm{SR}}}{d_{\mathrm{SD}}}\right)^{-\beta} \end{cases}$$

where d_{SD} is the distance between source and destination, d_{SR} is the distance between source and relay, and d_{RD} is the distance between relay and destination.

[5]The constraint allows a fair comparison of various power allocation techniques where the same total energy per symbol is assumed.

4.2 Performance Evaluation

THE BEP at the destination depends on the characterization of each link, the power allocation technique between source and relay, and the spatial position of the relay. In Section 4.2.1 a new class of upper bounds is proposed to characterize the mean BEP in each link; then the overall performance evaluation for the relay-assisted communication system is addressed in Section 4.2.2.

4.2.1 Links Characterization

Note that to characterize each link $\mathbb{L}$ the BEP behavior as a function of the SNR in dB is log-concave [57]. This implies that each tangent to the BEP in logarithmic scale versus the SNR in dB is an upper bound. In addition, by observing channel realizations it is possible to note the presence of dominant paths that become remarkable subsequently as the SNR increases.

These considerations motivate to consider a class of bounds tangent to the BEP and with the typical behavior of diversity systems performance in fading channel [58], with ordered diversity degree. In particular, the BEP on link $\mathbb{L}$ with short-term averaged SNR at the received $\gamma_{\mathbb{L}}$ is upper bounded by

$$P_{\mathrm{b}}^{(\mathbb{L})}(\gamma_{\mathbb{L}}) \leq f(\gamma_{\mathbb{L}}) \tag{4.2}$$

where $f(\gamma_{\mathbb{L}})$ is function of the SNR in the link $\mathbb{L}$ as given by

$$f(\gamma_{\mathbb{L}}) = \min\left\{\frac{k_{\mathbb{L}i}}{\gamma_{\mathbb{L}}^{i}},\ \ i = 0, 1, \ldots, I\right\} \tag{4.3}$$

where $k_{\mathbb{L}i}/\gamma_{\mathbb{L}}^{i}$ is a tangent with slope$-i$ in logarithmic scale. The value I is the maximum diversity captured by the system. For example, in the ROI with BEP from 10^{-4} to 0.5 it is possible verify that $I = 4$ for CM[6] 2 and 6. The corresponding values $k_{\mathbb{L}i}$ which make each function tangent to

[6]Channel model

CM	Parameters for single link BEP upper bound				
	$k_{\mathbb{L}0}$	$k_{\mathbb{L}1}$	$k_{\mathbb{L}2}$	$k_{\mathbb{L}3}$	$k_{\mathbb{L}4}$
2	0.50	0.11	0.68	37.46	2363.68
6	0.50	0.12	0.37	7.85	386.69

Table 4.1: Values of $k_{\mathbb{L}i}$ for channel model 2 and 6.

the BEP are given in Table 4.1 for CM 2 and 6 that will be considered for numerical results. Figure 4.2 compares the BEP bound for a generic link $\mathbb{L}$ with simulations as a function of the SNR E_S/N_0 for BPSK modulation and all Rake receiver [88].

The proposed class of bounds has up to I slopes ($I = 0$ would provide a BEP constant with the SNR). An interesting property of the class of bounds in (4.3) is that by setting some of the $k_{\mathbb{L}i} = 0$ the resulting function is still an upper bound. The most simple upper bound considers one-slope in the ROI.

4.2.2 Relay-Assisted Ultra-Wide Bandwidth Communications

The BEP at the destination for the considered UWB relay-assisted communication scheme is determined starting from the BEP of each single link, namely $P_b^{(SD)}$, $P_b^{(SR)}$, and $P_b^{(RD)}$ respectively for link SD, SR, and RD. The mean BEP at the destination results in

$$P_b = P_b^{(SD)} P_b^{(SR)} + P_b^{(SRD)} \left(1 - P_b^{(SR)}\right) \tag{4.4}$$

where $P_b^{(SD)}$, $P_b^{(SR)}$, and $P_b^{(SRD)}$ are functions of the relay position and the short-term averaged SNR as follows

$$\begin{aligned} P_b^{(SD)} &= f^{(SD)}\left(\gamma_{SD}\right) \\ P_b^{(SR)} &= f^{(SR)}\left(\gamma_{SR}\right) \\ P_b^{(SRD)} &= f^{(SRD)}\left(\gamma_{SD}, \gamma_{RD}\right) . \end{aligned} \tag{4.5}$$

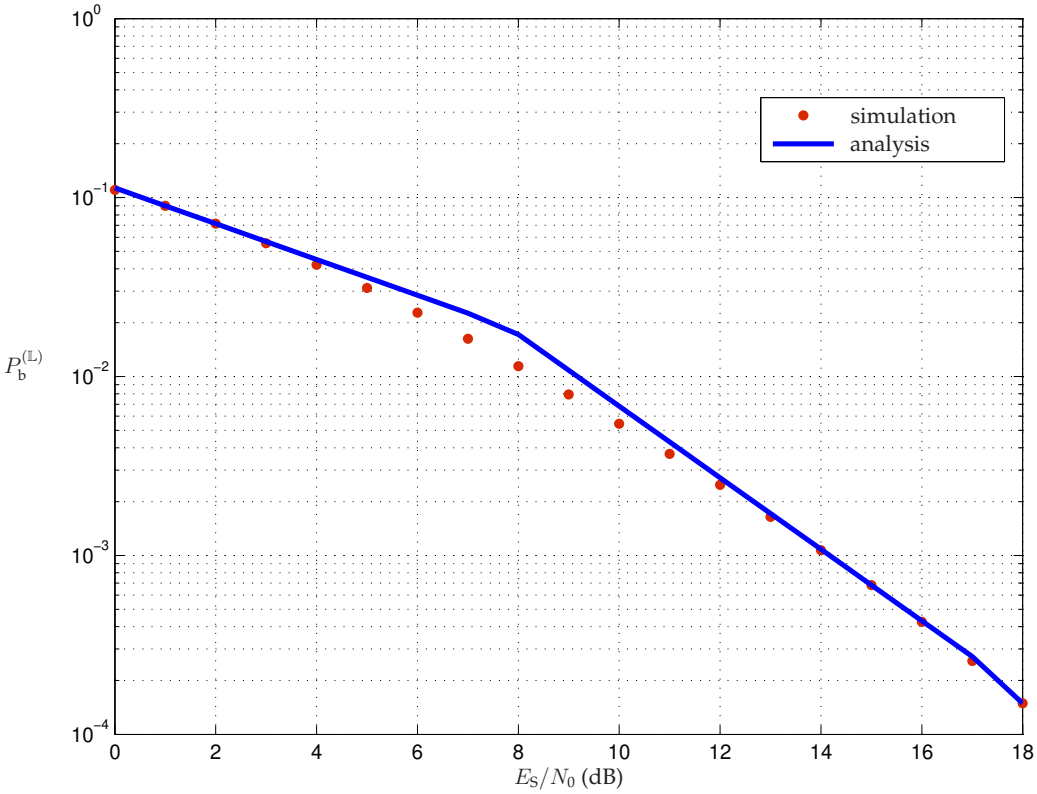

Figure 4.2: $P_b^{(\mathbb{L})}$ vs. E_S/N_0: comparison between simulation and upper bound.

In particular, the SNR in each single link results in

$$\gamma_{SD} = x_S \Delta_{SD} \gamma \tag{4.6a}$$

$$\gamma_{SR} = x_S \Delta_{SR} \gamma \tag{4.6b}$$

$$\gamma_{RD} = x_R \Delta_{RD} \gamma \tag{4.6c}$$

with $\gamma = E_S/N_0$. For the composite link SRD, the receiver coherently combines signals received in phase 1 from S with signals received in phase 2 from R in a composite all Rake structure. The mean BEP can be approximated as

$$P_b^{(SRD)} \simeq 2 P_b^{(SD)}(\gamma_{SD}) P_b^{(RD)}(\gamma_{RD}) \,. \tag{4.7}$$

which has been verified by simulation to be sufficiently accurate.

4.3 Power Allocation Techniques

SEVERAL power allocation techniques between source and relay are present in the literature (see, e.g., [54, 61]) based on known results for power control in wireless communications without relay (see, e.g., [46]). In addition to classical solutions such as uniform allocation and IPC, a power allocation technique is proposed with the purpose of minimize the BEP at the destination. The considered power allocation techniques are summarized below.

4.3.1 Uniform Power Allocation

In the case of uniform power allocation the source and the relay transmit with the same energy per symbol. Hence,

$$x_{\mathrm{S}} = x_{\mathrm{R}} = 1 \tag{4.8}$$

independently of the relay position.

4.3.2 Ideal Power Control

In the case of IPC x_{S} and x_{R} are such that the destination receives the signals from the source and from the relay with the same power, that is $\gamma_{\mathrm{SD}} = \gamma_{\mathrm{RD}}$. Thus the power allocation depends on the relay position. In particular, x_{S} results in [54]

$$x_{\mathrm{S}} = \frac{2\Delta_{\mathrm{RD}}}{1 + \Delta_{\mathrm{RD}}} \tag{4.9}$$

and $x_{\mathrm{R}} = 2 - x_{\mathrm{S}}$.

4.3.3 BEP-Optimal Power Allocation

This power allocation technique minimizes the BEP at the destination depending on relay position. By characterizing the performance of each

single link through the one-slope behavior with diversity L, that is $k_{\mathbb{L}}/\gamma_{\mathbb{L}}^{L}$, the BEP is then derived from (4.4). By minimizing the BEP with respect to x_{S} and x_{R}, and taking into account the constraint (4.1), the implicit solution for large γ results in

$$2\frac{k_{\mathrm{SR}}}{k_{\mathrm{RD}}}\left(\frac{\Delta_{\mathrm{RD}}}{\Delta_{\mathrm{SR}}}\right)^{L}=\left(\frac{x_{\mathrm{S}}}{x_{\mathrm{R}}}\right)^{L}\left(\frac{x_{\mathrm{S}}}{x_{\mathrm{R}}}-1\right) \tag{4.10}$$

The equation can be solved numerically to obtain $x_{\mathrm{S}}/x_{\mathrm{R}}$. By further approximating the numerical solution with the asymptotic behavior for $\Delta_{\mathrm{RD}}/\Delta_{\mathrm{SR}}\to 0$ and $\Delta_{\mathrm{RD}}/\Delta_{\mathrm{SR}}\to\infty$, the energy partition as given by[7]

$$\frac{x_{\mathrm{S}}}{x_{\mathrm{R}}}\approx\chi(L,k_{\mathbb{L}},d_{\mathbb{L}},\beta) \tag{4.11}$$

with $\mathbb{L}=\{\mathrm{SD},\mathrm{SR},\mathrm{RD}\}$ and

$$\chi=\max\left\{1,\left[2\frac{k_{\mathrm{SR}}}{k_{\mathrm{RD}}}\left(\frac{\Delta_{\mathrm{RD}}}{\Delta_{\mathrm{SR}}}\right)^{L}\right]^{\frac{1}{L+1}}\right\}. \tag{4.12}$$

By considering that $x_{\mathrm{S}}+x_{\mathrm{R}}=x_{\mathrm{T}}=2$, x_{S} can be written as

$$x_{\mathrm{S}}=\frac{2\chi}{1+\chi}. \tag{4.13}$$

and consequently $x_{\mathrm{R}}=2-x_{\mathrm{S}}$.

[7] In the following the argument of χ is omitted for conciseness.

4.4 Numerical Results

In this section results for UWB relay-assisted communications in IEEE 802.15.4a CM 2 (residential NLOS[8]) are provided, with parameters reported in [87], and for BPSK modulation and all Rake receiver. The path-loss coefficient $\beta = 3.5$ is considered and the distances between nodes are normalized to d_{SD}. A one-dimensional case is proposed, where a relay moves over a line between source and destination.

Figure 4.3 shows the portion of power x_{S} for various relay positions in the different cases of power allocation techniques described in Section 4.3. One can observe that when the relay moves from the source toward the destination, x_{S} increases in the case of IPC and BEP-optimal power allocation.

Figures 4.4 and 4.5 show the overall BEP at destination as a function of $d_{\mathrm{SR}}/d_{\mathrm{SD}}$ for $E_{\mathrm{S}}/N_0 = 2$ dB and various power allocation techniques (uniform, IPC, and BEP-optimal). In Figure 4.4 the one-slope BEP bound is assumed for each link, whereas in Figure 4.5 all tangents ($i = 0, 1, \ldots, 4$) are considered. As expected, the BEP evaluated with the one-slope behaviors is greater than the one evaluated with all tangents being obtained from a larger upper bound. In both cases the performance of the relay-assisted case outperforms that of the non cooperative case independently of the adopted techniques of power allocation. Note that the accuracy of the performance characterization of each link influences that of the overall BEP at destination; in fact the approximation with the complete class of tangents gives better performance than the one-slope approximation. Another important observation is on the impact of the power allocation technique on the BEP. By using BEP-optimal and uniform power allocation, the overall BEP is the same for $d_{\mathrm{SR}}/d_{\mathrm{SD}}$ in the range $[0.1, 0.5]$. However, the BEP-optimal outperforms the uniform power allocation for all the others relay positions. In addition, these results provide information on which

[8]Non-line-of-sight

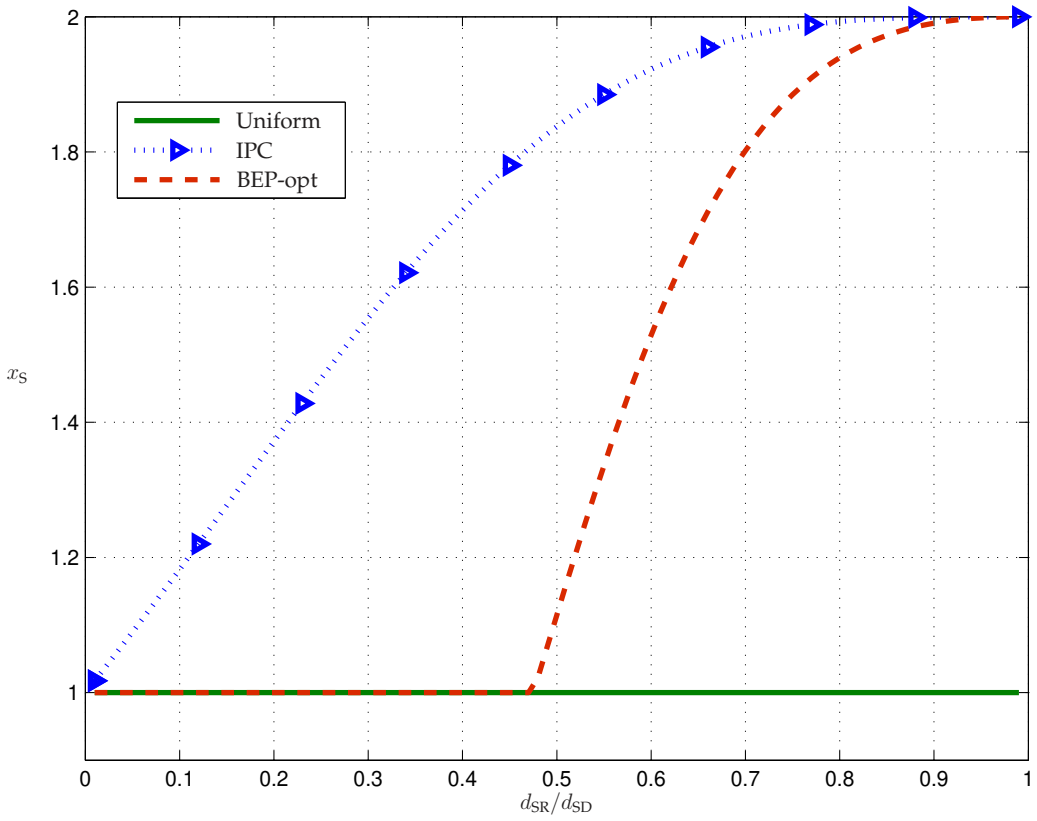

Figure 4.3: Portion of power allocated to the source, x_S, vs. d_{SR}/d_{SD} for different power allocation techniques (Uniform, IPC and BEP-optimal).

relay positions enable the fulfillment of a target BEP. As an example, for a given target BEP of 10^{-3}, Figure 4.5 shows that without cooperation or with cooperation and IPC it is not possible to satisfy the performance requirements. On the other hand, the target BEP is satisfied by uniform power allocation for relay positions such that d_{SR}/d_{SD} is in the range from 0.4 to 0.6; this range is larger with BEP-optimal power allocation for which the target BEP is fulfilled for d_{SR}/d_{SD} values from 0.41 to about 0.9.

Results are also provided for a bi-dimensional scenario. Figure 4.6 shows the BEP contours as a function of the relay position in a plane, using uniform, IPC, and BEP-optimal power allocation. The source and the destination are placed at the coordinates (0,0) and (1,0), respectively. The link

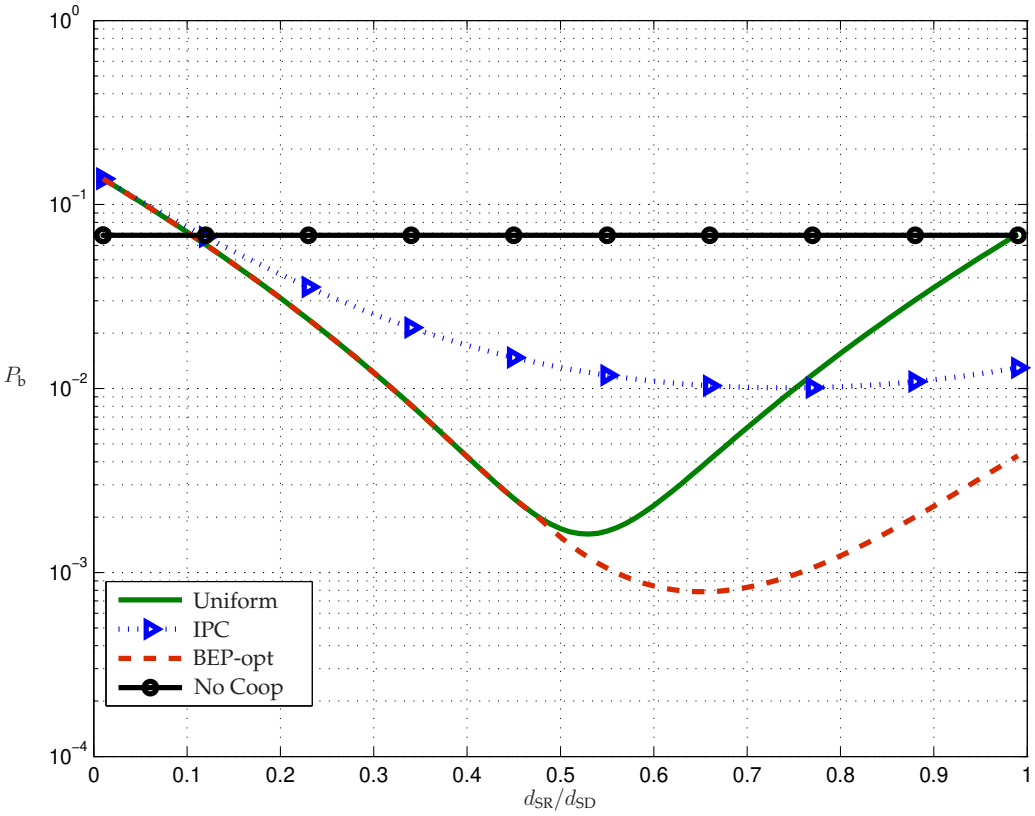

Figure 4.4: P_b vs d_{SR}/d_{SD} for different power allocation techniques with one-slope approximation and $E_S/N_0 = 2$ dB.

performance characterization given by a class of tangents with $I = 4$ and the overall BEP at destination as in (4.4) are considered. It is important to observe that the BEP-optimal power allocation gives the best performance and provides a larger region for possible relay positions satisfying the performance requirements.

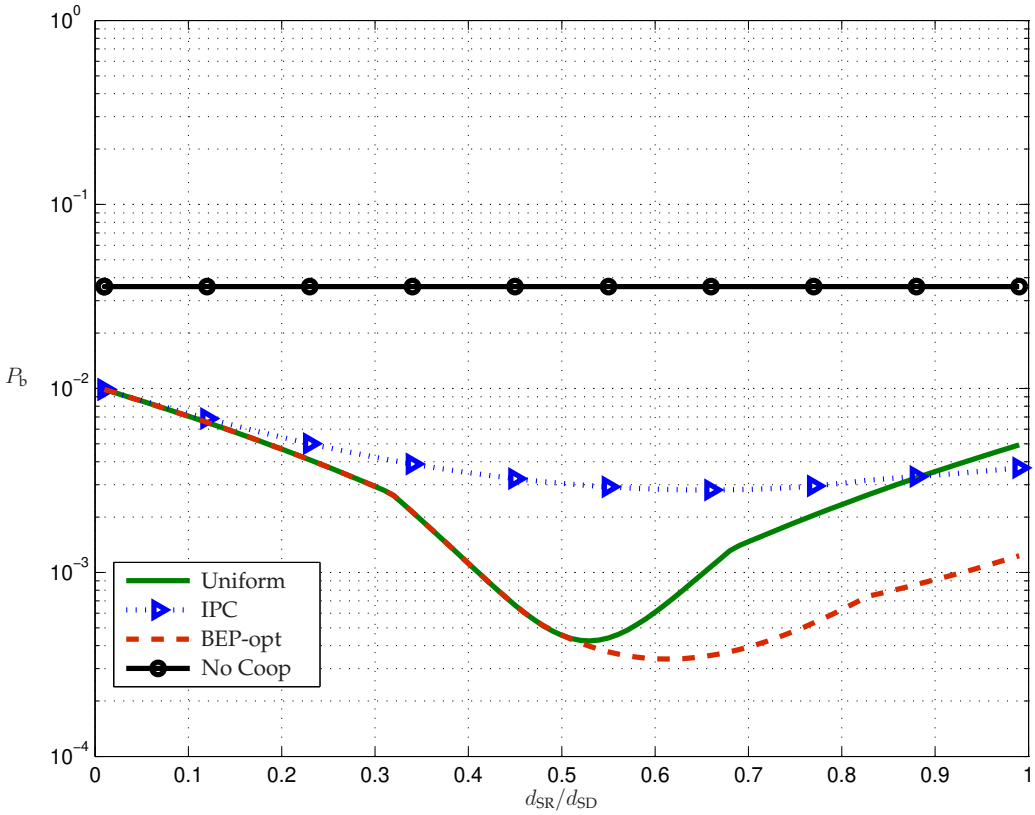

Figure 4.5: P_b vs d_{SR}/d_{SD} for different power allocation techniques using a class of tangents approximation with $I = 4$ and $E_S/N_0 = 2$ dB.

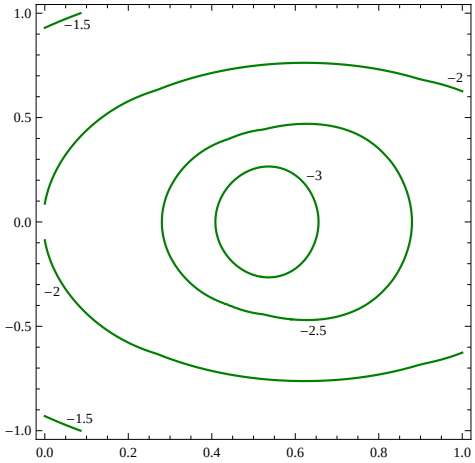

(a) Uniform power allocation technique.

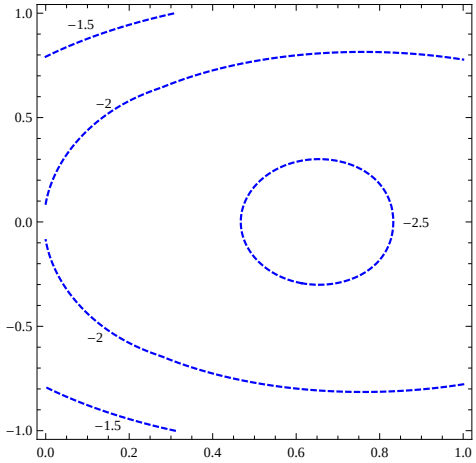

(b) IPC technique.

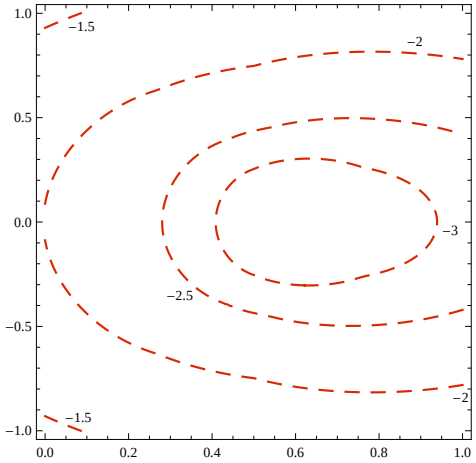

(c) BEP-opt power allocation technique.

Figure 4.6: $\log_{10}$ BEP contours vs relay position in the bi-dimenisonal scenario with source and destination in (0,0) and in (1,0), respectively.

Chapter 5

Network Synchronization

TIME synchronization plays an essential role in many distributed applications and assumes a fundamental importance in the interaction via the network. In fact, the coordination of events between entities is possible only sharing the same time. In addition, time synchronization can be useful for save energy in a network, by setting nodes in sleeping mode with a coordinated criteria. The necessity of a common time is essential for modern wireless networks, especially for an efficient management of resources, and results more critical for dense, distributed, and infrastructure-less wireless networks.

To realize time synchronization, various strategies have been analyzed for distributed wired networks [89] (e.g., computer cluster and set of processor) and new distributed solutions have been proposed for wireless topologies [90–93]. Solutions based on one or several main reference clocks are suggested in [94–96] for particular topologies (e.g., MANET, mesh). Distributed synchronization solutions are presented in [97–99], where a global convergence to a virtual common time and determinist bounds for timing errors are analyzed. However, these contributions do not jointly consider synchronization parameters simultaneously. A global distributed solution is proposed in [100], where synchronization and positioning are jointly analyzed in UWB networks.

The IR-UWB[1] technology, characterized by the high bandwidth and short pulses of the signal, allows a very precise temporal resolution that can be used for the localization process of the system [101–103] and for accurate synchronization between nodes [104–106]. An important advantage of the UWB synchronization if compared to that via cable and UHF[2] solutions is that it is completely based on the available hardware. However, the firmware and software will be adopted in accordance with the procedure laid down respectively by the synchronization protocol.

In this context, the master-slave synchronization is particularly attractive and provides high accuracy of synchronization based on the removal of the timing error of the slave node with respect to the master node time. By executing only the adaptation with respect to a reference node, no feedback is necessary from the slaves node to the master node. The variation of the relative value with respect to the reference value depends on the angular frequency of the node oscillator, that is equal to 1 (i.e., clock drift is equal to zero) when the hardware clock is perfect. However, the real clocks are imperfect and are characterized by clock drift [107,108]. The exact instantaneous drift is difficult to predict because it depends on certain environmental parameters (e.g., pressure, temperature, supply voltage).

In this chapter a time synchronization algorithm that jointly evaluate the drift and offset corrections is proposed [4]. The remainder of the chapter is organized as follows. Section 5.1 introduces the general network architecture. Section 5.2 analyzes the basis of the analytical model for timing synchronization and the assumption related to the used configuration. Section 5.3 details a time synchronization algorithm that jointly evaluate the drift and delay corrections for compensate the timing error of a slave clock. Section 5.4 describes the equivalent model of discrete-time synchronizer in the Z-domain and Section 5.5 provides numerical results for the proposed solution.

[1]Impulse-radio ultrawide bandwidth
[2]Ultra-high frequency

5.1 General Network Architecture

THE overall system design aims to obtain high-accuracy detection, real-time identification, and localization of objects and persons provided with small ultra-low power tags. In this context, the UWB technology is a good solution to overcome the limitation of current first and second generation of RFID[3] systems [109], such as identification and accurate localization at the submeter level, retaining low power consumption, small size, and low cost [110]. Various UWB systems based on the use of active RFID tags are proposed in [111–113], whereas passive tags that operate on UWB backscatter modulation are presented in [114, 115]. In the considered system, the IR-UWB technology is involved for RFID, characterized by the transmission of pulses with subnanosecond duration. This approach, useful when the low cost and small size are a crucial requirements, resolves multipath and garantees higth detection probability and high precision of the localization through ToA[4] estimation of the signal [78, 81, 116, 117].

A number of readers is located in several cells and covers the geographic area of interest [118]. All readers communicate with a central processing unit, which has the functions of data fusion, system configuration and synchronization. The location engines combine suitable algorithms for real-time spatial location of tracked objects. The obtained data are collected and create an object tracking database. The other tasks of the central unit include self-diagnostic, monitoring functionalities, and synchronization between readers. To improve the performance of the network by limiting the cost, an appropriate number of relays can be included. Figure 5.1 shows the considered general scenario characterized by a central unit, readers, relays, tagged and un-tagged objects.

The use of a dense relay network permits to extend coverage in the area of interest for complex propagation scenarios, when the link between

[3]Radio frequency identification
[4]Time-of-arrival

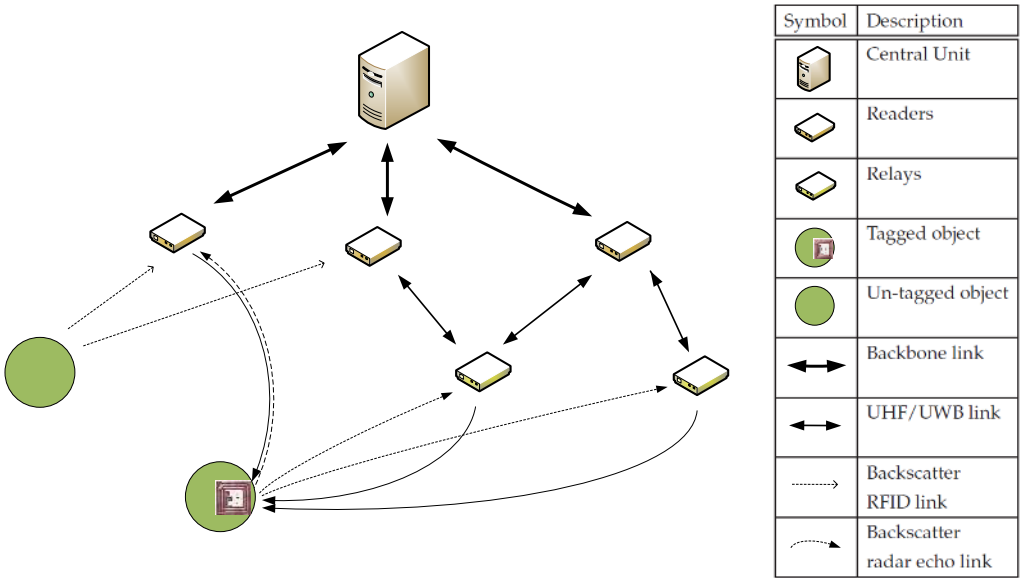

Figure 5.1: General architecture with a central unit, readers, relays, tagged and un-tagged objects.

readers and tags are in NLOS or in areas too far from the readers. Moreover, the use of relays plays an essential role also for extending the tag detection range in LOS[5] environments, as well as for improving the location capability and performance. In particular, the regulations for UWB system impose stringent power limit that restricts the tag detection range, especially for passive tags based on UWB backscatter modulation. This implies a LOS distance between readers and tags higher than the detection range. The localization through ToA estimation requires a minimum of three anchors, so relays are able to improve accuracy and robustness, by maintaining low cost.

The communication between tags and readers or relays is based on UWB and UHF functionalities and can be summarized as follows:

- Each reader interrogates all the small ultra-low power tags located in the same cell through the transmission of a wake-up signal that con-

[5]Line-of-sight

sists on an unmodulated UHF carrier. Each tag is usually in sleeping mode to save energy and does not present active transmitter. The energy of batteries is available only for modulation operation and memory access.

- After the transmission of the wake-up signal, readers radiate the UWB signal, which is backscattered by all tags according to their internal information bits. The analysis of the backscatter signals permit to localize the position of each tag in addition to their detection. Spreading codes are used to readers and tags sides for recognizing the backscattered signals. Each tag is associated with a unique speeding code allowing for unambiguous demodulation and detection.

- The targets of objects and people without a specific tags are detected through radar techniques, if they are moving in the area covered by readers. In this way, the presence or absence of a target is detected and its position is estimated.

In this context clock synchronization between readers has the essential role to guarantee satisfactory medium-access control performance and reduce tags wake-up synchronization offset. The synchronization process is achieved through the combination of Ethernet message exchanges (coarse synchronization) and ToA estimation of the UWB interrogation signals (fine synchronization) by reusing the same hardware developed for tag detection. Coarse synchronization has the main role of reduce the duration of the start-up synchronization procedure; the fine synchronization is realized to further refine the synchronization accuracy.

5.2 Analytical Model

THE network is characterized by N readers, which include a master node M and $N-1$ slave nodes S_n ($n \in 1, \ldots, N-1$). The master reader provides the reference time for the measurement process to which the slave nodes refer for synchronizing themselves. In other words, it is important that the nodes are synchronous to the same time base. In the following a constant drift term is considered, that means a local clock that varies linearly with time. The choice of the master node can be carried out during the network set up or through a dynamic self-assignment algorithm. To establish the same time among nodes of the network, the wireless synchronization algorithm provides exchange of messages between master reader and slave readers. The slave readers use the obtained information to adjust their clocks.

Each slave reader is equipped with a free-running oscillator from which the local clock reference is derived. The choice of free-running oscillator guarantees a relatively simple hardware implementation and avoids the inaccuracy provided by external analog frequency control. Due to the imprecision and tolerances of the oscillator, a real clock deviates from the reference time causing large timing errors. In other words, a real clock drift apart from the reference time, because the clock does not run at the exact right speed compared to another clock. The exact instantaneous drift is difficult to predict for its dependency on technical tolerances and environmental parameters (e.g., temperature, variation in driving voltage).

The k-th local time measurement of the slave clock timer of the n-th slave reader can be described as a function $t_k^{(n)}$ of the reference time t_k. For short time interval, $t_k^{(n)}$ can be written in a noisy scenario as

$$t_k^{(n)} = \left(1 + \tau_k^{(n)}\right) t_k + \mu_k^{(n)} + n_k^{(n)} \tag{5.1}$$

where $\tau_k^{(n)}$, $\mu_k^{(n)}$, and $n_k^{(n)}$ are the clock drift relative to the correct rate, the clock offset, and the estimated noise samples of the reader S_n at time instance t_k, respectively. Thus, the timing error $e_k^{(n)}$ between the slave clock

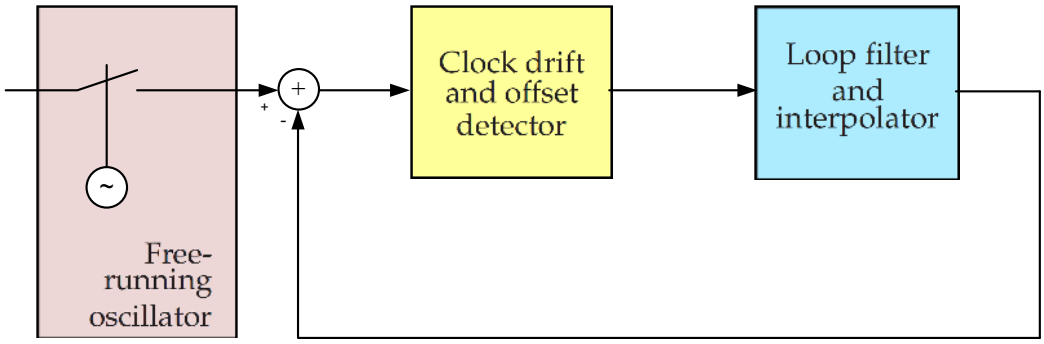

Figure 5.2: General timing synchronization loop.

timer $t_k^{(n)}$ and the master reference time t_k results in

$$e_k^{(n)} = \tau_k^{(n)} t_k + \mu_k^{(n)} + n_k^{(n)} \,. \tag{5.2}$$

A correction factor is necessary for the slave clock in order to obtain a synchronized local time value with the master clock.

The slave clock provided by a free-running oscillator is adjusted through a feedback timing synchronization loop [119]. The general scheme is shown in Fig. 5.2 and consists of:

- a clock drift and offset detector, which gives an indication of the timing error;
- a loop filter and interpolator, which filter the output of the previous block and adjusts the clock in order to reduce the timing error between the reference clock and the local clock.

5.3 Timing Synchronization Loop

5.3.1 Drift Compensation

To evaluate the master clock drift estimation, the $(k-1)$-th local time measurement of the n-th slave reader clock timer is considered. According to (5.1), it can be written as

$$t_{k-1}^{(n)} = \left(1 + \tau_{k-1}^{(n)}\right) t_{k-1} + \mu_{k-1}^{(n)} + n_{k-1}^{(n)} \tag{5.3}$$

where $\tau_{k-1}^{(n)}$, $\mu_{k-1}^{(n)}$, and $n_{k-1}^{(n)}$ are the clock drift, the clock offset, and the estimated noise samples of the reader S_n at time instance t_{k-1}, respectively.

Consequently, the clock drift can be evaluated starting from the difference between two consecutive local time measurements of the n-th slave reader in a temporal interval Δ. This difference results in

$$\begin{aligned} t_k^{(n)} - t_{k-1}^{(n)} &= \left(1 + \tau_k^{(n)}\right) t_k + \mu_k^{(n)} + n_k^{(n)} - \left(1 + \tau_{k-1}^{(n)}\right) t_{k-1} - \mu_{k-1}^{(n)} - n_{k-1}^{(n)} \\ &= t_k - t_{k-1} + \tau_k^{(n)} t_k - \tau_{k-1}^{(n)} t_{k-1} + \mu_k^{(n)} - \mu_{k-1}^{(n)} + n_k^{(n)} - n_{k-1}^{(n)} \\ &= \Delta + \tau_k^{(n)} t_k - \tau_{k-1}^{(n)} t_{k-1} + \mu_k^{(n)} - \mu_{k-1}^{(n)} + n_k^{(n)} - n_{k-1}^{(n)} \\ &= \Delta + \tau_k^{(n)} \Delta + \mu_k^{(n)} - \mu_{k-1}^{(n)} + n_k^{(n)} - n_{k-1}^{(n)} \,. \end{aligned} \tag{5.4}$$

By assuming the difference between two consecutive timing offset equal to zero, that is $\mu_k^{(n)} - \mu_{k-1}^{(n)} = 0$, (5.4) becomes

$$t_k^{(n)} - t_{k-1}^{(n)} = \Delta + \tau_k^{(n)} \Delta + n_k^{(n)} - n_{k-1}^{(n)} \,. \tag{5.5}$$

The assumption of no difference between two consecutive timing offset is not restrictive, because at this stage no offset compensation is considered. Other effects, such as jitter, are considered in the noise term.

By defining the estimated time offset value as

$$\hat{\tau}_k^{(n)} = \tau_k^{(n)} + \frac{n_k^{(n)} - n_{k-1}^{(n)}}{\Delta} \tag{5.6}$$

(5.7) can be written as

$$\frac{t_k^{(n)} - t_{k-1}^{(n)}}{\Delta} = 1 + \hat{\tau}_k^{(n)} \tag{5.7}$$

from which follows

$$\hat{\tau}_k^{(n)} = \frac{t_k^{(n)} - t_{k-1}^{(n)}}{\Delta} - 1\,. \tag{5.8}$$

Note that positive values of $\hat{\tau}_k^{(n)}$ refer to a local clock faster than the reference clock; on the contrary, negative values mean a local clock runs slower.

5.3.2 Loop Filter and Interpolator

The loop filter has the main task of reducing the effect of noise and can be implemented as a PI[6] controller characterized by two constant parameters, called integral constant and proportional constant. These values determinate the loop bandwidth, the noise level, and the speed of the loop output. Hence, the filter design parameters come out from the best trade-off during the implementation phase.

The loop filter output results in

$$\chi_k^{(n)} = K_{\mathrm{I}} \sum_{m=0}^{k-1} \hat{\tau}_m^{(n)} + K_{\mathrm{P}} \hat{\tau}_k^{(n)} \tag{5.9}$$

where K_{I} and K_{P} are the integral constant and the proportional constant, respectively. The two terms of (5.9) depend on the present estimated time offset $\hat{\tau}_k^{(n)}$ via the proportional constant K_{P} and on the accumulation of previous estimated time offset $\hat{\tau}_m^{(n)}$ via the integral constant K_{I}.

The NCO[7], or interpolator, is achieved by an integrator and its main task is to revert the inherent down-conversion performed in the drift estimator where only time measurements are usable. The interpolator output can be implemented recursively as

$$CF_\zeta = CF_{\zeta-1} + T_{\mathrm{clk}} \chi_k^{(n)} \tag{5.10}$$

where T_{clk} is the clock interval and $\zeta = k(\Delta/T_{\mathrm{clk}}) + \psi$ is the index between the measurements spaced by Δ with $0 \leq \psi \leq \Delta/T_{\mathrm{clk}}$. Specifically, (5.10)

[6] Proportional-integrator

[7] Numerically controlled oscillator

represents the correction factor necessary for the slave clock in order to synchronize its local clock with the master clock.

Figure 5.3 shows the drift synchronization loop at the n-th slave reader. As can be observed, a delay block is considered in the proposed configu-

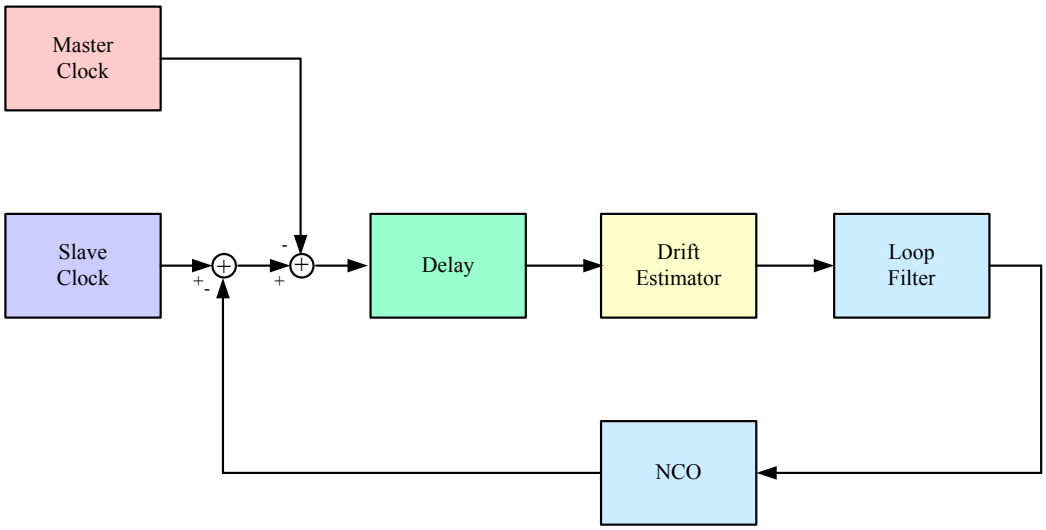

Figure 5.3: Timing synchronization loop with drift compensation.

ration. This delay D depends on the propagation delay t_{prop} and on the processing delay t_{proc} caused by the hardware implementation and can be written as

$$D = \frac{t_{\text{prop}} + t_{\text{proc}}}{\Delta}\,. \tag{5.11}$$

The delay influences the adaptation velocity of the loop, because a measured drift can only be compensate after that time.

5.3.3 Drift and Offset Compensation

The previous loop configuration is not able to compensate the offset effects. In order to remove the residual offset, a feed-forward solution based on averaging filter (sliding mean or recursive version of a exponential moving average) can be considered. Figure 5.4 shows the complete clock synchronization algorithm at the n-th slave reader.

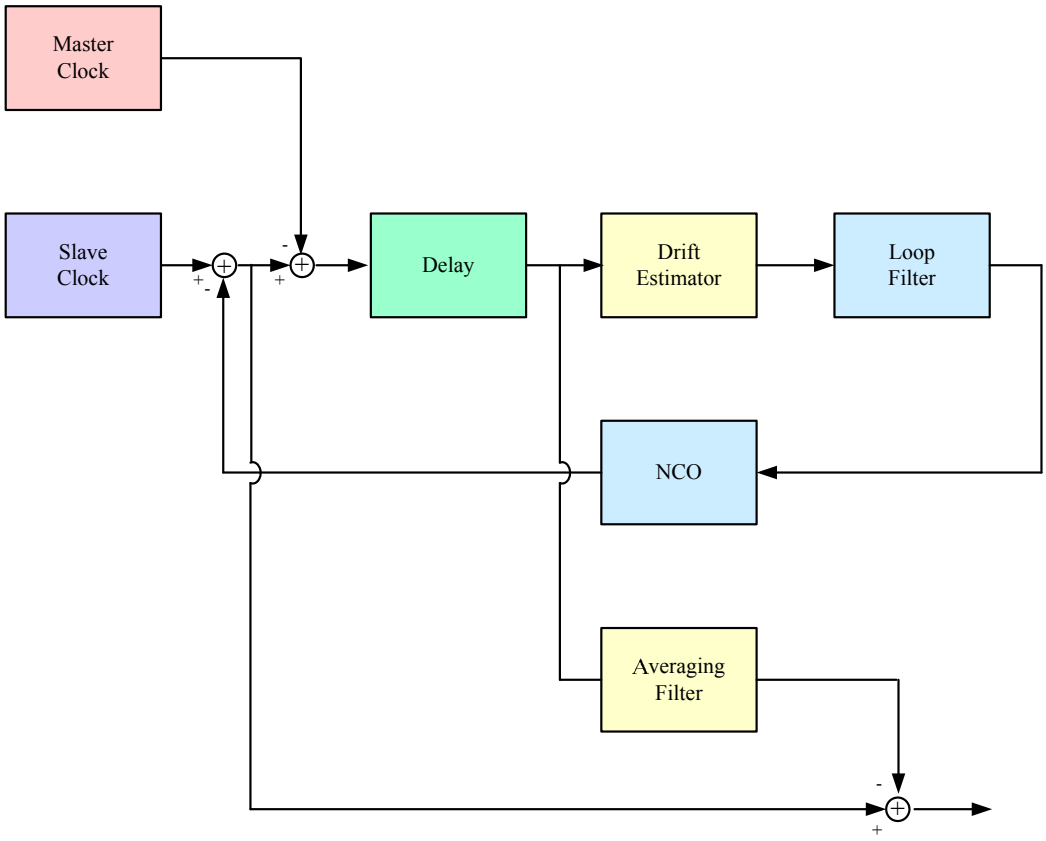

Figure 5.4: Timing synchronization loop with drift and offset compensation.

5.4 Discrete Z-Domain Analysis

By considering normal operating conditions, the timing error is characterized by small fluctuations around a stable equilibrium point; the appropriate performance evaluations for this mode of operation are the steady-state-error and the timing error variance. To analyze these small fluctuations it is more useful linearize the equivalent model around the stable equilibrium point and apply standard linear filter theory. This yields to the equivalent model for discrete-time synchronizer, as shown in Fig. 5.5 .

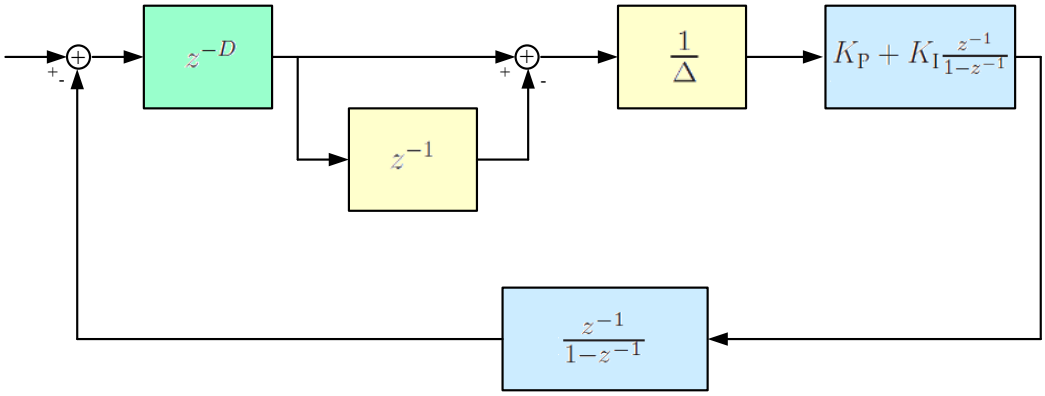

Figure 5.5: Equivalent model of discrete-time synchronizer.

The closed-loop frequency response $H(z)$ in the z-domain is given by

$$\begin{aligned}
H(z) &= \frac{z^{-D}(1-z^{-1})\frac{1}{\Delta}\left(K_\mathrm{P} + K_\mathrm{I}\frac{z^{-1}}{1-z^{-1}}\right)\frac{z^{-1}}{1-z^{-1}}}{1 + z^{-D}(1-z^{-1})\frac{1}{\Delta}\left(K_\mathrm{P} + K_\mathrm{I}\frac{z^{-1}}{1-z^{-1}}\right)\frac{z^{-1}}{1-z^{-1}}} \\
&= \frac{z^{-D}\frac{z-1}{z}\frac{1}{\Delta}\left(K_\mathrm{P} + K_\mathrm{I}\frac{1}{z-1}\right)\frac{1}{z-1}}{1 + z^{-D}\frac{z-1}{z}\frac{1}{\Delta}\left(K_\mathrm{P} + K_\mathrm{I}\frac{1}{z-1}\right)\frac{1}{z-1}} \\
&= \frac{z^{-D}\frac{1}{z}\frac{1}{\Delta}\left(K_\mathrm{P} + K_\mathrm{I}\frac{1}{z-1}\right)}{1 + z^{-D}\frac{1}{z}\frac{1}{\Delta}\left(K_\mathrm{P} + K_\mathrm{I}\frac{1}{z-1}\right)} \\
&= \frac{z^{-D}(K_\mathrm{P}z + K_\mathrm{I} - K_\mathrm{P})}{\Delta z^2 - \Delta z + z^{-D}K_\mathrm{P}z - z^{-D}K_\mathrm{P} + z^{-D}K_\mathrm{I}} \\
&= \frac{K_\mathrm{P}z + K_\mathrm{I} - K_\mathrm{P}}{\Delta z^{D+2} - \Delta z^{D+1} + K_\mathrm{P}z - K_\mathrm{P} + K_\mathrm{I}}\,.
\end{aligned} \tag{5.12}$$

The closed-loop frequency response in the frequency domain is obtained by replacing z with $e^{j\omega\Delta}$ and results in

$$H(j\omega) = \frac{K_{\mathrm{P}}e^{j\omega\Delta} + K_{\mathrm{I}} - K_{\mathrm{P}}}{\Delta e^{j\omega\Delta(D+2)} - \Delta e^{j\omega\Delta(D+1)} + K_{\mathrm{P}}e^{j\omega\Delta} - K_{\mathrm{P}} + K_{\mathrm{I}}}\,. \tag{5.13}$$

An important parameter is the one-sided loop bandwidth B_L, that denote the measure in Hertz of the bandwidth of the closed-loop response [119]. It is given by

$$B_L = \int_0^{\pi/\Delta} \left| \frac{K_{\mathrm{P}}e^{j\omega\Delta} + K_{\mathrm{I}} - K_{\mathrm{P}}}{\Delta e^{j\omega\Delta(D+2)} - \Delta T e^{j\omega\Delta(D+1)} + K_{\mathrm{P}}e^{j\omega\Delta} - K_{\mathrm{P}} + K_{\mathrm{I}}} \right|^2 \frac{d\omega}{2\pi}\,. \tag{5.14}$$

where T is the clock period. In many cases of interests, it is possible consider a small loop bandwidth in order to reduce the effect of loop noise. Typical value of $B_L T$ are in the order of one percent or much smaller.

The timing error variance due to the loop noise [119] results in

$$var[e_k] = \Delta \int_{\pi/\Delta}^{-\pi/\Delta} \left| \frac{K_{\mathrm{P}}e^{j\omega\Delta} + K_{\mathrm{I}} - K_{\mathrm{P}}}{\Delta e^{j\omega\Delta(D+2)} - \Delta e^{j\omega\Delta(D+1)} + K_{\mathrm{P}}e^{j\omega\Delta} - K_{\mathrm{P}} + K_{\mathrm{I}}} \right|^2 \frac{d\omega}{2\pi}\,. \tag{5.15}$$

5.4.1 Stability Criterion

By remembering the Jury's Stability Test [120], a given polynomial $P(z)$ has no roots on and outside the unit circle in the z-plane (i.e., for the digital or discrete data system to be stable) if the following conditions are satisfied:

$$\begin{aligned} &1.\ P(z)_{|z=1} = P(1) > 0 \\ &2.\ P(z)_{|z=-1} = P(-1) \begin{cases} > 0 \text{ for } n \text{ even} \\ < 0 \text{ for } n \text{ odd} \end{cases} \\ &3.\ |a_0| < |a_n|\,. \end{aligned} \tag{5.16}$$

In an ideal situation without delay (i.e., $D = 0$), (5.12) results in

$$H(z) = \frac{K_{\mathrm{P}}z + K_{\mathrm{I}} - K_{\mathrm{P}}}{\Delta z^2 + (K_{\mathrm{P}} - \Delta)z + K_{\mathrm{I}} - K_{\mathrm{P}}} \tag{5.17}$$

and the stability conditions are

$$\begin{aligned}
&1.\quad D(1) = \Delta + K_\mathrm{P} - \Delta + K_\mathrm{I} - K_\mathrm{P} \Rightarrow K_\mathrm{I} > 0 \\
&2.\quad D(-1) = \Delta + \Delta - K_\mathrm{P} + K_\mathrm{I} - K_\mathrm{P} \\
&\qquad\qquad = 2\Delta - 2K_\mathrm{P} + K_\mathrm{I} > 0 \\
&\qquad\qquad \Rightarrow K_\mathrm{P} < \frac{K_\mathrm{I} + 2\Delta}{2} \\
&3.\quad |K_\mathrm{I} - K_\mathrm{P}| < |\Delta| \,.
\end{aligned} \tag{5.18}$$

If the delay is equal to 1 (i.e., $D = 1$), (5.12) results in

$$H(z) = \frac{K_\mathrm{P} z + K_\mathrm{I} - K_\mathrm{P}}{\Delta z^3 - \Delta z^2 + K_\mathrm{P} z - K_\mathrm{P} + K_\mathrm{I}} \tag{5.19}$$

and the stability conditions are

$$\begin{aligned}
&1.\quad D(1) = \Delta - \Delta + K_\mathrm{P} - K_\mathrm{P} + K_\mathrm{I} \Rightarrow K_\mathrm{I} > 0 \\
&2.\quad D(-1) = -\Delta - \Delta - K_\mathrm{P} - K_\mathrm{P} + K_\mathrm{I} \\
&\qquad\qquad = -2\Delta - 2K_\mathrm{P} + K_\mathrm{I} < 0 \\
&\qquad\qquad \Rightarrow K_\mathrm{P} > \frac{K_\mathrm{I} - 2\Delta}{2} \\
&3.\quad |K_\mathrm{I} - K_\mathrm{P}| < |\Delta| \,.
\end{aligned} \tag{5.20}$$

The other cases with a delay bigger than one can be solved numerically.

5.5 Numerical Results

To show the range of validity of the analysis, in this section numerical results for a master-slave synchronization are provided. In particular, by assuming a typical ToA estimation error of about 1 ns, noise samples are characterized by an intensity of the same order of magnitude, whereas the measurement spacing is in the order of tens of milliseconds. Consequently, it results that $\left(n_k^{(n)} - n_{k-1}^{(n)}\right)/\Delta$ is about $(1 \text{ ns}/10 \text{ ms}) = 10^{-7}$, while $\hat{\tau}_k^{(n)}$ is expressed in terms of ppm[8] defined as the maximum number of extra (or missed) clock counts over a total of 10^{-6} counts (i.e., $\hat{\tau}_k^{(n)} \times 10^{-6}$). The propagation delay t_{prop} is in the order of ns and the processing delay t_{proc} is mainly determined by the fact that a complete symbol is received and processed before the ToA measurement becomes available and it is lower bounded by 16 ms. This value corresponds to the complete reception of a symbol in the current hardware implementation. Consequently, a total delay $t_{\text{proc}} + t_{\text{prop}} = 20$ ms and an interval between two measurements $\Delta = 50$ ms are considered.

The master clock runs at a reduced clock interval of 5 ms and the noise is a zero mean random variable with standard deviation $\sigma = 10$ ns. The k- th local time measurement of the slave clock of the n- th slave reader deviates from the master clock for a clock offset $\mu_k^{(n)} = 1$ µs. The values of the integral constant K_{I} and the proportional constant K_{P} satisfy the stability condition given by (5.16) and are obtained from (5.14) by fixing the one-sided loop bandwidth B_{L}. For $B_{\text{L}} = 0.5$, $K_{\text{I}} = 0.5$ and $K_{\text{P}} = 0.1$, respectively.

Figure 5.6 shows the timing error $e_k^{(n)}$ between the slave clock timer $t_k^{(n)}$ and the master reference time t_k as a function of the normalized master clock t_k/Δ for a case study with $\hat{\tau}_k^{(n)} = 10$ ppm. In particular, red line refers to the case without any kind of timing error compensation, green and blue lines represent the timing error of the configuration shown in

[8]Parts per million

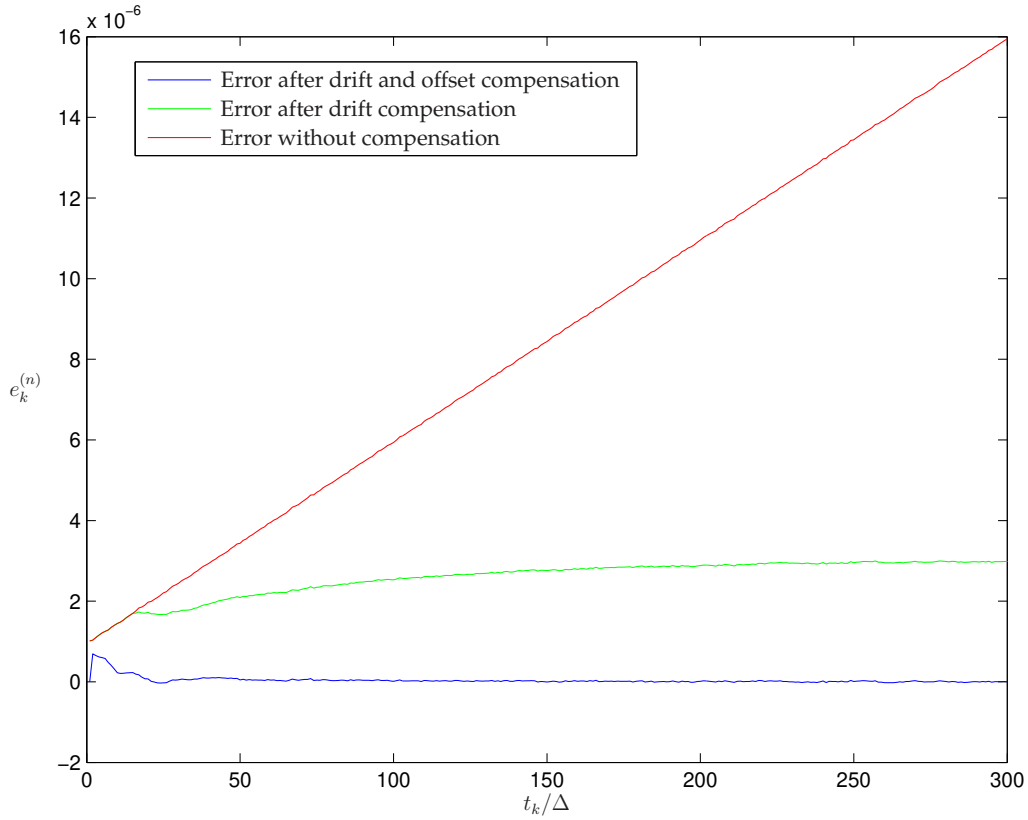

Figure 5.6: Comparison between begin timing error without compensation, with drift compensation, and with drift and offset compensation, respectively.

Figs. 5.3 and 5.4, respectively. From this comparison, it can be observed that without any compensation the begin error increases dramatically. The timing synchronization loop with drift compensation is not able to fully compensate the timing error due to the presence of the clock offset. In fact, there is only a reduction of the timing error in constant value. However, timing synchronization loop with drift and offset compensation reduces the clock drift and the clock offset and provides a timing error that tends to zero.

Figures 5.7 considers timing synchronization loop with drift and offset compensation and shows the absolute value of the timing error $e_k^{(n)}$

between the slave clock timer $t_k^{(n)}$ and the master reference time t_k in logarithmic scale as a function of the normalized master clock t_k/Δ for several clock drift values, namely 0 ppm, 10 ppm, and 20 ppm. The comparison of these case studies underline how a major settling time is necessary for the algorithm when the clock drift increases.

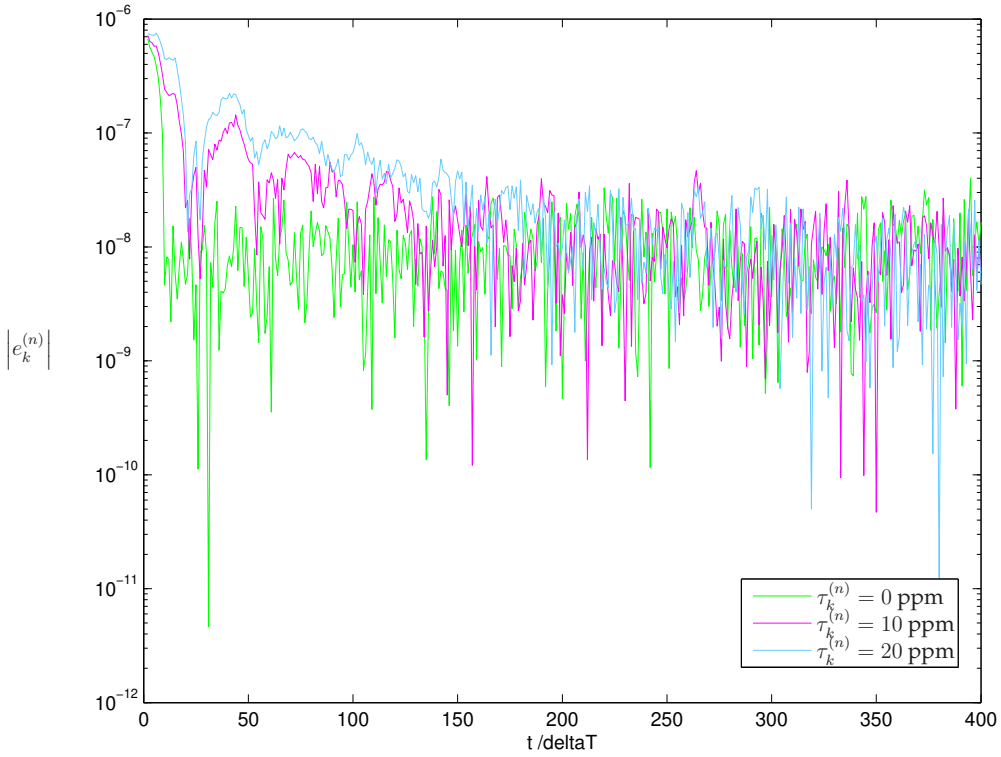

Figure 5.7: Absolute value of timing error in logarithmic scale after drift and offset compensation.

By fixing the loop bandwidth and the clock drift, it is possible obtain different performance in terms of error variance and settling time. In particular, Tables 5.1 and 5.2 show the error variance and the settling time for different case studies with a loop bandwidth $B_L = 0.5$ and $B_L = 0.05$ for a clock drift $\tau_k^{(n)} = 10$ ppm and $\tau_k^{(n)} = 20$ ppm, respectively. The settling time is defined as an elapsed time during which the output of the system settles to a desired accuracy. In the following an accuracy in the order

$B_L = 0.5$, $\tau_k^{(n)} = 10$ ppm		
Avg length	Error variance	Settling time [s]
10	1.431186e-016	10
100	1.993463e-016	10
1000	1.974805e-016	10
$B_L = 0.5$, $\tau_k^{(n)} = 20$ ppm		
Avg length	Error variance	Settling time [s]
10	1.458543e-016	10
100	1.854484e-016	10
1000	2.000589e-016	15

Table 5.1: Error variance and settling time for a loop bandwidth $B_L = 0.5$ with clock drift $\tau_k^{(n)} = 10$ ppm and $\tau_k^{(n)} = 20$ ppm, respectively.

of nanoseconds is considered. The loop bandwidth is responsible for the noise level and the velocity of the loop output. A low bandwidth means a low noise level, but corresponds to a slow response of the synchronization.

$B_L = 0.05$, $\tau_k^{(n)} = 10$ ppm		
Avg length	Error variance	Settling time [s]
10	1.403656e-016	35
100	1.713863e-016	75
1000	1.049814e-016	120
$B_L = 0.05$, $\tau_k^{(n)} = 20$ ppm		
Avg length	Error variance	Settling time [s]
10	1.593220e-016	50
100	1.493165e-016	90
1000	1.630983e-016	130

Table 5.2: Error variance and settling time for a loop bandwidth $B_L = 0.05$ with clock drift $\tau_k^{(n)} = 10$ ppm and $\tau_k^{(n)} = 20$ ppm, respectively.

Final Remark

THIS thesis underlines the importance of cooperative communications and the advantages of the use of a relay-assisted communication in terms of performance. In particular, after a preliminary overview on the state of art, a simple and general framework for the design and analysis of relay-assisted diversity communications is developed. It accounts for network geometry, links characterization, diversity methods, power allocation, and distributed coding. A new FEP-optimal power allocation technique is proposed and its benefits is quantified with respect to other techniques. The framework is applied to two case studies based on distributed P-STCs and distributed LDPC codes. Results provides the essence for design and operation of relay-assisted diversity communications with proper choice of relay position, power allocation, and system configurations.

UWB relay-assisted communications is analyzed through a mathematical framework which enables to investigate the BEP performance at destination for various network topologies and power allocation techniques between source and relay. The channels modeled following the IEEE 802.15.4a standards and proposed a new class of bounds to characterize the performance of each link. A BEP-optimal power allocation technique that minimizes the BEP at the destination depending on the relay position and its comparison with classical uniform allocation and IPC techniques are proposed. Results clearly show the performance improvement provided by relay-assisted communications and the spatial regions where the relay is

more effective. The analytical framework can be extended to others settings, in terms of network topology, number of relays, modulation and coding techniques, diversity techniques, and power allocation methods once the performance characterization of each link is available.

In addition, a timing synchronization algorithm is proposed for master-slave communications. After a preliminary overview of the general system, a simple analysis for obtaining a common time among nodes is developed. The aim of this algorithm is compensate the clock drift and offset, that dramatically influence the performance of the system. It accounts also the propagation and processing delay, and the presence of the noise. The equivalent model of discrete-time synchronizer is analyzed for studying the stability of the system and for obtaining the expression of important parameters, as loop bandwidth and error variance. Results clearly show the performance improvement provided by the proposed timing synchronization algorithm.

Bibliography

[1] C. La Palombara, V. Tralli, B. Masini, and A. Conti, "Relay-assisted diversity communications," *IEEE Trans. Veh. Technol.*, vol. 62, no. 1, pp. 415 –421, Jan. 2013.

[2] C. La Palombara, A. Conti, B. M. Masini, and V. Tralli, "On the impact of links characterization and power allocation in relay assisted communications," in *Proc. Int. Wireless Commun. and Mobile Computing (IWCMC)*, Jul. 2011, pp. 2076 –2081.

[3] C. La Palombara, A. Conti, and V. Tralli, "Relay-assisted UWB communications: links characterization and power allocation," in *Proc. IEEE Int. Conf. on Ultra-Wideband (ICUWB)*, Sep. 2011, pp. 293 –297.

[4] *SELECT Project Deliverable D2.3.2. Multi-functional network design: final system specification*, Jun. 2012.

[5] A. Goldsmith, *Wireless Communications*. Cambridge, 2005.

[6] V. Garg, *Wireless Communications and Networking*. Morgan Kaufmann, 2007.

[7] A. Molisch, *Wireless Communications- Second Edition*. John Wiley & Sons, 2010.

[8] H. Holma and A. Toskala, *LTE for UMTS: Evolution to LTE-Advanced*. John Wiley & Sons, 2011.

[9] M. Katz and F. H. P. Fitzek, *WiMAX Evolution: Emerging Technologies and Applications*. John Wiley & Sons, 2009.

[10] R. Kraemer and M. Katz, *Short-Range Wireless Communications: Emerging Technologies and Applications*. John Wiley & Sons, 2009.

[11] R. Daher and A. Vinel, *Roadside Networks for Vehicular Communications: Architectures, Applications, and Test Fields*. Information Science Reference, 2012.

[12] J. Mietzner, R. Schober, L. Lampe, W. Gerstacker, and P. Hoeher, "Multiple-antenna techniques for wireless communications - a comprehensive literature survey," *IEEE Commun. Surveys Tuts.*, vol. 11, no. 2, pp. 87 –105, Second Quarter 2009.

[13] A. Sibille, C. Oestges, and A. Zanella, *MIMO: From Theory to Implementation*. Academic Press, 2010.

[14] G. Foschini and M. Gans, "On limits of wireless communications in a fading environment when using multiple antennas," *Wireless Personal Communications*, vol. 6, pp. 311–335, Mar. 1998.

[15] E. Telatar, "Capacity of multiantenna gaussian channels," *AT&T Bell Laboratories, Tech. Memo.*, Jun. 1995.

[16] G. Raleigh and J. Cioffi, "Spatio-temporal coding for wireless communication," *IEEE Trans. Commun.*, vol. 46, no. 3, pp. 357 –366, Mar. 1998.

[17] H. Bolcskei, D. Gesbert, and A. Paulraj, "On the capacity of OFDM-based spatial multiplexing systems," *IEEE Trans. Commun.*, vol. 50, no. 2, pp. 225 –234, Feb. 2002.

[18] M. Dohler and Y. Li, *Cooperative Communications: Hardware, Channel & PHY*. Wiley & Sons, 2010.

[19] A. Nosratinia, T. Hunter, and A. Hedayat, "Cooperative communication in wireless networks," *IEEE Commun. Mag.*, vol. 42, no. 10, pp. 74 – 80, Oct. 2004.

[20] Y. Li, "Distributed coding for cooperative wireless networks: An overview and recent advances," *IEEE Commun. Mag.*, vol. 47, no. 8, pp. 71 – 77, Aug. 2009.

[21] Y. Zhang, H. H. Chen, and M. Giuzani, *Cooperative Wireless Communications (Wireless Networks and Mobile Communications)*. Auerbach Publications, 2009.

[22] S. G. Glisic, *Advanced Wireless Communications and Internet: Future Evolving Technologies*. Wiley, 2011.

[23] F. Fitzek and M. D. Katz, *Cooperation in Wireless Network: Principles and Applications- Real Egoistic Behavior is to Cooperate!* Springer, 2006.

[24] Y. Shen, H. Wymeersch, and M. Win, "Fundamental limits of wideband cooperative localization via fisher information," in *Proc. IEEE Wireless Commun. and Networking Conf.*, Mar. 2007, pp. 3951–3955.

[25] D. Dardari, A. Conti, J. Lien, and M. Z. Win, "The effect of cooperation on UWB- based positioning systems using experimental data," *EURASIP J. Adv. Signal Process*, vol. 2008, pp. 1–11, Jan. 2008.

[26] H. Wymeersch, U. Ferner, and M. Z. Win, "Cooperative Bayesian self- tracking for wireless networks," *IEEE Commun. Lett.*, vol. 12, no. 7, pp. 505–507, 2008.

[27] N. Patwari, J. N. Ash, S. Kyperountas, A. O. Hero, III, R. L. Moses, and N. S. Correal, "Locating the nodes: Cooperative localization in wireless sensor networks," *IEEE Signal Process. Mag.*, vol. 22, no. 4, pp. 54–69, 2005.

[28] J. Zhao, *Analysis and Design of Communication Techniques in Spectrally Efficient Wireless Relaying Systems*. Logos Verlag, 2010.

[29] K. J. R. Liu, A. K. Sadek, W. Su, and A. Kwasinski, *Advanced Wireless Communications and Internet: Future Evolving Technologies*. Cambridge University Press, 2009.

[30] E. Zimmermann, P. Herhold, and G. Fettweis, "On the performance of cooperative diversity protocols in practical wireless systems," in *Proc. IEEE Semiannual Veh. Technol. Conf.*, vol. 4, Oct. 2003, pp. 2212 – 2216.

[31] S. Sugiura, S. Chen, and L. Hanzo, "Cooperative differential space-time spreading for the asynchronous relay aided CDMA uplink using interference rejection spreading code," *IEEE Signal Process. Lett.*, vol. 17, no. 2, pp. 117 –120, Feb. 2010.

[32] L. Wang and L. Hanzo, "The resource-optimized differentially modulated hybrid AF/DF cooperative cellular uplink using multiple-symbol differential sphere detection," *IEEE Signal Process. Lett.*, vol. 16, no. 11, pp. 965 –968, Nov. 2009.

[33] B. Gedik and M. Uysal, "Impact of imperfect channel estimation on the performance of amplify-and-forward relaying," *IEEE Trans. Wireless Commun.*, vol. 8, no. 3, pp. 1468 –1479, Mar. 2009.

[34] C. Patel and G. Stuber, "Channel estimation for amplify and forward relay based cooperation diversity systems," *IEEE Trans. Wireless Commun.*, vol. 6, no. 6, pp. 2348 –2356, Jun. 2007.

[35] S. Borade, L. Zheng, and R. Gallager, "Amplify-and-forward in wireless relay networks: Rate, diversity, and network size," *IEEE Trans. Inf. Theory*, vol. 53, no. 10, pp. 3302 –3318, Oct. 2007.

[36] A. Bletsas, H. Shin, and M. Win, "Outage optimality of opportunistic amplify-and-forward relaying," *IEEE Commun. Lett.*, vol. 11, no. 3, pp. 261 –263, Mar. 2007.

[37] I. Abou-Faycal and M. Medard, "Optimal uncoded regeneration for binary antipodal signaling," in *Proc. IEEE Int. Conf. on Commun.*, vol. 2, Jun. 2004, pp. 742–746.

[38] H. Xiong, J. Xu, and P. Wang, "Frequency-domain equalization and diversity combining for demodulate-and-forward cooperative systems," in *Proc. IEEE Int. Conf. Acoustics, Speech, and Signal Processing*, 31 Mar.- 4 Apr. 2008, pp. 3245 –3248.

[39] K. S. Gomadam and S. A. Jafar, "Optimal relay functionality for SNR maximization in memoryless relay networks," *IEEE J. Sel. Areas Commun.*, vol. 25, no. 2, pp. 390 –401, Feb. 2007.

[40] Z. Yi and I.-M. Kim, "Diversity order analysis of the decode-and-forward cooperative networks with relay selection," *IEEE Trans. Wireless Commun.*, vol. 7, no. 5, pp. 1792 –1799, May 2008.

[41] J. Laneman, D. Tse, and G. Wornell, "Cooperative diversity in wireless networks: Efficient protocols and outage behavior," *IEEE Trans. Inf. Theory*, vol. 50, no. 12, pp. 3062 – 3080, Dec. 2004.

[42] Y. Li and B. Vucetic, "On the performance of a simple adaptive relaying protocol for wireless relay networks," in *Proc. IEEE Semiannual Veh. Technol. Conf.*, May 2008, pp. 2400 –2405.

[43] B. Akhbari, M. Mirmohseni, and M. Aref, "Compress-and-forward strategy for the relay channel with non-causal state information," *Proc. IEEE Int. Symp. on Inf. Theory*, pp. 1169–1173, 28 Jun.- 3 Jul. 2009.

[44] M. Dohler, Y. Li, B. Vucetic, A. Aghvami, M. Arndt, and D. Barthel, "Performance analysis of distributed space-time block-encoded sensor networks," *IEEE Trans. Veh. Technol.*, vol. 55, no. 6, pp. 1776 – 1789, Nov. 2006.

[45] R. Pabst, B. Walke, D. Schultz, P. Herhold, H. Yanikomeroglu, S. Mukherjee, H. Viswanathan, M. Lott, W. Zirwas, M. Dohler, H. Aghvami, D. Falconer, and G. Fettweis, "Relay-based deployment concepts for wireless and mobile broadband radio," *IEEE Commun. Mag.*, vol. 42, no. 9, pp. 80 – 89, Sep. 2004.

[46] M. Chiani, A. Conti, and R. Verdone, "Partial compensation signal-level-based up-link power control to extend terminal battery duration," *IEEE Trans. Veh. Technol.*, vol. 50, no. 4, pp. 1125–1131, Jul. 2001.

[47] A. Sendonaris, E. Erkip, and B. Aazhang, "User cooperation diversity. Part I. System description," *IEEE Trans. Commun.*, vol. 51, no. 11, pp. 1927 – 1938, Nov. 2003.

[48] ——, "User cooperation diversity. Part II. Implementation aspects and performance analysis," *IEEE Trans. Commun.*, vol. 51, no. 11, pp. 1939 – 1948, Nov. 2003.

[49] A. Bletsas, H. Shin, and M. Win, "Cooperative communications with outage-optimal opportunistic relaying," *IEEE Trans. Wireless Commun.*, vol. 6, no. 9, pp. 3450 –3460, Sep. 2007.

[50] A. Bletsas, A. Khisti, and M. Win, "Opportunistic cooperative diversity with feedback and cheap radios," *IEEE Trans. Wireless Commun.*, vol. 7, no. 5, pp. 1823 –1827, May 2008.

[51] J. Laneman and G. Wornell, "Distributed space-time-coded protocols for exploiting cooperative diversity in wireless networks," *IEEE Trans. Inf. Theory*, vol. 49, no. 10, pp. 2415 – 2425, Oct. 2003.

[52] V. Tralli, A. Conti, and M. Chiani, "Pragmatic Space-Time Trellis Codes: GTF-Based Design for Block Fading Channels," *IEEE Trans. Signal Process.*, vol. 59, no. 6, Jun. 2011.

[53] A. Conti, V. Tralli, and M. Chiani, "Pragmatic space-time codes for cooperative relaying in block fading channels," *EURASIP J. Appl. Signal Process. (special issue on Wireless Cooperative Networks)*, vol. 2008, pp. Article ID 872 151, 1–11, 2008.

[54] L. Zuari, A. Conti, and V. Tralli, "Effects of nodes geometry and power allocation in space-time coded cooperative wireless systems," *Mobile Networks and Applications*, pp. 1–13. [Online]. Available: http://dx.doi.org/10.1007/s11036-010-0263-5

[55] V. Tralli, A. Conti, and M. Chiani, "Pragmatic Space-Time Trellis Codes: GTF-Based Design for Block Fading Channels," *IEEE Trans. Signal Process.*, vol. 59, no. 6, Jun. 2011.

[56] J. Hu and T. Duman, "Low density parity check codes over wireless relay channels," *IEEE Trans. Wireless Commun.*, vol. 6, no. 9, pp. 3384–3394, Sep. 2007.

[57] A. Conti, D. Panchenko, S. Sidenko, and V. Tralli, "Log-concavity property of the error probability with application to local bounds for wireless communications," *IEEE Trans. Inf. Theory*, vol. 55, no. 6, pp. 2766–2775, Jun. 2009.

[58] A. Conti, W. M. Gifford, M. Z. Win, and M. Chiani, "Optimized simple bounds for diversity systems," *IEEE Trans. Commun.*, vol. 57, no. 9, pp. 2674–2685, Sep. 2009.

[59] M. Chiani, A. Conti, M. Mazzotti, E. Paolini, and A. Zanella, "Outage capacity for MIMO-OFDM systems in block fading channels," in *Asilomar Conf. on Signals, Systems, and Computers*, Nov. 2011, pp. –.

[60] G. Scutari and S. Barbarossa, "Distributed space-time coding for regenerative relay networks," *IEEE Trans. Wireless Commun.*, vol. 4, no. 5, pp. 2387 – 2399, Sep. 2005.

[61] J. Luo, R. Blum, L. Cimini, L. Greenstein, and A. Haimovich, "Decode-and-forward cooperative diversity with power allocation in wireless networks," *IEEE Trans. Wireless Commun.*, vol. 6, no. 3, pp. 793 –799, Mar. 2007.

[62] A. Host-Madsen and J. Zhang, "Capacity bounds and power allocation for wireless relay channels," *IEEE Trans. Inf. Theory*, vol. 51, no. 6, pp. 2020 –2040, Jun. 2005.

[63] IEEE Std 802.16j 2009, "IEEE Std 802.16j-2009 IEEE Standard for Local and metropolitan area networks Part 16: Air Interface for Broadband Wireless Access Systems Amendment 1: Multihop Relay Specification," Jun. 2009.

[64] A. Ghosh, R. Ratasuk, B. Mondal, N. Mangalvedhe, and T. Thomas, "LTE-advanced: next-generation wireless broadband technology [invited paper]," *IEEE Wireless Comm.*, vol. 17, no. 3, pp. 10–22, Jun. 2010.

[65] G. Farhadi and N. Beaulieu, "On the ergodic capacity of multi-hop wireless relaying systems," *IEEE Trans. Wireless Commun.*, vol. 8, no. 5, pp. 2286–2291, May 2009.

[66] L. Wang and L. Hanzo, "The resource-optimized differentially modulated hybrid AF/DF cooperative cellular uplink using multiple-symbol differential sphere detection," *IEEE Signal Process. Lett.*, vol. 16, no. 11, pp. 965–968, Nov. 2009.

[67] W. Webb and R. Steele, "Variable rate QAM for mobile radio," *IEEE Trans. Commun.*, vol. 43, no. 7, pp. 2223–2230, Jul. 1995.

[68] S. T. Chung and A. Goldsmith, "Degrees of freedom in adaptive modulation: a unified view," *IEEE Trans. Commun.*, vol. 49, no. 9, pp. 1561–1571, Sep. 2001.

[69] A. Conti, M. Z. Win, and M. Chiani, "Slow adaptive M -QAM with diversity in fast fading and shadowing," *IEEE Trans. Commun.*, vol. 55, no. 5, pp. 895–905, May 2007.

[70] H. Skjevling, D. Gesbert, and A. Hjorungnes, "Precoded distributed space-time block codes in cooperative diversity-based downlink," *IEEE Trans. Wireless Commun.*, vol. 6, no. 12, pp. 4209–4214, Dec. 2007.

[71] S. Yiu, R. Schober, and L. Lampe, "Decentralized distributed space-time trellis coding," *IEEE Trans. Wireless Commun.*, vol. 6, no. 11, pp. 3985–3993, Nov. 2007.

[72] A. Stefanov and E. Erkip, "Cooperative coding for wireless networks," *IEEE Trans. Commun.*, vol. 52, no. 9, pp. 1470 – 1476, Sept. 2004.

[73] M. Win and J. Winters, "Virtual branch analysis of symbol error probability for hybrid selection/maximal-ratio combining in Rayleigh fading," *IEEE Trans. Commun.*, vol. 49, no. 11, pp. 1926–1934, Nov. 2001.

[74] A. Molisch and M. Win, "MIMO systems with antenna selection- An overview," *IEEE Microw. Mag.*, vol. 5, no. 1, pp. 46–56, Mar. 2004.

[75] M. Hasna and M.-S. Alouini, "Optimal power allocation for relayed transmissions over Rayleigh-fading channels," *IEEE Trans. Wireless Commun.*, vol. 3, no. 6, pp. 1999 – 2004, Nov. 2004.

[76] W. Mesbah and T. Davidson, "Optimized power allocation for pairwise cooperative multiple access," *IEEE Trans. Signal Process.*, vol. 56, no. 7, pp. 2994 –3008, Jul. 2008.

[77] Y. Zhao, R. Adve, and T. Lim, "Improving amplify-and-forward relay networks: optimal power allocation versus selection," *IEEE Trans. Wireless Commun.*, vol. 6, no. 8, pp. 3114 –3123, Aug. 2007.

[78] M. Win and R. Scholtz, "Impulse radio: how it works," *IEEE Commun. Lett.*, vol. 2, no. 2, pp. 36 –38, Feb. 1998.

[79] ——, "Ultra-wide bandwidth time-hopping spread-spectrum impulse radio for wireless multiple-access communications," *IEEE Trans. Commun.*, vol. 48, no. 4, pp. 679–691, Apr. 2000.

[80] S. Gezici, Z. Tian, G. B. Giannakis, H. Kobayashi, A. F. Molisch, H. V. Poor, and Z. Sahinoglu, "Localization via ultra-wideband radios: a look at positioning aspects for future sensor networks," *IEEE Signal Process. Mag.*, vol. 22, no. 4, pp. 70–84, Jul. 2005.

[81] D. Dardari, A. Conti, U. J. Ferner, A. Giorgetti, and M. Z. Win, "Ranging with ultrawide bandwidth signals in multipath environments," *Proc. IEEE*, vol. 97, no. 2, pp. 404–426, Feb. 2009, special issue on *Ultra-Wide Bandwidth (UWB) Technology & Emerging Applications*.

[82] M. Z. Win, A. Conti, S. Mazuelas, Y. Shen, W. M. Gifford, D. Dardari, and M. Chiani, "Network localization and navigation via cooperation," *IEEE Commun. Mag.*, vol. 49, no. 5, pp. 56–62, May 2011.

[83] "IEEE standard for information technology - telecommunications and information exchange between systems - local and metropolitan area networks - specific requirement part 15.4: Wireless medium access control (MAC) and physical layer (PHY) specifications for low-rate wireless personal area networks (WPANs)," *IEEE Std 802.15.4a-2007 (Amendment to IEEE Std 802.15.4-2006)*, pp. 1 –203, 2007.

[84] M. Dohler, Y. Li, B. Vucetic, A. H. Aghvami, M. Arndt, and D. Barthel, "Performance analysis of distributed space-time block-

encoded sensor networks," *IEEE Trans. Veh. Technol.*, vol. 55, no. 6, pp. 1776–1789, Nov. 2006.

[85] Z. Zeinalpour-Yazdi, M. Nasiri-Kenari, and B. Aazhang, "Bit error probability analysis of UWB communications with a relay node," *IEEE Trans. Wireless Commun.*, vol. 9, no. 2, pp. 802 –813, Feb. 2010.

[86] F. Z. K. Maichalernnukul and T. Kaiser, "UWB MIMO cooperative relay systems: BER analysis and relay regions," in *Proc. Conf. on Inform. Sci. and Sys. (CISS)*, Mar. 2010, pp. 1 –6.

[87] A. F. Molisch, K. Balakrishnan, D. Cassioli, C. Chong, S. Emami, A. Fort, J. Karedal, J. Kunisch, H. Schantz, U. Schuster, and K. Siwiak, "IEEE 802.15.4a channel model - final report," in *Converging: Technology, work and learning. Australian Government Printing Service*. Online Available, 2004.

[88] M. Win, G. Chrisikos, and N. Sollenberger, "Performance of RAKE reception in dense multipath channels: implications of spreading bandwidth and selection diversity order," *IEEE J. Sel. Areas Commun.*, vol. 18, no. 8, pp. 1516 –1525, Aug. 2000.

[89] R. Bittel, W. Elsner, H. Helm, R. Mukundan, and D. Perreault, "Clock synchronization through discrete control correction," *IEEE Trans. Commun.*, vol. 22, no. 6, pp. 836 – 839, Jun. 1974.

[90] J. Elson and K. Römer, "Wireless sensor networks: A new regime for time synchronization," *ACM SIGCOMM Computer Commun. Review*, vol. 33, no. 1, pp. 149–154, 2003.

[91] R. Solis, V. S. Borkar, and P. Kumar, "A new distributed time synchronization protocol for multihop wireless networks," in *45th IEEE Conf. on Decision and Control*, 2006, pp. 2734–2739.

[92] K. Römer, P. Blum, and L. Meier, "Time synchronization and calibration in wireless sensor networks," *Handbook of Sensor Networks: Algorithms and Architectures*, pp. 199–237, 2005.

[93] P. Ranganathan and K. Nygard, "Time synchronization in wireless sensor networks: a survey," *Int. J. of UbiComp (IJU)*, vol. 1, no. 2, p. 92, 2010.

[94] G. Cao and J. Welch, "Accurate multihop clock synchronization in mobile ad hoc networks," in *Proc. Int. Conf. on Parallel Processing Workshops (ICPPW)*, Aug. 2004, pp. 13 – 20.

[95] K. Römer, "Time synchronization in ad hoc networks," in *Proceedings of the 2nd ACM international symposium on Mobile ad hoc networking & computing*, ser. MobiHoc '01, 2001, pp. 173–182.

[96] "IEEE Standard Profile for Use of IEEE 1588 Precision Time Protocol in Power System Applications," *IEEE Std C37.238-2011*, pp. 1 –66, 14 Jul. 2011.

[97] P. Blum, L. Meier, and L. Thiele, "Improved interval-based clock synchronization in sensor networks," in *Proc. IEEE Inform. Processing in Sensor Networks*, Apr. 2004, pp. 349 – 358.

[98] F. Sivrikaya and B. Yener, "Time synchronization in sensor networks: a survey," *IEEE Netw.*, vol. 18, no. 4, pp. 45 – 50, Jul.-Aug. 2004.

[99] Q. Li and D. Rus, "Global clock synchronization in sensor networks," *IEEE Trans. Computers*, vol. 55, no. 2, pp. 214 – 226, Feb. 2006.

[100] B. Denis, J.-B. Pierrot, and C. Abou-Rjeily, "Joint distributed synchronization and positioning in UWB ad hoc networks using TOA," *IEEE Trans. Microw. Theory and Techniques*, vol. 54, no. 4, pp. 1896 – 1911, Jun. 2006.

[101] D. Dardari and R. D'Errico, "Passive ultrawide bandwidth RFID," in *Proc. IEEE Global Telecomm. Conf.*, Dec. 2008, pp. 1 –6.

[102] D. Arnitz, U. Muehlmann, and K. Witrisal, "UWB ranging in passive UHF RFID: proof of concept," *Electron. Lett.*, vol. 46, no. 20, pp. 1401 –1402, 2010.

[103] K. K. Lee, H. A. Hjortland, and T. S. Lande, "IR-UWB technology on next generation RFID systems," in *NORCHIP*. IEEE, 2011, pp. 1–4.

[104] J. R. Fernandes and D. Wentzloff, "Recent advances in IR-UWB transceivers: An overview," in *IEEE Int. Symp. on Circuits and Systems*, 2010, pp. 3284–3287.

[105] L. Zheng, Z. Liu, and M. Wang, "Synchronization for IR-UWB system using a switching phase detector-based impulse phase-locked loop," *ETRI Journal*, vol. 34, no. 2, 2012.

[106] M. A. Matin, *Ultra Wideband: Current Status and Future Trends*. In-Tech, 2012.

[107] G. Coulouris, J. Dollimore, and T. Kindberg, *Distributed Systems: Concepts And Design*, ser. International Computer Science Series. Addison-Wesley, 2005.

[108] H. Kopetz, *Real-Time Systems: Design Principles for Distributed Embedded Applications*, ser. Realtime Systems. Springer, 2011.

[109] E. Ngai, K. K. Moon, F. Riggins, and Y. Candace, "RFID research: An academic literature review (1995-2005) and future research directions," *International Journal of Production Economics*, vol. 112, no. 2, pp. 510 – 520, 2008.

[110] "To strengthen european technology: The support of RFID within FP7," *European Commission DG Information Society and Media/Unit G2 Microsystems*, Sep. 2007.

[111] R. Fontana and S. Gunderson, "Ultra-wideband precision asset location system," in *Proc. IEEE Conf. on Ultra Wideband Syst. and Technol. (UWBST)*, May 2002, pp. 147 –150.

[112] L. Stoica, A. Rabbachin, H. Repo, T. Tiuraniemi, and I. Oppermann, "An ultrawideband system architecture for tag based wireless sensor networks," *IEEE Trans. Veh. Technol.*, vol. 54, no. 5, pp. 1632 – 1645, Sep. 2005.

[113] D. Dardari, "Pseudorandom active UWB reflectors for accurate ranging," *IEEE Commun. Lett.*, vol. 8, no. 10, pp. 608 – 610, Oct. 2004.

[114] J. Reunamaki, "Ultra wideband radio frequency identification techniques," U.S. Patent 7, 154, 396, Dec., 2006.

[115] D. Dardari, R. D'Errico, C. Roblin, A. Sibille, and M. Win, "Ultra-wide bandwidth RFID: The next generation?" *Proc. IEEE*, vol. 98, no. 9, pp. 1570 –1582, Sep. 2010.

[116] Y. Shen and M. Win, "Fundamental limits of wideband localization-part I: A general framework," *IEEE Trans. Inf. Theory*, vol. 56, no. 10, pp. 4956 –4980, Oct. 2010.

[117] Y. Shen, H. Wymeersch, and M. Win, "Fundamental limits of wideband localization- part II: Cooperative networks," *IEEE Trans. Inf. Theory*, vol. 56, no. 10, pp. 4981 –5000, Oct. 2010.

[118] *SELECT Project Deliverable D2.3.1. Multi-functional network design: intermediate system specification*, Oct. 2011.

[119] H. Meyr, M. Moeneclaey, and S. A. Fechtel, *Digital Communication Receivers. Sinchronization, Channel Estimation, and Signal Processing*. Wiley, 1997.

[120] M. Gopal, *Digital Control & Stat Var Methd 3e*. McGraw-Hill Education (India) Pvt Limited, 2008.

List of Figures